# UNIVERSITY OF MINNESOTA
# SPACE SCIENCE CENTER

(E81-10028) A STUDY OF MINNESOTA LAND AND WATER RESOURCES USING REMOTE SENSING, VOLUME 13 Progress Report, 1 Jan. - 31 Dec. 1979 (Minnesota Univ.) 140 p HC A07/MF A01 CSCL 08B G3/43

N81-12505
THRU
N81-12510
Unclas
00028

N81-12506

## SECTION A

# LANDSAT APPLICATIONS TO WETLANDS CLASSIFICATION IN THE UPPER MISSISSIPPI RIVER VALLEY

(Final Report)

Dr. T. M. Lillesand and Lee F. Werth
Remote Sensing Laboratory
Institute of Agriculture
University of Minnesota
St. Paul, Minnesota

## INDEX

5

SPACE SCIENCE CENTER

University of Minnesota

Minneapolis, Minnesota 55455

# A STUDY OF MINNESOTA LAND AND WATER RESOURCES USING REMOTE SENSING

PROGRESS REPORT

January 1, 1980

Supported By:

NASA GRANT NGL 24-005-263

Submitted to:

NATIONAL AERONAUTICS AND SPACE ADMINISTRATION
Washington, D.C. 20546

# TABLE OF CONTENTS

# SPACE SCIENCE CENTER

# PROGRESS REPORT

January, 1980

This report covers research at the University of Minnesota from January 1, to December 31, 1979.

Section A is a final report by T. M. Lillesand and L. F. Werth describing the use of LANDSAT data to classify wetlands in the Upper Mississippi River Valley. As the benefits of wetlands are recognized, accurate maps of the wetlands are needed to implement a number of federal, state and local programs. They used both LANDSAT MSS data and digitized infrared aerial photographs to recognize wetlands and to classify them. There were inaccuracies in distinguishing some types of wetland cover from non-wetland areas. However, it is relatively easy to distinguish wetland from non-wetland manually; once that is done, the more tedious task of preparing an inventory of types of wetland cover can be done automatically with 87% accuracy.

Section B reports initial efforts by Dr. Lillesand and Douglas Meisner to develop data analysis techniques which separate those activities requiring extensive computing from those involving a great deal of user interaction. This will allow the latter to be done in the user's office or in the field. So far, some programs have been written to process images at the University Computer Center. An initial study has been made of user interaction with color prints (instead of expensive graphics terminals). Preliminary analyses of wetlands and forests have been made, with the goal of studying the analysis techniques. Some relatively inexpensive digital display equipment has been purchased and is now operating. Several cooperative projects with both state and federal agencies have already grown out of this work.

Section C describes work by Drs. Joseph Goebel and Matt Walton and the staff of the Minnesota Geological Survey. They combine several different kinds of remote sensing data in order to identify bedrock near the surface. While no single set of data nor mathematical combination of the data was able to indicate areas of bedrock within 3-15 meters of the surface, they were able to develop a recommended procedure for locating areas of near-surface bedrock.

The efforts of Dr. R. H. Rust and P. Robert of the Department of Soil Science to evaluate moisture stress in corn and soybean crops are described in Section D. As in previous years, their efforts were hampered by superb growing conditions during the summer of 1979. A few areas received too much moisture, and these could be identified in LANDSAT pictures.

Laboratory measurements were made of plant leaf reflectance vs. moisture, and of the water content of various soil samples. LANDSAT data from the summer of 1977 were analyzed. One difficulty with using LANDSAT data for crop management has been the delay of two months or more before the LANDSAT data become available. A cooperative project with local farmers using color infrared aerial photography was tried. Although hampered by cloud cover, the technique showed enough promise so that the farmers wish to continue the project. They will, in fact, help to finance it.

In section E, Dr. Michael Sydor and his colleagues at the University of Minnesota-Duluth report their success using satellite remote sensing data to measure particle concentrations in Lake Superior. They have been able to measure red clay, taconite tailings and tannin. They also describe checks of the data for internal consistency. These checks can warn of problems with atmospheric turbidity or of light scattering from the water's surface.

I am also happy to report that a technique described in last year's annual report, the work of Professor H. Stefan on using LANDSAT images for reconnaissance of ice cover on lakes and reservoirs, has been adopted by the U. S. Army Corps of Engineers (R. K. Haugen, R. E. Bates and R. L Mead, Ice Formation, Thickness and Breakup on Impoundments Within the Contiguous United States. U. S. Army Corps of Engineers, Cold Regions Research and Engineering Laboratory, Hanover, N. H., Draft, Oct. 1979).

D,

N81-12506

## SECTION A

# LANDSAT APPLICATIONS TO WETLANDS CLASSIFICATION IN THE UPPER MISSISSIPPI RIVER VALLEY

(Final Report)

Dr. T. M. Lillesand and Lee F. Werth
Remote Sensing Laboratory
Institute of Agriculture
University of Minnesota
St. Paul, Minnesota

INDEX

5

Even with increased recognition since the 1960's of wetland importance, growing world population and food demand have resulted in extensive wetland drainage. Since World War II nearly 25% of the wetlands in the Prairie Pothole Region of the Dakotas and Minnesota has been drained. Sound federal, state, and local management decisions on acquisition, preservation or drainage of wetlands must be based on sound inventory data. Currently, the U.S. Fish and Wildlife Service is involved in a National Wetland Inventory to satisfy these data needs at the federal level. Likewise, various state and local agencies are undertaking, or have completed weltand inventories for a range of purposes. For example, in Minnesota wetland inventories serve as baseline data to evaluate site modification permits, non-point pollution sources, and generally to execute the public water law.

In short, accurate classification and mapping of wetland cover types is considered essential to the implementation of a number of federal, state, and local legislative mandates and resource management programs. At the same time, the task of mapping wetlands on a statewide basis is challenging in terms of cost, time and manpower. On a national level, the task is monumental.

The general objective of the federal wetland inventory is to classify and locate the nation's wetlands as accurately as possible on 1:100,000 (or in some cases 1:24,000) scale maps (Cowardin et al., 1977). To accomplish this, two possible remote sensing data bases suggest themselves: (a) high altitude, small-scale aerial photography and/or (b) LANDSAT. Of the two, aerial photography appears to be the favored choice from the standpoint of spatial resolution - but photography is not always available and, when available, it not always adequate for the purpose.

Neither technique, LANDSAT in particular, had been sufficiently tested in areas representative of Minnesota prior to this study. Thus, this study was proposed to test the applicability of automated processing of LANDSAT multispectral scanner (MSS) in the Minnesota regional context.

## STUDY OBJECTIVES

Initially, the sole objective of this study was to test, under local conditions, the capability of Landsat data analysis techniques to position adequately and classify wetlands in support of the National Wetlands Inventory. This involved a comparison of single-date vs. double-date sets as well as a comparison of data sets preprocessed with a coarse vs. a precision geometric correction. The test area chosen for these comparisons consisted of five contiguous 7.5-minute quadrangles located within the western part of the Twin City 7-County Metropolitan Area (Figure 1). The entire Metropolitan Area has been mapped previously through airphoto interpretation by the Remote Sensing Laboratory under contract with a consortium of funding agencies.[1] (In addition, in-house funds had already been used to perform the single-date Landsat analysis of the study area.)[2] The large amount of existing data on this area provided a good test base for the study. The test site contains one of the most concentrated areas of wetland diversity in the west half of the Metropolitan Area. It is a

---

[1] The Minnesota Department of Natural Resources, the U.S. Army Corps of Engineers, the U.S. Fish and Wildlife Service, the USDA Soil Conservation Service, and the Twin Cities Metropolitan Council. (Werth et al., 1977; Owens and Meyer, 1978).

[2] The University of Minnesota Agricultural Experiment Station and the College of Forestry.

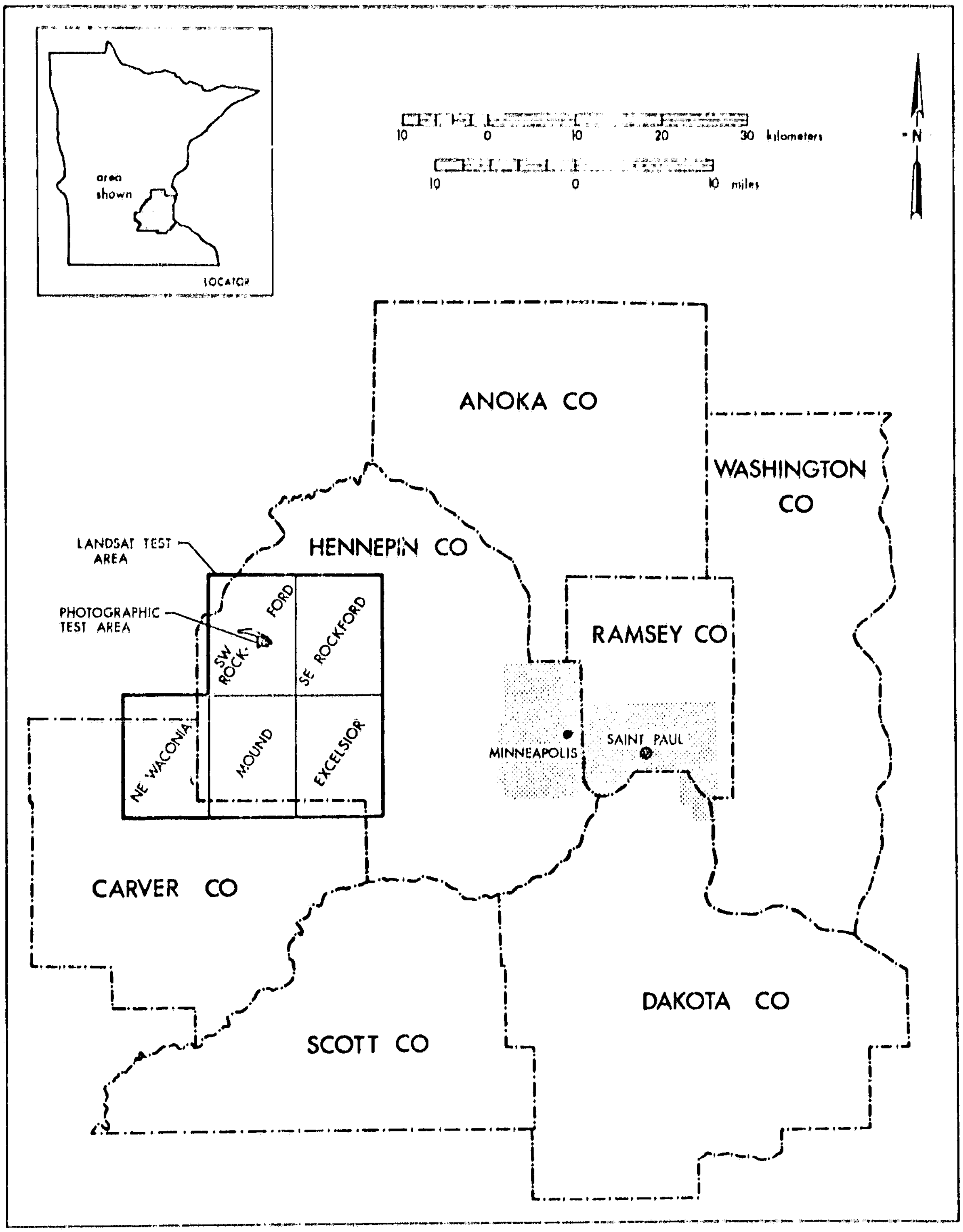

Figure 1. Study Site (located in the western part of Hennepin County, Minnesota).

complex, heterogeneous area of undulating glacial topography representatime of a transition zone between tall grass prairie and northern hardwood forest. The landscape is interspersed with small farms, villages, cities, subdivisions, parks and golf courses.

As the tests of tne various LANDSAT data analysis techniques were being applied to the 5 quadrangle test area, a parallel test of digitized color infrared photographic data was undertaken in a limited sub-area (see Figure 1). The digitized photographic data virtually removed the spatial resolution restrictions inherent in the LANDSAT data. These restrictions were found to be acute due to the spatial complexity of land cover in this area. In this way, the photographic analysis permitted a more basic test of the spectral characteristics and separability of the wetland types. This was deemed important for judging the potential applicability of Landsat data analysis procedures in areas which are less complex spatially than those in the Metropolitan study area. It also provided some insight into the potential advantages to be realized with the improved spatial resolution of the Thematic Mapper on LANDSAT-D. In addition, the photographic research permitted an initial investigation into the potential utility of using digitized color infrared photography per se as a data source for wetland mapping in spatially complex areas.

The methods and results of the LANDSAT test and the test of the digitized photography comprise, respectively, the next two sections of this report.

## LANDSAT DATA ANALYSIS

As previously indicated, both single-date and double-date LANDSAT data sets were analyzed in this study. Both data sets were processed at the Purdue University Laboratory for Applications of Remote Sensing (LARS). The single-date analysis was performed on data acquired on July 6, 1976. A coarse geometric correction (i.e., not using ground control points) was applied to this data set. The correction resulted in an average pixel positioning error of approximately 2 pixels N-S and 4.5 pixels E-W when image data were compared to a 1:24,000 map base. This correction uses a transformation model based on nominal satellite parameters and the geographic position of the test site, to rescale, deskew and rotate the original data. Following the geometric correction, classification was performed using the LARS hybrid multi-block cluster classification procedure (Hoffer and Fleming, 1978). This procedure entails selecting blocks of training areas containing heterogeneous cover types, clustering these blocks individually (unsupervised), identifying the informational identity of cluster classes, pooling training statistics from similar classes in various blocks, and using these statistics to perform a maximum likelihood classification of the entire area of interest. Following this procedure, thirty-five spectral classes were extracted from the single-date data to represent the following information classes: Non-wetland, Forest, Shrub, Emergent, Submergent and Water. Overall classification accuracy as measured from 2555 randomly selected pixels of verified identity was 72%. (That is, the total number of pixels classified correctly, ÷ 2555 = 0.72). However, the individual classes had highly variable classification accuracies. For example, 96% of the Water test pixels were classified correctly, whereas only 10% of pixels known to be of the Shrub class were classified correctly. The average of all of the class accuracies was 41%, which was deemed inadequate for the application at hand.

The generally poor classification performance and geometric correction results of the single-date analysis were improved upon in the double-date analysis process. First, application of the LARS geometric correction, using ground control points, resulted in average additional pixel positional corrections of approximately 0.5 pixels N-S and 0.75 pixels E-W. The geometrically corrected data for two dates were registered and the multi-block cluster technique was used for classification. (In this case the July 5, 1976 data were merged with those of August 7, 1975). The LARSYS feature selection process was employed to judge which of the eight available bands of data was optimum for subsequent classification. Using this process, bands 5 and 6 from both dates were deemed best suited for the classification. Given the poor performance of the Shrub class in the single-date analysis, this class was eliminated from the double-date classification. Also, it was hypothesized that separation between the Non-wetland class (basically corn) and Emergents (cattail) would improve with the introduction of the August data, since the corn had tasseled by this date.

The test field accuracy of the double-date classification was evaluated in a manner similar to the single-date effort. This involved evaluation of some 450 randomly selected test fields that varied in size from one to nine homogeneous pixels. The cover type present in each field was verified by ground site visits. Table 1 summarizes the results of comparing the LANDSAT and ground data. As can be seen from Table 1, the

Table 1. Test Field Accuracy Assessment of Double-Date LANDSAT Classification†

| Known Cover Types | | % Classified As Indicated Cover Type | | | |
|---|---|---|---|---|---|
| Cover Type | No. of Test Pixels | Non-wetland | Forest | Emergent | Water |
| Nonwetland | 1,706 | 75 | 8 | 17 | |
| Forest | 120 | 34 | 56 | 10 | |
| Emergent | 121 | 33 | 30 | 35 | 2 |
| Water | 523 | | | 2 | 98 |

Overall Classification Accuracy: 77%

Average Accuracy Per Class: 66%

---

†A detailed discussion of the classification and mapping accuracy of the single and double-date LANDSAT analyses is given in Werth (1980).

overall classification accuracy for the double-date analysis was 77%. The accuracy for the various information classes ranged from a low of 35% for the Emergent class to 98% for Water. The per class average accuracy was 66%. The comparative levels of errors of omission and commission for each class are also shown in Table 1.

In short, the two-date results indicated an increase in overall classification accuracy of approximately 5% (from 72 to 77%) and an improvement in per class classification accuracy of about 25% (from 41 to 66%). Additional classification accuracy appears to be precluded by the spatial and spectral resolution limits of the LANDSAT MSS relative to the complexity of the study area. This is not to say that LANDSAT has limited application to wetland mapping in general. Rather, we have simply concluded that one should expect poor success in single-date analyses and only moderate success in double-date analyses of wetland areas which are as complex as those in our study area.

## ANALYSIS OF DIGITIZED PHOTOGRAPHY

As mentioned previously, digitized color infrared aerial photography was also analyzed in this study as an extension of the LANDSAT analysis effort. Again, this source of digital data virtually removes the spatial resolution restrictions limiting the LANDSAT automated classification process, thereby permitting more thorough study of the spectral properties of the wetland cover types under investigation. Constraints of time and funding limited the photographic analysis to coverage of a single study site located within the LANDSAT test area (Figure 1). This site contains a number of small wetland areas which generally characterize those of the surrounding region.

Figure 2a is a (1.7x) enlargement of the original 70mm position transparency used in the photographic analysis. The original image was a 1:50,000 photograph (Kodak type 2443) taken with a Hasselblad 500 EL (f=50mm) camera on July 21, 1977, in support of previous wetland research efforts conducted by the Remote Sensing Laboratory. The image was digitized using a modified P-1700 Optronics drum scanner made available by the University of Wisconsin Environmental Monitoring and Data Acquisition Group (UW/EMDAG). Density readings from 0-3D were digitized into 256 levels and recorded on computer compatible tape. Broad band separation filters were used to obtain the approximate image density record for each of the three film layers. A measurement spot size of 50μm was employed, so that each pixel represented a ground area approximately 2.5m square. The spectral and spatial quality of the resulting digital data can be seen in the color rendering of the digitized data shown in Figure 2b. This figure was generated with the University of Minnesota D-47 Dicomed Color Image Recorder. The digital data from each image band were contrast enhanced by a histogram equilization algorithm prior to being recorded. This algorithm alters the distribution of original image values so that each display level comprises approximately an equal area portion of the display image in each band of data. Figure 2b represents a digitally generated color composite of the three original bands enhanced in this manner.

The photographic analysis effort took on two forms: 1) a <u>full-scene classification</u>, the intent of which was to classify <u>all</u> pixels and cover types present in the scene, and 2) a <u>sub-scene classification</u>,

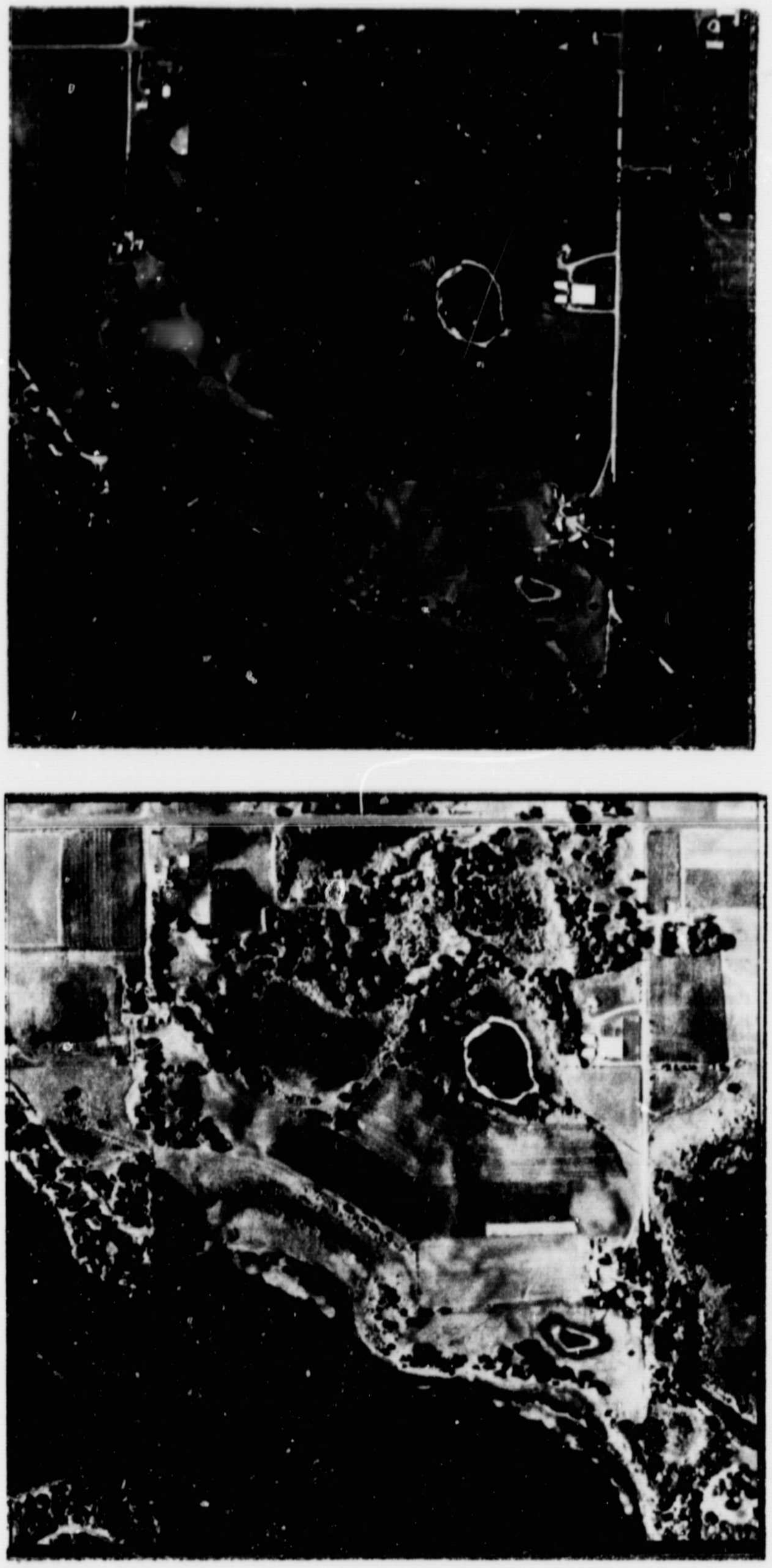

Figure 2. Original color infrared aerial photograph of test area (a) and film recorder output of digital microdensitometer data (b).

to classify wetland areas and cover types only. In both cases, a supervised classification approach was employed using the "Eppler Optimization" form of the maximum likelihood classifier that is integrated into the University of Minnesota Image Processing Software (UMIPS). A description of the two classification procedures follows.

Full-Scene Classification

Training for the photographic classifications was accomplished by photo-interpreting training areas on prints produced from the enhanced Dicomed image. The boundary of each training area was then digitized in terms of x and y image coordinates. In turn, these coordinates were converted to column and row addresses in the scanning microdensitometer data using a polynomial two-dimensional coordinate transformation. This transformation took the form

$$\text{column no.} = a_1 + a_2 x + a_3 y + a_5 x^2 + a_6 y^2$$

$$\text{row no.} = a_7 + a_8 x + a_9 y + a_{10} xy + a_{11} x^2 + a_{12} y^2$$

A least squares observation equation solution for coefficients $a_1$, $a_2 \ldots a_{12}$ was performed by measuring both the image and line printer output coordinates of readily identifiable ground control points in the scene. Using 10 points for this purpose, the root mean square error (rms) of the transformation was found to be 0.89 pixels in the x and 0.74 pixels in the y image direction.

Training statistics were developed for the 13 major cover types appearing in the scene: Water, Duckweed (Lemna minor), Water Lily (Nymphaea spp.- Nuphar spp.), Cattail (Typha spp.), Reed Canary Grass (Phalaris arundinacea), Willow (Salix spp.), Forest, Cropland, Pasture, Bare

Soil, Road, Roof, and Shadow. Multiple spectral classes (25) were derived from 35 training areas to adequately train for the 13 cover types.

Table 2 is a confusion matrix indicating the training field classification accuracy obtained in the full-scene analysis. Note that for some types the accuracy of classificaion in the training areas was excellent (e.g., Pasture = 97%). Other types, most notably Willow, were very poorly classified (25%). Figure 3 is a color-coded Dicomed image showing the results of applying the full-scene classification. As can be seen from both Table 2 and Figure 3, similar to the case with the LANDSAT data, many of the cover types present in the scene could not be spectrally separated. However, of particular note is the fact that virtually all wetland types were mutually separable. That is, errors of omission and commission in each wetland type were primarily attributable to the spectral confusion between wetland and non-wetland cover types, rather than between wetland cover types themselves.

## Sub-Scene Classification

Because of the spectral confusion between the wetland and non-wetland cover types, it was hypothesized that if the training and classification procedures were limited to wetland areas only, the classification accuracy would improve greatly. Hence, the training process was repeated in wetland areas only, using the following classes: Duckweed, Water, Water Lily, Cattail, Reed Canary Grass, and Willow. The boundaries of the wetland areas were delineated again using conventional image interpretation. This process requires much less labor than discriminating all cover type boundaries occurring within the wetlands. The purpose here was simply to separate wetland and non-wetland image areas. Spectral pattern

Table 2. Classification Performance for Training Fields Used in Full-Scene Analysis

| Known Cover Type | | % Classified As Indicated Cover Type | | | | | | | | | | | | |
|---|---|---|---|---|---|---|---|---|---|---|---|---|---|---|
| Cover Type | No. of Train. Pixels | Duckweed | Water | Water Lily | Cattail | Reed Canary | Willow | Forest | Cropland | Pasture | Bare Soil | Road | Roof | Shadow |
| Duckweed | 67 | 87 | | 2 | | | | | 4 | | 1 | 6 | | |
| Water | 1,700 | | 81 | | | | | | | | 1 | | | 18 |
| Water Lily | 240 | | | 89 | | | | | 10 | 1 | | | | |
| Cattail | 119 | | | | 91 | | 9 | | | | | | | |
| Reed Canary | 664 | | | | | 74 | | 10 | 16 | | | | | |
| Willow | 255 | | | | 17 | 3 | 25 | | 55 | | | | | |
| Forest | 48 | | | 2 | | 4 | | 73 | 17 | 4 | | | | |
| Cropland | 3,392 | | | 4 | | 2 | 6 | 1 | 86 | | 1 | | | |
| Pasture | 815 | | | 1 | | | | | 2 | 97 | | | | |
| Bare Soil | 232 | 7 | | | | | | | 11 | | 81 | 1 | | |
| Road | 400 | 2 | | | | | | | 1 | 3 | 1 | 93 | | |
| Roof | 56 | | | | | | | | | | | | 100 | |
| Shadow | 86 | | 7 | | | | | | | | | | | 93 |

Overall Classification Accuracy: 84%

Average Accuracy Per Class: 82%

Color Key

Duckweed - magenta

Water - blue

Water Lily - magenta

Cattail - orange

Reed Canary - red

Willow - yellow

Forest - black

Cropland - tan

Pasture - green

Bare Soil - brown

Road/Roof - white

Shadow - black

Figure 3. Full-scene classification of digital photographic data.

Table 3. Classification Performance for Training Fields Used in

| Known Cover Type | | % Classified As Indicated Cover Type | | | | | |
|---|---|---|---|---|---|---|---|
| Cover Type | No. of Train. Pixels | Duckweed | Water | Water Lily | Cattail | Reed Canary | Willow |
| Duckweed | 67 | 88 | | 4 | 8 | | |
| Water | 1,700 | | 100 | | | | |
| Water Lily | 240 | | | 100 | | | |
| Cattail | 119 | 1 | | | 89 | | 10 |
| Reed Canary | 664 | | | | | 97 | 3 |
| Willow | 255 | | | | 40 | 21 | 39 |

Overall Classification Accuracy: 94%

Average Accuracy Per Class: 85.5%

Table 4. Classification Performance in Eight Wetland Test Areas

| Known Cover Type | | % Classified As Indicated Cover Type | | | | |
|---|---|---|---|---|---|---|
| Cover Type | No. of Test Pixels | Duckweed | Water | Water Lily | Cattail | Reed Canary |
| Duckweed | 984 | 95 | | 3 | 2 | |
| Water | 6,173 | 2 | 97 | | | 1 |
| Water Lily | 2,240 | 11 | | 72 | 1 | 16 |
| Cattail | 13,586 | | | | 81 | 19 |
| Reed Canary | 9,920 | 1 | | 5 | 2 | 92 |

Overall Classification Accuracy: 87%

Average Accuracy Per Class: 87%

recognition was then used to provide the more subtle delineation of wetland species, a more time consuming process for the photo-interpreter. Table 3 indicates the classification accuracy obtained in the "wetland only" training areas. Note the improvement in training field classification accuracy which results when non-wetland classes are eliminated from the analysis. Figure 4 shows the results of the sub-scene classification. As can be seen from Table 3 and Figure 4 the Willow type introduced the largest errors in the sub-scene classification.

As a final classification effort, the Willow type was dropped and the resulting statistics were again applied to the "wetland only" subset (with predominantly willow areas excluded) of the original image. The accuracy of this classification was evaluated in eight test areas located in the scene. The result of the classification in these areas is shown in Figure 5. The classification accuracy in each of the eight test areas was obtained by comparing the computer-derived classification to that obtained by photointerpretation. This was done for all pixels in the eight areas (approximately 33,000). In those cases where the photointerpretation was ambiguous, a field visit to the site was made to be certain of the correct identification of the cover type present.

The results of the pixel-by-pixel accuracy assessment are given in Table 4. Errors in the classification of Duckweed and Water are believed to be caused by edge effects, in which a given pixel actually overlays two cover types near a boundary between the two types. To some extent, this effect enters into the accuracy problems for Water Lily as well. It is felt that the classification accuracy of the Water Lily and Reed Canary classes could be improved somewhat with additional training. Most of the Water Lily/Reed Canary confusion occurred in an

Color Key

Duckweed - magenta

Water - blue

Water Lily - magenta

Cattail - orange

Reed Canary - red

Willow - yellow

Figure 4. Sub-scene classification of photgraphic data in wetland areas only.

Color Key

Duckweed - magenta

Water - blue

Water Lily - magenta

Cattail - orange

Reed Canary - red

Figure 5. Sub-scene classification excluding the Willow cover type.

area of the scene which was not used for training. The errors in classification of Cattail are believed to be due to the presence of mixed Cattail/Willow in many areas. A sparse scattering of Willow occurred in many areas of both the Cattail and the Reed Canary cover types. Wherever present, Willow tended to cause misclassification due to the highly variable spectral characteristics of this cover type. These difficulties may be resolvable by the inclusion of a "texture" variable in future analysis procedures.

## CONCLUSIONS

Based on the results of this investigation, the following general conclusions have been reached:

1. If, within the accuracy levels it is capable of providing, LANDSAT data are judged to be acceptable for wetlands classification, a precision geometric correction should be applied and multi-date data sets should be used. In this study a 25% improvement in average classification accuracy was realized by processing double-date vs. single-date data (from 41% to 66%). Under the spectrally and spatially complex site conditions characterizing the geographical area used in this study, further improvement in wetland classification accuracy is apparently precluded by the spectral and spatial resolution restrictions of the LANDSAT MSS.
2. Full-scene analysis of scanning densitometer data extracted from small scale color infrared photography failed to permit discrimination of many wetland and non-wetland cover types. This was due essentially to the same spectral confusion between cover types that

was realized in the LANDSAT analysis. When classification of photographic data was limited to wetland areas only, much more detailed and accurate classification could be made. The final subset classification made in this study yielded an average classification accuracy of 87% with a 2.5m spatial resolution.

3. The integration of conventional image interpretation (to simply delineate wetland boundaries) and machine-assisted classification (to discriminate among cover types present within the wetland areas) appears to warrant further research. Though both the delineation of wetland boundaries and the development of valid training area statistics are labor-intensive tasks, the results from the combined approach appear to be much more accurate and economical than those obtained in conventional full-scene digital analysis. Additional research is needed to study the feasibility and cost of extending this methodology over a large area using LANDSAT and/or small scale photography.

## ACKNOWLEDGEMENTS

The LANDSAT data analysis performed in this study represents partial fulfillment, by Lee F. Werth, of the requirements for the Ph. D. degree at the University of Minnesota. Many aspects of this study were supported directly or indirectly by funding from the University of Minnesota College of Forestry and Agricultural Experiment Station (Proj. MIN-42-003 and 037). The cooperation of the Purdue University Laboratory for Applications of Remote Sensing (LARS) in the LANDSAT analysis is recognized, as is that of the University of Wisconsin Environmental

Monitoring and Data Acquisition Group (EMDAG) in the photographic analysis. Douglas E. Meisner developed the University of Minnesota Image Processing Software used in the photographic analysis and Mark Columbo, Carl Markon, John Minor and Mark A. Springan assisted in the LANDSAT accuracy assessment. William L. Johnson and Katherine A. Knutson assisted in the production of this report. Finally, the University of Minnesota Space Science Center is acknowledged for administering the NASA Grant funding this research.

## LITERATURE CITED

Cowardin, L. M., V. Carter, F. C. Golet, and E. T. LaRoe, 1977. Classification of Wetlands and Deep-Water Habitats of the United States (an operational draft). USDI Fish and Wildlife Services. 100pp.

Hoffer, R. M. and M. D. Fleming, 1978. Mapping Vegetation Cover by Computer-Aided Analysis of Satellite Data, LARS Technical Report 011178. 12pp.

Owens, T. and M. Meyer, 1978. A Wetlands Survey of the Twin Cities 7-County Metropolitan Area - East Half. IAFHE RSL Res. Report 78-2, St. Paul, MN. 19pp.

Werth, L. 1980. A Comparison of Remote Sensing Technique Applications to Wetland Classification in Minnesota's 7-County Metropolitan Area, Ph. D. Dissertation, University of Minnesota, (in preparation).

Werth, L., M. Meyer and K. Brooks, 1977. A Wetlands Survey of the Twin Cities 7-County Metropolitan Area - West Half. IAFHE RSL Res. Report 77-10, St. Paul, MN. 18pp.

N81-12507

# SECTION B

# DEVELOPMENT OF ALTERNATIVE DATA ANALYSIS TECHNIQUES FOR IMPROVING THE ACCURACY AND SPECIFICITY OF NATURAL RESOURCE INVENTORIES MADE WITH DIGITAL REMOTE SENSING DATA

(Progress Report)

(July 1, 1979 - December 31, 1979)

Dr. T. M. Lillesand and Douglas E. Meisner
Remote Sensing Laboratory
Institute of Agriculture
University of Minnesota
St. Paul, Minnesota

INDEX

30

# DEVELOPMENT OF ALTERNATIVE DATA ANALYSIS TECHNIQUES FOR IMPROVING THE ACCURACY AND SPECIFICITY OF NATURAL RESOURCE INVENTORIES MADE WITH DIGITAL REMOTE SENSING DATA

Investigators: Dr. Thomas M. Lillesand
Douglas E. Meisner
Remote Sensing Laboratory
Institute of Agriculture
University of Minnesota
St. Paul, Minnesota

## INTRODUCTION

General application of digital remote sensing technology has gone through considerable change in the recent past. In spite of growing user interest in applications of digital classification for thematic mapping, the private sector has shifted its focus somewhat away from this activity. Attention is being concentrated more on hardware development and provision of digital image enhancement services, rather than on classification per se. This shift is partly due to the increasing sophistication of end users as the "gee whiz" allure of the technology wears off, a smaller core of more serious users is emerging. This is a healthy development. Another reason for the shift, however, is the difficulty and cost inherent in performing digital classification services in a non-research environment. The need for active involvement of field personnel, coupled with the problems of training those personnel in the generally complex procedures, has frustrated many analysis efforts. At the same time, as accessible as remote job entry terminals have become, line printer output simply does not afford the graphic interaction required for most sophisticated classification procedures. In this context, one can understand the shift toward image enhancement procedures; these activities are greatly simplified by the clear and convenient separation of digital processing efforts from subsequent field analysis. Yet, as training courses (e.g. at the three NASA regional centers and at the EROS Data Center) continue to nurture interest in the use of digital classification techniques, the need for serving those users will increase. This is particularly critical as applications spread to the state and regional level, since these users are less able to obtain specialized equipment in-house.

The work begun under this grant is an investigation into the ways to improve the involvement of state and local user personnel in the digital image analysis process. The intent is to isolate those elements of the analysis process which require extensive involvement by field personnel and to provide means for performing those activities apart from a computer facility. In this way, the analysis procedure can be converted from a centralized activity focused on a computer facility to a distributed activity in which users can interact with the data at the field office level (or indeed in the field itself). This concept is illustrated in Figure 1. If successfully implemented, the distributed approach would offer these advantages:

1. Provide more efficient use of computer resources, by reducing the digital image processing effort to a highly standardized procedure which can be run in a batch mode.
2. Provide more economical use of field personnel, by eliminating the expense of transporting them to the analysis facility and lodging them while there. "Day to day" work could then be handled while

A second preliminary analysis involved forest typing with LANDSAT data on a College of Forestry test site for which detailed ground data and high altitude color infrared photography were available. In this case, training sets were delineated on high altitude photography and digitally transformed into LANDSAT scene coordinates. Unfortunately, the second order least squares polynominal fit used in the transformation was inadequate for relating the photographic base to the LANDSAT data. Due to the spatial complexity of the study area, even the slight displacements resulting from the transformation process affected the training statistics excessively. An interesting sidelight was the fact that the RMS errors computed in the polynomial fitting process were very low, suggesting a higher accuracy than was actually realized on a training area by area basis.

Subsequently, the training process was performed by visually relating the high altitude images and the hard copy LANDSAT enlargement in a Zoom Transfer Scope. This approach enabled features in the LANDSAT enlargement to be identified with much more certainty and led to successful training. This process was found to be impossible using line printer output.

3. Procurement of digital display equipment. In-house funds have been used to acquire a stand-alone microcomputer-based image display system which will be used on this project. Installation of this equipment was completed in November. The system consists of a Spatial Data Eye-Com video digitizer and display, a DEC LSI-11 microcomputer with Fortran compiler, a DeAnza Visacom color display system, color

vs. Dicomed output, log vs. linear recording, various contrast stretch techniques, and different film and print paper types.

The use of film recorder images as a base for supervised training was tested in several pilot studies. This began with several student projects in which the color data were used for visual analysis but actual training set delineation was performed on line printer image output. The availability of the color data for interpretation of spectral characteristics enhanced the analysis process greatly, but the training set delineation was still a cumbersome task.

Two other preliminary analyses have been performed. The first involved classification of wetland types on a photograph which had been digitized using a scanning densitometer.[1] Training sites were located on the color image base and digitally transformed (using a polynomial transformation model) into scene coordinates. Because the encoding was done by hand, the process was still cumbersome. However, this was seen as a simulation of a coordinate digitizer-based procedure to be developed in the near future.

The polygon processing software was also used in this study to mask the image data set, in order to restrict the classification to selected sub-scenes (in this case, wetland areas). This permitted successful classification of within-wetland species, a task which had been previously impossible because of spectral confusion between some wetland and non-wetland classes.

---

See Section A of this report.

## PROGRESS TO DATE

In the past six months of work on this project, the following four general areas of activity have been pursued:

1. Development of general image processing software on the University of Minnesota computer system (Control Data Cyber models 172 and 74). This software enables us to read CCT's in several formats, including the old and new LANDSAT tape formats, scanning microdensitometer tapes obtained from the University of Wisconsin, and tapes generated by the Data Analysis Laboratory of the EROS Data Center. Programs to support supervised training and optimized maximum likelihood classification have been written and used in this and other research projects. Interfaces to the U of M Dicomed color image recorder have been developed, both to display contrast enhanced original image data and to record classification output results.
2. Initial investigation into the use of color hardcopy image data as a primary medium in supervised training procedures. The procedure we employ is to generate digitally enlarged and contrast enhanced hard copy color prints of image data within study areas. These prints are then used to analyze visually (rather than statistically) the spectral properties of the data before supervised training sites are selected on the hard copy print. This technique of supervised training on hard copy images is perceived as a "first look" at a distributed analysis approach.

   The investigation began with a basic examination of image recording techniques, including comparisons of video displays working on the classification project. State employees in Minnesota have stressed the importance of this point. By making agency involvement more economical in various ways, a larger number of personnel may participate for longer periods of time.

3. Reduce the difficulties of working with untrained personnel by eliminating their direct involvement with a computer system and somewhat standardizing the analysis procedure they employ. This would remove the user's exposure to the computer operating system and the inevitable system downtime, which are generally frustrating to the new user.

4. Reduce the time pressure on the user frequently caused by the need to tightly schedule his or her time and to schedule the expensive interactive analysis equipment. Taking sufficient time to analyze computer output during the classification process is a critical element too frequently missed in digital analyses. In addition, the distributed approach would give the user the option of suspending the analysis if it is deemed necessary to revisit the field or obtain other reference data.

5. Eliminate the need to invest in specialized computer equipment, and to handle the staffing and maintenance requirements of such equipment.

Thus, our effort is oriented not towards developing new quantitative classification techniques, but rather toward finding ways to implement current techniques in a way better suited to non-research applications.

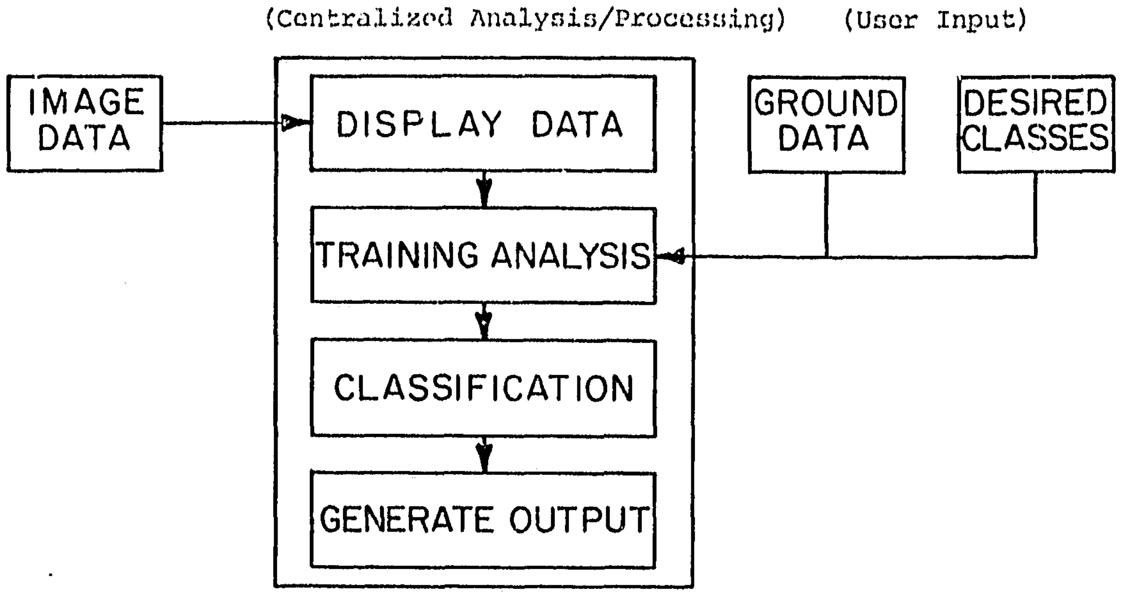

(a) Centralized Data Analysis Process.

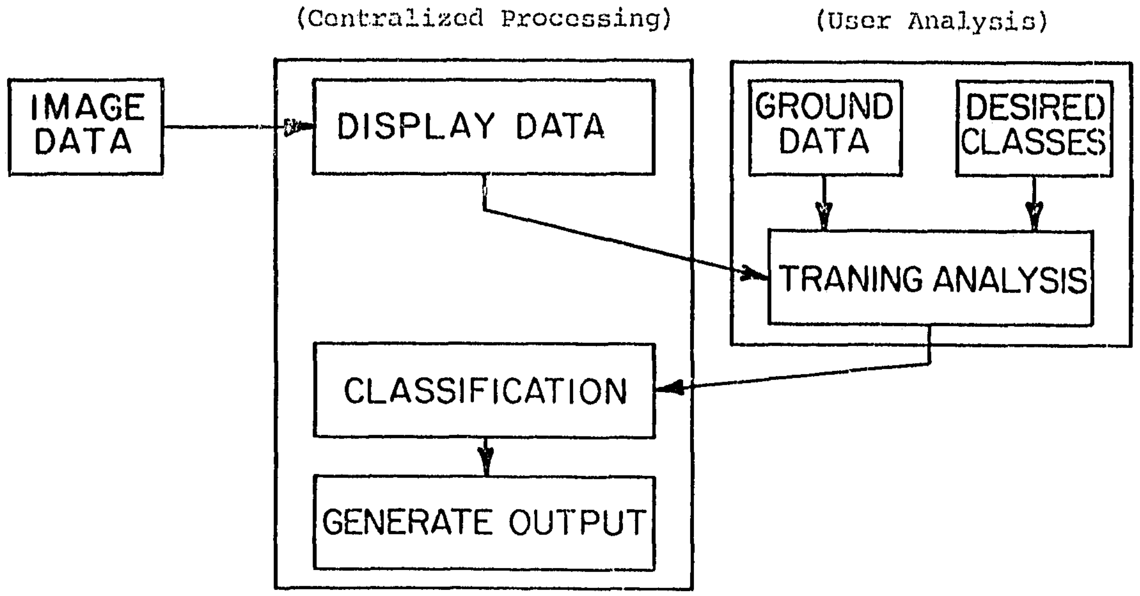

(b) Distributed Data Analysis Process

Figure 1. Comparison Between Centralized and Distributed Analysis Concepts.

monitor, and flexible disk drive. The system can communicate over a high speed phone link to the Universtiy computer system.

In addition to being used as a development tool for the hard-copy based analysis techniques, this equipment will be explored as an additional tool for decentralized data analyses where modest equipment investment is feasible. Microcomputer-based systems like the Visacom have considerable potential for enabling equipment to be more widely distributed, particularly as their cost continues to decline. We will evaluate the pros and cons of this approach as the research continues.

4. Procurement of coordinate digitizer. Again using in-house funds, a digitizing tablet has been obtained which will be connected to the microcomputer system. Software will be developed to enable supervised training site entry, interactive masking of image data to restrict classification to subscene areas, and test site entry for detailed accuracy assessment. The first and last of these activities are currently being explored using an IDIMS system in a cooperative project with the EROS Data Center. This work is described on page B9 report.

In addition to the progress described above, we have been fortunate in the past six months to have been involved in several Federal-State cooperative projects which have had input to this research. Agencies involved include:

1. NASA Eastern Regional Applications Center (ERRSAC). In the past year, ERRSAC began a program of remote sensing technology transfer to state and local governments. Minnesota was one of the first states

selected to be involved, and the Remote Sensing Laboratory has participated in the activities in a technical assistance role. This involvement has included giving a seminar on image processing to state employees, participating in a week-long training course at Goddard, and attending a conference organized by ERRSAC. The ERRSAC training course and conference have provided attitional exposure to the problems involved in training new users. They have further confirmed the potential utility of a decentralized approach to digital classification.

2. Earth Resources Laboratory, NASA Space Technology Laboratory. As an outgrowth of the ERRSAC activity, we have provided consultation to the Land Management Information Center of the Minnesota State Planning Agency. This group has operated a digital geo-based resource information system for the state for ten years. They have recently obtained funds to purchase specialized computer hardware to further support and enhance that activity. Part of that equipment will be for remote sensing image processing, on which we have provided technical advice. As part of that activity, a trip was arranged for a demonstration of the ELAS image analysis system at ERL in Mississippi. This demonstration provided an interesting comparison to the IDIMS system used at Goddard. In particular, the effective use of an unsupervised classification technique was impressive. Applications staff at ERL reported almost exclusive use of this classification technique. We hope to integrate such an option in our decentralized processing approach.

3. Data Analysis Laboratory, EROS Data Center. We are currently participating in a cooperative project with EROS and Minnesota State

Planning. The project is intended to investigate the incorporation of LANDSAT-derived data into the statewide land information system. A wide range of analysis techniques was proposed, and we were able to expand this to include the techniques which we have been exploring under this grant, particularly the use of a coordinate digitizer to enter supervised training set polygons and test areas for accuracy assessment. Subsequent computer work will be performed on the IDIMS image processing system at EROS. This should prove very advantageous to us, since it will permit the various analysis strategies to be tested without the time consuming task of software development. The results of the comparisons will then allow us to concentrate our future efforts on those techniques which look most promising.

The demonstration project is being performed on a study site located north of the city of St. Paul. The area under analysis covers part of four 7.5 minute quadrangles containing a range of urban fringe land uses, from medium density suburban residential to large scale agricultural. Image data for the area have been extracted from an April, 1979, Landsat 3 scene. The system corrections to this image by the new NASA Master Data Processing Facility include a geometric resampling to the Hotine Mercator Projection. The data analysis and processing techniques which are being compared in the study are:

Training techniques:

a. Supervised training using CRT display and joystick to enter polygons

b. Supervised training using color hard copy and a digitized tablet to enter polygons

c. Unsupervised classification

d. Supervised training using digital land cover data currently in the Minnesota Land Management Information System.

Classification techniques

a. Minimum distance to mean

b. Maximum likelihood with threshold

c. Canonical transformation with minimum distance to mean

d. Post-classification smoothing algorithms

Geometric correction techniques

a. Use of NASA corrected data resampled to Hotine Mercator Projection

b. Resampling to convert from Hotine to UTM projection prior to classification

c. Same as (b) but resampled after classification

Data resulting from combinations of the above techniques will be compared to a photo-interpreted reference data set prepared by the Remote Sensing Lab. The reference data consist of six randomly selected photographs covering approximately one quarter of the study area. The interpreted reference data are being geocoded at EROS to enable automatic, full pixel comparisons to the test data sets.

Currently, about half of the above work has been completed.

## FUTURE ACTIVITIES

Assuming continued funding under this program, the following areas will be pursued in the coming year:

1. Basic software development on the microcomputer/display system. This will involve programs to transfer data from the University Computer Center, provide optimized disk data storage, and display the data. Down-loading of image processing programs will be attempted. Interface software will be developed to operate the digitizer tablet.
2. Completion of the EROS cooperative project. As has been mentioned, these results will be used to define the direction of our development efforts. At present, it appears likely that this will involve additional attention to unsupervised analysis.
3. Implementation of software based on the results in (2) but designed for decentralized operation.
4. Sample projects to test the decentralized approach using field personnel with limited digital image analysis background. Several prospects for sample projects are available within Minnesota, but attempts will be made to arrange additional demonstrations through NASA ERRSAC and/or EROS.

We feel that the activities of the past six months have put us in a good position to develop the proposed alternative analysis approach. Our involvement with the technology transfer groups at NASA and EROS have further emphasized the needs which formed the basis for our proposal last year. In addition, these contacts should improve our ability to publicize and acquire feedback on the alternative techniques we develop. The exposure to analysis systems at NASA ERRSAC and ERL and the hands-on experience at EROS have brought us up to date on the state of the art. This is critical to avoid "reinventing the wheel." Finally, the availability of the microcomputer and color display system will permit the investigation of a potentially important alternative approach to decentralized analysis.

In short, we feel we are making substantial progress toward defining the technological components of an alternative approach to digital classification which will improve the accuracy and specificity of natural resource inventories made with digital image data. During the next year we will begin testing this system in the "real world".

N81-12508

# SECTION C

# SYNERGISTIC RELATIONSHIPS AMONG REMOTE-SENSING AND GEOPHYSICAL MEDIA: GEOLOGICAL AND HYDROLOGICAL APPLICATIONS

Dr. Joseph E. Goebel
Dr. Matt Walton
Mr. Lawrence G. Batten
Minnesota Geological Survey

## INDEX

44

## C. SYNERGISTIC RELATIONSHIPS AMONG REMOTE-SENSING AND GEOPHYSICAL MEDIA:

## GEOLOGICAL AND HYDROLOGICAL APPLICATIONS

Investigators: Dr. Joseph E. Goebel
Dr. Matt Walton
Mr. Lawrence G. Batten
Minnesota Geological Survey

### STATUS OF REMOTE SENSING AT THE MINNESOTA GEOLOGICAL SURVEY, 1979

The Minnesota Geological Survey continues to expand the use of remote sensing to understand better and interpret the geology of Minnesota. Space imagery was employed in 1979 to identify and locate bedrock outcrops. A low-level, high-resolution aeromagnetic survey of the state, which began in the fall of 1979, will ultimately provide the best coverage of this sort in the country. Gravity mapping was completed in the St. Cloud and New Ulm sheets at a compilation scale of 1:250,000.

Geochemical methods of remote sensing employed during the past year entailed the measurement of radon in well water in three areas of the state, as well as measurement of gamma radiation taken manually on the ground.

### 1. Photo Interpretation of Surficial Quaternary Geology

Mapping the Quaternary geology proceeds in various parts of the state. Dr. Saul Aronow mapped the glacial deposits of Dakota County with the assistance of aerial photographs. Dr. Mary Savina used aerial photography to identify and delineate glaciofluvial deposits in Dakota County.

## 2. Statewide Aeromagnetic Survey

A low-altitude, high-density aeromagnetic survey of the entire state is a major new project for the Minnesota Geological Survey. The current stage involves acquisition of data over Cook, Lake, St. Louis, Carlton and Pine Counties with a 400-meter flight interval at an average terrain clearance of 150 meters. This work is being supervised by Dr. Val Chandler who is interpreting the results as they become available. As will be demonstrated later in this report, aeromagnetic data can be used successfully in combination with other remotely sensed data and traditional geological data sources to make geologic interpretations which none of these sources of data can achieve alone.

## 3. Radon Survey

In geochemical surveying, given elements may be found to vary in concentration in samples taken systematically over a selected region. When variations in radon activity in ground water are plotted geographically, as contour maps, the resulting image may reveal environmental influences on radon concentration in addition to primary variations in radion emissions from geologic sources. The interpretation of the image depends on consideration of bedrock type and structure, drift thickness, and hydrologic parameters. Richard Lively has demonstrated a relationship between contour maps of radon concentration, kinds of till, and bedrock structure.

### 4. Ground Survey of Gamma Radiation

A similar imaging technique has been applied to gamma radiation data taken by hand on the ground. This study was initially intended for locating uranium, but the resultant contour map of gamma radiation intensity shows a weak correlation with the distribution of tills and outwash and may separate some till units.

## PRESENT STUDY -- SYNERGISTIC RELATIONSHIPS BETWEEN REMOTE-SENSING MEDIA IN IDENTIFYING AREAS OF NEAR-SURFACE BEDROCK

### 1. Introduction

Although the original intention of this investigation was to locate specific areas in which bedrock is at or very near the surface, bedrock exposures vary too much in character and site, and most are too small to be identified individually by remote sensing. The best example of the problem is the extensive exposures along the Mississippi River which were an important part of this study. Although this bedrock is well exposed in vertical sections, it is covered with about 100 feet of glacial drift behind the river cut. Because all of the media collect data vertically, the outcrop itself is less than the resolution of most remote-sensing media. This investigation therefore reports the identification of areas where bedrock is near the surface and outcrops are likely to occur.

Synergism, as understood here, is the combination of two or more data sources to recognize a geologic characteristic which is not identifiable on any single image. This study was directed toward quantitative evaluation of the usefulness of the data sources and toward developing a procedure to use them for locating bedrock outcrop areas, rather than toward systematic mapping of outcrops.

## 2. Materials

The following sources of geological data were used in this study:

(1) Topographic maps, for elevation control and geomorphic information.

(2) The aeromagnetic map of Minnesota, at scale 1:1,000,000 as published by the U.S. Geological Survey.

(3) The Bouguer gravity map of Minnesota. Although the primary gravity anomaly sources are within the Precambrian bedrock, the gravity field may locally reflect changes in thickness of the surficial deposits.

(4) Skylab photographs. It was expected that the broad coverage would reveal local changes related to near-surface bedrock that would be more difficult to ascertain on aerial photographs. Also the Skylab photos were made with different filters which might enhance moisture content variations or other factors in areas of thin surficial cover. Skylab coverage included photographs in visual color, color infrared, visual black and white in the red and green range, and black and white infrared in the 0.7-0.8 μm range.

(5) Seven seasons of LANDSAT images, including all four MSS bands for a dry and a wet summer-spring-fall and one winter scene.

(6) Aerial photographs, for information on geomorphology.

(7) A contour map of regional thickness of unconsolidated sediments, supplemented by the Minnesota Geological Survey data base of water-well drillers' logs, was used to reduce the search area to the one-third of the state which has less than 100 feet of glacial drift.

(8) The set of maps of lineaments previously prepared for this study (Goebel and others, 1978). Glacial, fluvial and tectonic processes are responsible for many of the lineaments. We felt that outcrops would occur near these linear features.

(9) A map of glaciofluvial features. Because melt water eroded the soft new glacial drift, outcrops predominantly occur in glaciofluvial deposits.

(10) Side Looking Radar (SLAR) images, reviewed for indications of textural changes of the soils regardless of moisture content.

(11) Blue-line print orthophotos for 7.5-minute topographic quadrangles in Minnesota, at the quadrangle scale. Although the resolution and gray-scale change in density are not very good on these prints, their registration to the topographic sheets permits comparison of patterns on other imagery with topographic features, and allowed us to assure ourselves of feature locations on all remote-sensing media.

(12) Airborne gamma radiation maps. We expected that the outwash should at least be distinguishable from the till because of the differing mineral content in the two sediment types.

(13) The SMS-GOES imagery was considered because it recorded a different spectrum, but we could not locate cloud-free images of Minnesota without browsing through all of the images. No record is kept, that we could find, of cloud-free periods. Imagery from these satellites seems to be considered temporal and is used only for weather observation.

## 3. Methods

This study was organized to determine which of the remote-sensing media contributed most to the identification and location of areas with shallow bedrock, and to evaluate them quantitatively.

After all of the remote-sensing or imaging media over Minnesota were located and collected, eight sites were chosen which had all of the kinds of image coverage listed above. USGS 7.5-minute topographic maps were used for locating outcrops in the eight sites and for compiling the results of the study.

Four of the eight sites were designated as training sites. The other four sites (referred to hereafter as test sites) were retained to test the procedure developed in the study of the first four sites. All four training sites were first investigated in the field, and bedrock outcrops, near-surface topographic features and stream conditions were plotted on the USGS topographic maps. Two of the training sites had no outcrops, but the Twin Cities and St. Cloud sites had ample outcrops (see site maps in appendix). The rock outcrop locations were then transferred to a 1:250,000 and a 1:1,000,000 scale USGS topographic map to facilitate location of these features on the various remote-sensing imagery.

We then tabulated the responses of each of the remote-sensing media to areas of observed bedrock outcrop (areas where bedrock was within 12 feet of the land surface) to determine which media seemed to distinguish the bedrock areas. Next we determined correlations between media for outcrop areas. This was particularly important in sorting through all of the bands of LANDSAT used in this study.

The Bausch & Lomb Stereo Zoom Transferscope was used to transfer and locate features from different media and different scales onto the same scale. This transferscope also proved useful in transposing two different images onto each other.

We constructed our own densitometer using a sensitive light meter to register multiseasonal LANDSAT imagery to a base map. We did not have, nor could we find, a densitometer which met our specifications. This densitometer is not an exact instrument. Its only function was to select those images which seem to respond consistently in areas of outcrop.

The test sites were field checked after examination of the foregoing media had indicated specific sites to be checked.

We attempted to confirm near-surface (within 10 to 50 feet) bedrock with a portable power drill, but the drill was not successful, especially in saturated sands. Because no other drill was available, we checked the remaining areas to a depth of 20 feet with a hand auger.

## 4. Results

Near-surface bedrock areas as identified in this study were areas covered with less than 100 feet of glacial drift. Areas where the bedrock is less than 12 feet below the surface are defined for this study as outcrops. When appropriate remote-sensing data were used, bedrock was located about half of the time predicted.

The synergistic relationships among LANDSAT imagery, Skylab photographs, and aerial photographs were useful for establishing areas of near-surface bedrock. Lineaments were located on LANDSAT imagery and aerial photographs during 1978, and near-surface water tables will be located during 1980. Both of these subjects can be identified by remote-sensing methods more reliably than individual outcrops, which are small and occur in a wide variety of environments with a wide range of responses. Bedrock outcrops themselves could not be resolved by any of the data sources used, nor did any combination of data sources specifically identify rock at the ground surface. The data sources could not simply be combined mathemetically to produce a visual image of probable areas of near-surface bedrock. Outcrops and near-surface bedrock had to be verified visually at the site. Despite these drawbacks, the study resulted in a procedure for locating areas of near-surface bedrock within which actual surface outcrops may occur.

## Field Criteria Indicative of Near-surface Bedrock

1. Surface rock rubble on the shoulder of hills can cover either bedrock or till.

2. Bluffs, especially along major streams, are often the result of a bedrock resistant to erosion.

3. Trees are somewhat shorter and sparser, but surprisingly stouter, in areas of near-surface bedrock, and they appear darker on photographs. Juniper was observed in some areas where bedrock is less than 40 feet deep, but we made no attempt to validate this observation statistically.

4. Constrictions in the width of floodplains and steepened stream gradients may be caused by near-surface bedrock.

5. Swamps at elevations well above local streams or the regional water table may indicate bedrock control of the flow of the ground water. Constriction at swamp outlets and broad backwater flats indicate possible bedrock influence on surficial morphology.

## Sequence of Image Examination

Anomalies specifically related to areas of near-surface bedrock could not be identified in any of the data sources. A stepwise method of restricting the evidence of one source by the evidence of the next source was the most useful procedure for determining outcrop areas. The following procedure evolved in this study:

Step One: A map of the regional thickness of the unconsolidated surficial sediments was used to reduce the search area to the one-third of the state which is known to have less than 100 feet of cover.

Step Two: Broad regional imagery, such as Skylab photographs or leaf-off, early spring LANDSAT images, multispectral bands 4, 5 and 6 was studied to further distinguish candidate sites for near surface bedrock.

Step Three: Potential outcrop areas identified from step two were examined on the aeromagnetic map. We noted a correlation between spectrally-identified areas of potential outcrop and aeromagnetic anomaly levels (relative to arbitrary datum) of 11,000 to 11,500 gammas, but this relationship requires further study.

Step Four: Some statistical correspondence between gravity values within the range of -30 to + 35 milligals and bedrock outcrop areas was observed, but half of the state is within this range. Areas within these limits were considered only if the conditions in the first three stages had been met.

Step Five: After large areas of potential outcrop have been identified, more site-specific methods can be used. Conventional aerial photography is especially useful at this stage. Numerous criteria for outcrop recognition on aerial photographs have been developed over the last 5 years (Cooper, 1978; in press), and these were applied to photographs of the test sites.

Step Six: The areas selected on the basis of the previous steps were located on 7.5-minute topographic maps. Areas less than 50 feet above the elevation of the nearest stream and within 2,500 feet of it were searched for.

Step Seven: The final step was to verify the outcrop on the land.

## Comments and Recommendations on Image Types

Of the methods employed in this study, LANDSAT images were analyzed the most thoroughly. We had four MSS bands with seven scenes for each scene center. These seven scenes included a wet and dry spring, a wet and dry summer, a wet and dry fall and a winter image. Of the 28 possible combinations of MSS bands, the bands which had the most uniform intensity of response, as measured on the photographic negatives, and also as deduced from comparing two different scene centers, were:

A dry spring - bands 4, 5 and 6
A wet spring - bands 4 and 5
A dry summer - band 4

Combinations of two or three of the above were best for identifying areas of probable outcrops.

An objective of this study was to establish a method for selecting other bands as possible sources of information about bedrock outcrops. It will require another phase of investigation to acquire these CCT's, develop the training sets, and then predict all of the outcrop areas in each scene.

The areas of shallow bedrock appeared very dark on radar (SLAR) images, as they did on aerial photographs, but because the detail and resolution were better on the aerial photographs we did not pursue the radar imagery as an indication of bedrock outcrop. Skylab photos, visual and infrared, color and black and white, also showed shallow bedrock as very dark or intense colors.

The map of natural gamma radiation intensities, which vary according to surficial conditions, indicated the location of sand, gravel and organic material, but the resolution was not sufficient to identify bedrock near the surface. There was radioactivity coverage over only the study training areas so we could not project this information on the test areas. With better resolution, and with actual flight-line data if they were available, natural gamma radiation data possibly would be a useful indicator of surface or near-surface bedrock.

When aeromagnetic data with higher resolution are available, it will be useful to investigate areas characterized by concurrence of magnetic anomalies and topographic lineaments, and by localized, sharp magnetic anomalies with high gradients and intensity values. This was not practical with the resolution of the available map.

The new, more detailed gravity map now partly completed for Minnesota will be potentially more useful in future studies. The gravity anomaly characteristics at known outcrops for an area would be useful criteria in evaluating gravity data for other areas of possible outcrops.

## Relations of Outcrop to Lineaments, Drainage, and Elevation

We looked at lineaments interpreted from many sources (see Goebel and others, 1978) and counted the number of outcrops located within 1 mile and within 2 miles of a lineament. We found that of the lineaments, those interpreted from winter LANDSAT imagery occurred most frequently near outcrops. Although there were many lineaments in the two training areas that had outcrops, there were few in the test areas. Therefore, we could not assess the usefulness of lineaments in predicting outcrops. It would be advisable to review the lineaments in application of this study to other areas.

We tested the hypothesis that bedrock outcrop elevations should be near the base levels of the closest streams, and that they should be fairly close to the nearest stream beds. Topographic maps provided information on elevations above sea level. Two-thirds of the outcrops in the St. Cloud site have elevations less than 50 feet above the elevation of the nearest stream and two-thirds of the outcrops in the Twin Cities site are within 124 feet of nearest-stream elevations.

It was further determined that outcrop is likely to be higher in elevation the farther it occurs from the stream. Most outcrops located were at distances between 1,400 and 5,000 feet from streams, although we found outcrops in streambeds and as far as 8,000 feet away. Except where other evidence is available, it would be useful to concentrate the search in areas less than 50 feet higher than a streambed but no farther than 2,500 feet, or at most 5,000 feet from a stream.

Outcrops occurred dominantly in or very near glaciofluvial and alluvial areas shown on Quaternary Geologic Map of Minnesota. Glaciofluvial excavation of bedrock is consistent with the relationship between stream erosion and outcrops.

## CONCLUSIONS

Systematic application of procedures developed in this study can narrow the search area to reasonable limits, and can help define areas where bedrock is near the surface. Some media should be further investigated to understand their contribution to recognizing outcrop areas. More specific attention could be given to quantifying the usefulness and constraints of the recommended procedure for locating bedrock near the surface.

Table 1. Mean and standard deviation of the response values derived for selected remote-sensing media used in this study.

| Remote-sensing Medium | Twin Cities | | St Cloud | |
|---|---|---|---|---|
| | M | SD | M | SD |
| Aeromagnetic map (in gammas mag. rad.) | 11,300 | 246 | 11,200 | 180 |
| Bouguer gravity map (in milligals) | 3 | 33 | -16 | 3 |
| Aerial photos (light to dark scale 1-5) | 4.5 | 2.1 | 4.4 | .9 |
| Thickness unconsolidated sediments (ft.) | 94 | 54 | 53 | 36 |
| Bedrock outcrop elevation (feet) | 852 | 86 | 1,072 | 42 |
| Streambed elevation (feet) | 759 | 29 | 1,038 | 35 |
| Distance from outcrop to streambed (ft.) | 5,180 | 7,800 | 1,421 | 1,484 |
| SLAR radar (light to dark scale 1-5) | 4.7 | .5 | 4.6 | .6 |
| Natural gamma radiation (counts/second) | 2.9 | 32.8 | -15.7 | 2.5 |

| | Twin Cities | St. Cloud |
|---|---|---|
| Percentage of outcrops occurring in fluvial deposits | 79 | 77 |

Table 2. Mean and standard deviation for the density values recorded for outcrops in the training sites on LANDSAT Imagery. (Measured on photographic negatives, low numbers are greater film densities.)

| | Band 4 | | Band 5 | | Band 6 | | Band 7 | |
|---|---|---|---|---|---|---|---|---|
| Site and Season | M | SD | M | SD | M | SD | M | SD |
| Winter | | | | | | | | |
| Twin Cities | 2.7 | 1.0 | 2.1 | .8 | 2.1 | .9 | 3.0 | 1.4 |
| St. Cloud | .8 | .2 | .7 | .1 | .7 | .1 | .9 | .2 |
| Wet Spring | | | | | | | | |
| Twin Cities | 3.9 | .6 | 4.5 | 1.0 | 4.4 | 1.4 | 4.9 | 1.8 |
| St. Cloud | 3.2 | .2 | 3.8 | .3 | 3.1 | 1.4 | 3.3 | .5 |
| Dry Spring | | | | | | | | |
| Twin Cities | 7.0 | 1.0 | 5.5 | .1 | 5.1 | .8 | 6.2 | 1.6 |
| St. Cloud | 6.2 | .6 | 5.3 | .5 | 3.6 | .5 | 4.2 | .7 |
| Wet Summer | | | | | | | | |
| Twin Cities | 7.4 | 1.3 | 6.8 | 1.4 | 3.5 | 1.3 | 3.8 | 2.0 |
| St. Cloud | 6.9 | .8 | 5.7 | 1.1 | 2.8 | .6 | 2.8 | .6 |
| Dry Summer | | | | | | | | |
| Twin Cities | 4.9 | .8 | 4.2 | 1.0 | 3.2 | 1.1 | 4.3 | 1.7 |
| St. Cloud | 3.4 | .4 | 2.7 | .6 | 1.4 | .3 | 1.6 | .6 |
| Wet Fall | | | | | | | | |
| Twin Cities | 7.3 | 1.1 | 6.8 | 1.3 | 5.6 | 1.2 | 6.2 | 2.2 |
| St. Cloud | | (NO COVERAGE) | | | | | | |
| Dry Fall | | | | | | | | |
| Twin Cities | 8.0 | 1.6 | 7.4 | 1.5 | 6.9 | 1.5 | 8.0 | 1.8 |
| St. Cloud | 6.1 | .5 | 4.6 | .6 | 3.8 | .6 | 4.5 | .8 |

Table 3. Lineaments, Twin Cities Site

| Number of lineaments per outcrop | 0 | | 1 | | 2 | | 3 | | 4 | | 5 | |
|---|---|---|---|---|---|---|---|---|---|---|---|---|
| Distance from outcrop to lineament (km) | 1-1/2 | 6 | 1-1/2 | 6 | 1-1/2 | 6 | 1-1/2 | 6 | 1-1/2 | 6 | 1-1/2 | 6 |
| Rectilinears from the river map | 79 | 27 | 27 | 67 | 4 | 6 | | | | | | |
| Rectilinears from the contour map | 62 | 17 | 24 | 51 | 11 | 19 | 1 | 7 | | 3 | | 3 |
| Rectilinears of rivers on winter LANDSAT | 69 | 13 | 31 | 77 | | 4 | | 4 | | | | |
| Rectilinears of rivers on Spring LANDSAT | 81 | 74 | 19 | 4 | | | | | | | | |
| Rectilinears contacts on Winter LANDSAT | 74 | 64 | 27 | 36 | | | | | | | | |
| Rectilinears tonal contacts on Spring LANDSAT | 100 | 91 | | 9 | | | | | | | | |
| Lineaments of tonal stripe on Winter LANDSAT | 100 | 100 | | | | | | | | | | |
| Lineaments of tonal stripes on Spring LANDSAT | 100 | 100 | | | | | | | | | | |
| Lineaments from the lakes map | 87 | 67 | 13 | 29 | | | | | | | | |
| Lineaments of lakes on Winter LANDSAT | 87 | 56 | 13 | 27 | | 26 | | | | 6 | | |
| Lineaments of lakes on Spring LANDSAT | 96 | 60 | 4 | 40 | | 10 | | 10 | | | | |
| Curvilinear from the river map | 73 | 57 | 24 | 37 | 4 | 14 | | 4 | | | | |
| Curvilinear from the contour map | 74 | 36 | 19 | 26 | 7 | 33 | | 7 | | | | |
| Curvilinear of rivers on Winter LANDSAT | 77 | 61 | 16 | 24 | 7 | 14 | | | | | | |
| Curvilinear of rivers on Spring LANDSAT | 71 | 61 | 24 | 30 | 1 | | 3 | 9 | | | | |
| Curvilinear of tonal contacts on Winter LANDSAT | 81 | 66 | 19 | 24 | | 9 | | | | | | |
| Curvilinear of tonal contacts of Spring LANDSAT | 100 | 94 | | 6 | | | | | | | | |

These results are the percentage of all of the outcrops occuring within the indicated distance to the assigned number of nearby lineaments. (For maps of lineaments see Goebel, and others, 1978)

Table 4. Lineaments, St. Cloud Site

| Number of lineaments per outcrop | 0 | | 1 | | 2 | | 3 | | 4 | | 5 | |
|---|---|---|---|---|---|---|---|---|---|---|---|---|
| Distance from outcrop to lineament (km) | 1-1/2 | 6 | 1-1/2 | 6 | 1-1/2 | 6 | 1-1/2 | 6 | 1-1/2 | 6 | 1-1/2 | 6 |
| Rectilinears from the river map | 97 | 90 | 3 | 10 | | | | | | | | |
| Rectilinears from the contour map | 100 | 100 | | | | | | | | | | |
| Rectilinears of rivers on winter LANDSAT | 87 | 0 | 10 | 70 | 3 | 26 | | 3 | | | | |
| Rectilinears of rivers on Spring LANDSAT | 93 | 63 | 6 | 36 | | | | | | | | |
| Rectilinears contacts on Winter LANDSAT | 97 | 37 | 3 | 63 | | | | | | | | |
| Rectilinears tonal contants on Spring LANDSAT | 0 | 60 | | 33 | | 6 | | | | | | |
| Lineaments of tonal stripe on Winter LANDSAT | 100 | 87 | | 13 | | | | | | | | |
| Lineaments of tonal stripes on Spring LANDSAT | 100 | 100 | | | | | | | | | | |
| Lineaments from the lakes map | 97 | 97 | 3 | 3 | | | | | | | | |
| Lineaments of lakes on Winter LANDSAT | 100 | 100 | | | | | | | | | | |
| Lineaments of lakes on Spring LANDSAT | 100 | 97 | | 3 | | | | | | | | |
| Curvilinear from the river map | 87 | 6 | 13 | 83 | 3 | 10 | | | | | | |
| Curvilinear from the contour map | 100 | 93 | | 6 | | | | | | | | |
| Curvilinear of rivers on Winter LANDSAT | 90 | 0 | 6 | 46 | 3 | 53 | | | | | | |
| Curvilinear of rivers on Spring LANDSAT | 90 | 0 | 10 | 65 | | 36 | | | | | | |
| Curvilinear of tonal contacts on Winter LANDSAT | 97 | 17 | 10 | 63 | | 3 | | | | | | |
| Curvilinear of tonal contacts of Spring LANDSAT | 90 | 6 | 10 | 10 | | 66 | | | | | | |

These results are the percentage of all of the outcrops occuring within the indicated distance to the assigned number of nearby lineaments. (For maps of lineaments see Goebel, and others, 1978)

Table 5. Mean and standard deviation of the color density values on Skylab photographs with a scale of 1-5 from light to dark. The Twin Cities site was not included on any of the Skylab photographs and these data apply to the St. Cloud site only.

| Type of photography | M | SD |
|---|---|---|
| Infra-red, color | 4.3 | 1.3 |
| Infra-red, black and white (.7 - .8 um) | 4.9 | .7 |
| Infra-red, black and white (.8 - .9 um) | 4.5 | .8 |
| Visible, color | 4.1 | .9 |
| Visible, black and white (.6 - .7um) | 1.7 | .8 |
| Visible, black and white (.5 - .6 um) | 3.8 | .7 |

Table 6. Correlation between the responses of the remote-sensing media used in this study to near surface bedrock.

| Site | Remote-sensing media | Pearson's r |
|---|---|---|
| St. Cloud | Gravity vs. aeromagnetics | -.14 |
| Twin Cities | Gravity vs. aeromagnetics | -.01 |
| St. Cloud | Aeromagnetics vs. natural gamma radiation | .00 |
| Twin Cities | Aeromagnetics vs. natural gamma radiation | .14 |
| St. Cloud | Gravity vs. natural gamma radiation | .34 |
| Twin Cities | Gravity vs. natural gamma radiation | -.29 |
| St. Cloud | Aerial photograph vs. radar imagery | -.12 |
| Twin Cities | Aerial photograph vs. radar imagery | .30 |
| St. Cloud | Radar imagery vs. visible color | -.21 |
| St. Cloud | Outcrop elevation vs. stream bed elevation | .83 |
| Twin Cities | Outcrop elevation vs. stream bed elevation | .62 |
| St. Cloud | Outcrop elevation vs. distance to elevation | .29 |
| Twin Cities | Outcrop elevation vs. distance to elevation | .32 |
| St. Cloud | Outcrop elevation vs. sediment thickness | -.57 |
| Twin Cities | Outcrop elevation vs. sediment thickness | -.29 |
| | Skylab Photography (Twin Cities without coverage) | |
| St. Cloud | Visible color vs. I.R. color | .15 |
| St. Cloud | I.R. color vs. black and white .6-.7 um | -.09 |
| St. Cloud | Black and white .6-.7 um vs. black and white .5-.6 um | .11 |
| St. Cloud | Black and white .5-.6 um vs. black and white .8-.9um | .00 |
| St. Cloud | Black and white .8-.9 um vs. black and white .7-.8 um | .41 |
| St. Cloud | Visible color vs. black and white .8-.9 um | .07 |
| | LANDSAT Image negatives | |
| St. Cloud | Wet summer band 4 vs. dry summer band 6 | .04 |
| St. Cloud | Dry summer band 6 vs. day fall band 4 | .53 |
| St. Cloud | Dry spring band 4 vs. dry summer band 6 | .62 |
| St. Cloud | Dry spring band 4 vs. dry fall band 4 | .72 |
| St. Cloud | Wet summer band 7 vs. dry summer band 6 | .91 |
| St. Cloud | Dry spring band 4 vs. wet summer band 7 | .66 |
| St. Cloud | Winter band 4 vs. dry spring band 4 | .09 |
| St. Cloud | Winter band 6 vs. dry spring band 4 | .11 |

# DATA SOURCES

## Aerial Photographs

Study Area A - Marshall and Pennington Counties, 1966, U.S. Department of Agriculture, Agricultural Stabilization and Conservation Service, Aerial Survey, Inc., Louisville, KY, 1:20,000.

BXY - 1GG-(65-76), (142-154), (182-189)
BXY - 2GG-(107-114), (161-172), (192-203), (267-278)
BXY - 3GG-(44-48), (68-81), (146-159), (181-194), (264-276)
BXY - 4GG-(79-84), (167-169)
BYC - 1GG-(46-55), (88-97), (163-171)
BYC - 2GG-(56-65), (116-124), (132-141), (206-215)

Study Area $B^1$ - Lake of the Woods County, 1941, Abrams Aerial Survey Corp. - Mark Hurd Aerial Mapping Corp., 1:20,000.

C1Q-1-(38-145)
C1Q-3-(23-31)
C1Q-5-(119-125), (156-162), (165-171)

Study Area $B^2$ - Roseau County, 1966, U.S. Dept. of Agriculture, Agricultural Stabilization and Conservation Service, Park Aerial Surveys, 1:20,000.

BYG-2GG-(113-138)
BYG-3GG-(36-48), (50-55)
BYG-4GG-(1-13), (120-132)

Study Area C - Beltrami County, 1939, U.S. Dept. of Agriculture, Agricultural Adjustment Administration, Abrams Aerial Survey Corp. -

Mark Hurd Aerial Mapping Corp., 1:20,000.

CIN-1-(60-77), (83-91), (102-114), (124-133), (140-159)

CIN-2-(36-45), (65-80)

CIN-4-(182-197), (205-217)

CIN-5-(62-83), (122-128)

CIN-6-(4-21), (88-106), (111-116), (124-128)

CIN-7-(33-35)

CIN-10-(79-82)

Study Area D - St. Louis County, 1953, Arrowhead Aerial Surveys, Hibbing, MN.

CIR-1G-(140-156), (163-179), (191-207)

Study Area E - Crow Wing County, 1940, U.S. Department of Agriculture, Agricultural Adjustment Administration, Abrams Aerial Survey Corp. - Mark Hurd Aerial Mapping Corp., 1:20,000.

BXT-1-(55-60), (94-108), (113-128), (161-175)

BXT-4-(106-117), (123-142)

Study Area F - Crow Wing County, 1939, U.S. Dept. of Agriculture, Agricultural Adjustment Administration, Abrams Aerial Survey Corp. - Mark Hurd Aerial Mapping Corp., 1:20,000.

BXT-2-17-(49-59), 72-79), (101-110), (144-154)

BXT-3-(41-52), (95-104), (122-133), (171-181)

BXT-5-(2-15), (27-38), (69-86), (101-113)

Study Area G - Benton, Sherburne, Stearns, and Wright Counties, 1963, U.S. Dept. of Agriculture, Agricultural Stabilization and Conservation

Service, Mark Hurd Aerial Surveys, Inc., 1:20,000.

BIN-1DD-(75-82), (92-93), (142-143)

BIN-2DD-(19-20), (58-63), (100-101), (133-134), (171-172), (228-229)
(266-267)

BJL-1DD-(38-39), (84-91), (143-154), (156-176), (181-201), (204-268)

BJL-2DD-(21-39), (40-57), (101-118), (124-132), (210-227), (267-279)

BJL-3DD-(5-11)

Study Area $H^1$ - Hennepin County, 1951, Mark Hurd Aerial Surveys, Inc. Wide Angle, 1:9,600.

BF-2-(1-8), (76-93)

BF-3-(35-43), (64-70)

BF-6-(60-65)

Study Area $H^2$ - Hennepin and Ramsey Counties, 1957, U.S. Dept. of Agriculture, Commodity Stabilization Service, Mark Hurd Aerial Surveys, Inc., 1:20,000.

BIM-2T-1

WO-2T-(52-72), (128-135). (201-209)

WO-3T-(2-10)

WO-9T-(65-71)

Study Area $H^3$ - Dakota and Washington Counties, 1964, U.S. Dept. of Agriculture, Agricultural Stabilization and Conservation Service, Mark Hurd Aerial Surveys, Inc., 1:20,000.

CZ-2EE-(22-38), (107-125)

CZ-3EE-(1-27), (83-107)

C22

CZ-4EE-(53-63), (190-216)

CZ-5EE-(45-62)

## LANDSAT IMAGES

EROS Data Center, LANDSAT Imagery, U.S. Dept. of the Interior, Geological Survey, EROS Data Center, Sioux Falls, S.D., 1:1,000,000

Black & White Negatives:

8-2359-16173-4,5,6,7

8-5353-15515-4,5,6,7

8-2197-16201-4,5,6,7

8-2269-16192-4,5,6,7

8-2791-16043-4,5,6,7

8-2593-16121-4,5,6,7

8-2665-16094-4,5,6,7

8-2018-16236-4,5,6,7

8-5354-15571-4-4a,5,6,7

8-2198-16253-4,5,6,7,

8-2828-16075-4,5,6,7

8-2594-16172-4,5,6,7

8-2648-16154-4,5,6,7

# SKYLAB Images

EROS Data Center, SKYLAB Images S190A, U.S. Dept. of the Interior, Geological Survey, EROS Data Center, Sioux Falls, S.D., 1:2,822,434.

| G30A043216000 | Infrared Positive | Black & White Positive |
|---|---|---|
| G30A044216000 | IR | BW |
| G30A047216000 | | BW |
| G30A048216000 | | BW |
| G30A045216000 | IR | Color |
| G30A046216000 | Normal | Color |
| G30A043217000 | IR | BW |
| G30A044217000 | IR | BW |
| G30A047217000 | | BW |
| G30A048217000 | | BW |
| G30A045217000 | IR | Color |
| G30A046217000 | | Color |
| G30A043218000 | IR | BW |
| G30A044218000 | IR | BW |
| G30A047218000 | | BW |
| G30A048218000 | | BW |
| G30A045218000 | IR | Color |
| G20A013134000 | IR | BW |
| G20A014134000 | IR | BW |
| G20A017134000 | | BW |

| | | |
|---|---|---|
| G20A018134000 | | BW |
| G20A015142000 | IR | Color |
| G20A025008000 | | Color |
| G30A025008000 | IR | BW |
| G30A026008000 | IR | BW |
| G30A029008000 | | BW |
| G30A030008000 | | BW |
| G30A027008000 | IR | Color |
| G30A028008000 | | Color |

## SLAR Images

Goodyear Aerospace Corp., Side Looking Airborne Radar Imagery (SLAR): Goodyear Aerospace Corp., Litchfield Park, Arizona, 1:200,000.

| | | | | |
|---|---|---|---|---|
| RNI | FN | 1068X | Poss#03 | Pos. Paper and Film |
| RN3792 | FN | 129X | Poss#07 | Pos. Paper and Film |

## Orthophotographs

Blue-line orthophotographs, Mark Hurd Aerial Surveys, Inc., 345 Pennsylvania Ave. So., Mpls., MN. 55426, 1:24,000.

| | | |
|---|---|---|
| Sucker Creek | 392-2 | 1977 |
| Nebish | 361-2 | 1977 |
| Redby N.E. | 361-1 | 1977 |
| Borden Lake | 360-2 | 1977 |
| O'Brien Lookout Tower | 360-3 | 1977 |

| | | |
|---|---|---|
| Saum | 360-4 | 1977 |
| Saum N.E. | 360-1 | 1977 |
| Shotley | 391-3 | 1977 |
| Shotley Brook | 391-2 | 1977 |
| South Long Lake | 213-2 | 1977 |
| Merrifield | 213-4 | 1977 |
| Riverton | 213-1 | 1977 |
| Brainerd | 213-2 | 1977 |
| Prescott | 103-2 | 1977 |
| St. Paul Park | 103-3 | 1977 |
| Lake Elmo | 104-4 | 1977 |
| Hudson | 103-1 | 1977 |
| St. Paul West | 104-4 | 1977 |
| St. Paul East | 104-1 | 1977 |
| St. Paul S.W. | 104-3 | 1977 |
| Inver Grove Heights | 104-2 | 1977 |
| Viking S.W | 399-3 | 1969 |
| Viking S.E. | 399-2 | 1969 |
| Warroad S.E. | 446-2 | 1969 |
| Roosevelt | 445-2 | 1969 |
| Winter Road Lake N.W. | 434-4 | 1969 |
| Winter Road Lake | 434-1 | 1969 |
| Milligan Lake N.E. | 435-1 | 1969 |
| Monticello | 139-2 | 1977 |
| Silver Creek | 139-3 | 1977 |

| | | |
|---|---|---|
| Clear Lake | 139-4 | 1977 |
| Elk River | 138-2 | 1977 |
| Big Lake | 138-3 | 1977 |
| Orrock | 138-4 | 1977 |
| Lake Fremont | 138-1 | 1977 |
| Becker | 139-1 | 1977 |
| Boulder Lk. Reservoir | 269-3 | 1969 |
| Boulder Lk. Reserv. N.E. | 269-1 | 1969 |
| Comstock Lake | 269-4 | 1969 |
| Thompson Lake | 269-2 | 1969 |
| Arnold | 246-1 | 1969 |
| Fredenberg | 246-4 | 1969 |
| Shaw | 270-2 | 1969 |
| Trommald | 233-2 | 1977 |
| Pelican Lake | 233-3 | 1977 |
| Stewart Lake | 254-3 | 1977 |
| Mitchell Lake | 254-2 | 1977 |
| Roosevelt Lake | 253-3 | 1977 |
| Edna Lake | 253-2 | 1977 |
| Twig | 247-1 | 1969 |
| St. Cloud | 158-3 | 1977 |
| Cable | 158-2 | 1977 |
| St. Augusta | 140-4 | 1977 |
| Clearwater | 140-1 | 1977 |
| Minneapolis North | 121-2 | 1977 |

| | | |
|---|---|---|
| Minneapolis South | 105-1 | 1977 |
| Stillwater | 119-2 | 1977 |

# Maps

## Aeromagnetic

Zietz, Isidore and Kirby, John R., 1970, Aeromagnetic Map of Minnesota, U.S. Geological Survey, Geophysical Investigations Map GP-725.

## Gravity

Craddock, Campbell, Mooney, H.M. and Kolehmainen, Victoria, 1970, Simple Bouguer Gravity Map of Minnesota and Northwestern Wisconsin, Minnesota Geological Survey, University of Minnesota, Miscellaneous Map Series Map M-10, 1:1,000,000.

## Geologic

Goebel, J.E., and Walton, M., 1979, Geologic Map of Minnesota, Quaternary Geology: Minnesota Geological Survey State Map Series Map S-4, 1:3,168,000.

## Radioactivity

Neuschel, S.K., 1969, Natural Gamma Aeroradioactivity Map of Minneapolis-St. Paul Area, Minnesota-Wisconsin: U.S. Geological Survey, Geophysical Investigations Map GP 658, 1:250,000.

## Topographic

U.S. Army Map Service (BEAM), Western United States, 1:250,000 Topographic Map Series, U.S. Army Corps of Engineers, Wash., D.C., for sale by U.S. Dept. of the Interior Geological Survey.

Bemidji, Minnesota Sheet, 1954 (Limited Revision 1965)

Brainerd, Minnesota Sheet, 1953 (Limited Revision 1965)

Duluth, Minnesota-Wisconsin Sheet, 1953 (Limited Revision 1963)

Hibbing, Minnesota Sheet, 1954 (Limited Revision 1965)

Roseau, Minnesota, U.S.-Ontario, Can. Sheet, 1954 (Limited Revision 1968)

U.S. Dept. of the Interior Geological Survey, 1965, State of Minnesota (Base Map), U.S Dept. of the Interior Geological Survey, 1:1,000,000.

U.S. Dept. of the Interior Geological Survey, Topographic Quadrangles, U.S. Dept. of the Interior Geological Survey, Wash., D.C.

| | | |
|---|---|---|
| Arnold MN | 7.5' | 1953 |
| Becker, MN | 7.5' | 1961 |
| Big Lake, MN | 7.5' | 1961 |
| Borden Lake, MN | 7.5' | 1972 |
| BoulderLk.Reservoir, MN | 7.5' | 1953 photorevised 1969 |
| BoulderLk.Reservoir N.E.,MN | 7.5' | 1957 |
| Brainerd, MN | 7.5' | 1973 |
| Cable, MN | 7.5' | 1974 |
| Clear Lake, MN | 7.5' | 1961 |
| Clearwater, MN | 7.5' | 1974 |
| Comstock Lake, MN | 7.5' | 1957 |
| Edna Lake, MN | 7.5' | 1970 |
| Elk River, MN | 7.5' | 1961 |
| Fredenberg, MN | 7.5' | 1953 photorevised 1972 |

| | | |
|---|---|---|
| Hudson, MN-WI | 7.5' | 1967 photorevised 1972 |
| Inver Grove Heights, MN | 7.5' | 1967 photorevised 1972 |
| Lake Elmo, MN | 7.5' | 1967 photorevised 1972 |
| Lake Freemont, MN | 7.5' | 1961 |
| Merrifield, MN | 7.5' | 1973 |
| Minneapolis North, MN | 7.5' | 1967 photorevised 1972 |
| Minneapolis South, MN | 7.5' | 1967 photorevised 1972 |
| Mitchell Lake, MN | 7.5' | 1970 |
| Monticello, MN | 7.5' | 1961 |
| Mulligan Lake N.E., MN | 7.5' | 1968 |
| Nebish, MN | 7.5' | 1972 |
| Newfolden, MN | 15 ' | 1957 |
| O'Brien Lookout Tower, MN | 7.5' | 1972 |
| Orrock, MN | 7.5' | 1961 |
| Pelican Lake, MN | 7.5' | 1959 |
| Prescott, MN | 7.5' | 1967 photorevised 1972 |
| Redby N.E., MN | 7.5' | 1972 |
| Riverton, MN | 7.5' | 1973 |
| Roosevelt, MN | 7.5' | 1967 |
| Roosevelt Lake, MN | 7.5' | 1970 |
| Rosewood, MN | 7.5' | 1959 |
| St. Augusta, MN | 7.5' | 1974 |
| St. Cloud, MN | 7.5' | 1974 |
| St. Paul East, MN | 7.5' | 1967 photorevised 1972 |
| St. Paul Park, MN | 7.5' | 1967 photorevised 1972 |

| | | |
|---|---|---|
| St. Paul S.W., MN | 7.5' | 1967 photorevised 1972 |
| St. Paul West, MN | 7.5' | 1967 photorevised 1972 |
| Saum, MN | 7.5' | 1972 |
| Saum, N.E., MN | 7.5 | 1972 |
| Shaw, MN | 7.5' | 1953 |
| Shotley, MN | 7.5' | 1973 |
| Shotley Brook, MN | 7.5' | 1974 |
| Silver Creek, MN | 7.5' | 1961 |
| South Long Lake, MN | 7.5' | 1973 |
| Stewart Lake, MN | 7.5' | 1971 |
| Stillwater, MN-WI | 7.5' | 1951 photorevised 1972 |
| Sucker Creek, MN | 7.5' | 1973 |
| Swift, MN | 7.5' | 1967 |
| Thompson Lake, MN | 7.5' | 1954 photorevised 1969 |
| Trommald, MN | 7.5' | 1959 |
| Twig, MN | 7.5' | 1953 photorevised 1969 and 1972 |
| Viking, MN | 7.5' | 1959 photorevised 1976 |
| Viking S.E., MN | 7.5' | 1959 |
| Viking S.W., MN | 7.5' | 1959 |
| Warroad S.E., MN | 7.5' | 1967 |
| Whiteface, MN | 7.5' | 1956 |
| Winter Road Lake, MN | 7.5' | 1958 |
| Winter Road Lake N.W., MN | 7.5' | 1968 |

## Other

Goebel, J.E., 1980, Isopach map of thickness of unconsolidated sediments in Minnesota: Minnesota Geological Survey file map, 1:500,000.

Goebel, J.E., in preparation, Areas in Minnesota where the bedrock is inferred to be within 50 feet of the present land surface: Minnesota Geological Survey file map, 1:3,168,000.

## References

Cooper, R.W., 1978, Lineament and structural analysis of the Duluth Complex, Hoyt Lakes-Kawishiwi area, northeastern Minnesota: unpub. Ph.D. thesis, University of Minnesota, Minneapolis, 180 p.

Cooper, R.W., Morey, G.B., and Weiblen, P.W., in press, Topographic and aeromagnetic lineaments and their relationship to bedrock geology in a glaciated Precambrian terrane, northeastern Minnesota: International Conference on Basement Tectonics, 3rd, Proceedings (May 15-19, 1978).

Goebel, J.E., Walton, M., and Batten, L.G., 1978, Synergistic relationship between lineaments located on LANDSAT imagery and traditional sources of topographic information, _in_ A study of Minnesota land and water resources using remote sensing: University of Minnesota Space Science Center, NASA Grant NGL 24-005-263, v. XII, p. C1-C50.

Sims, P.K., and Morey, G.B., _eds_., 1972, Geology of Minnesota: a centennial volume: Minnesota Geological Survey, 632 p.

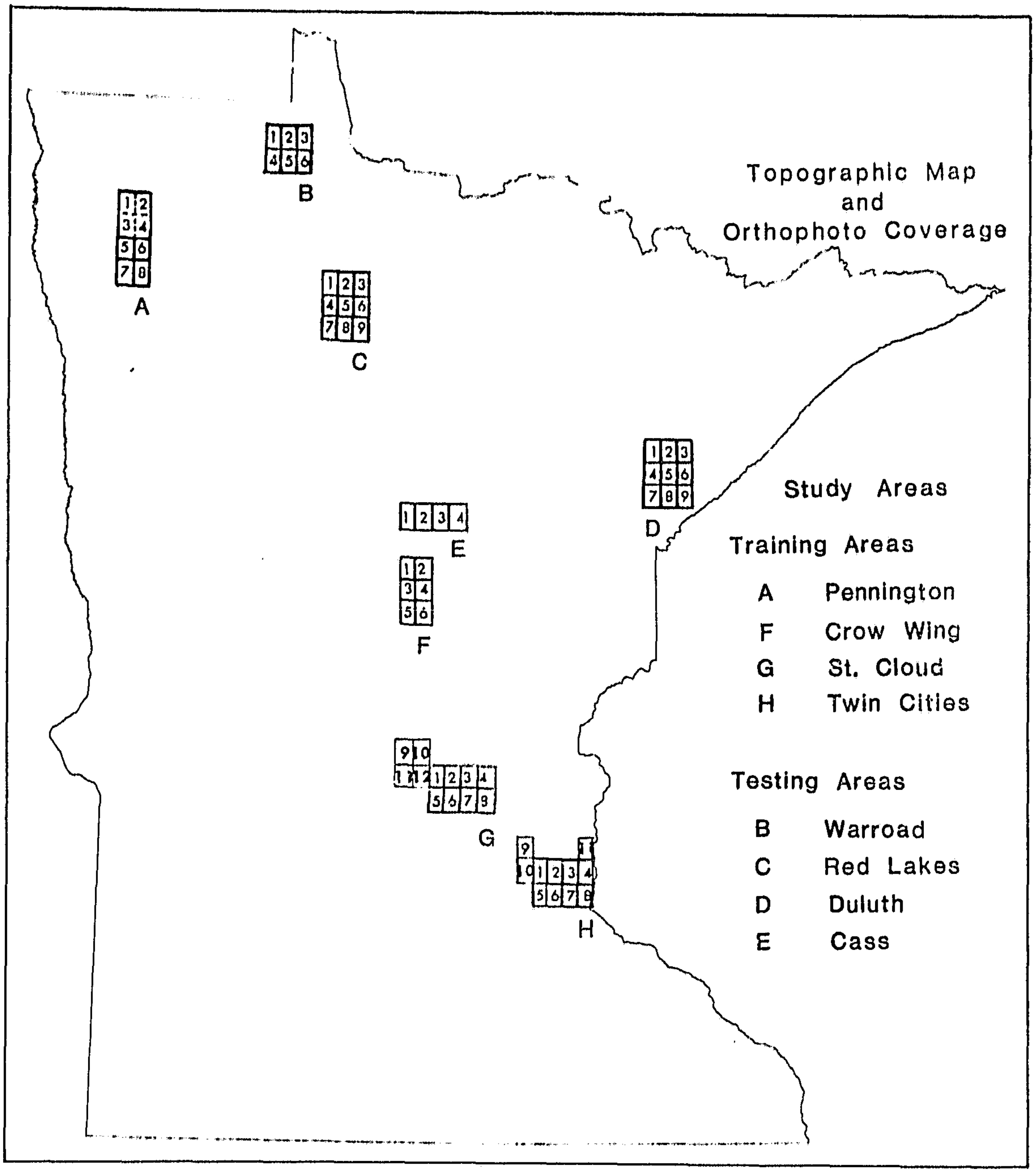

Figure 1. Index map of topographic maps and orthophotos coverage used in this study. For the list of each map or orthophoto see Data Sources.

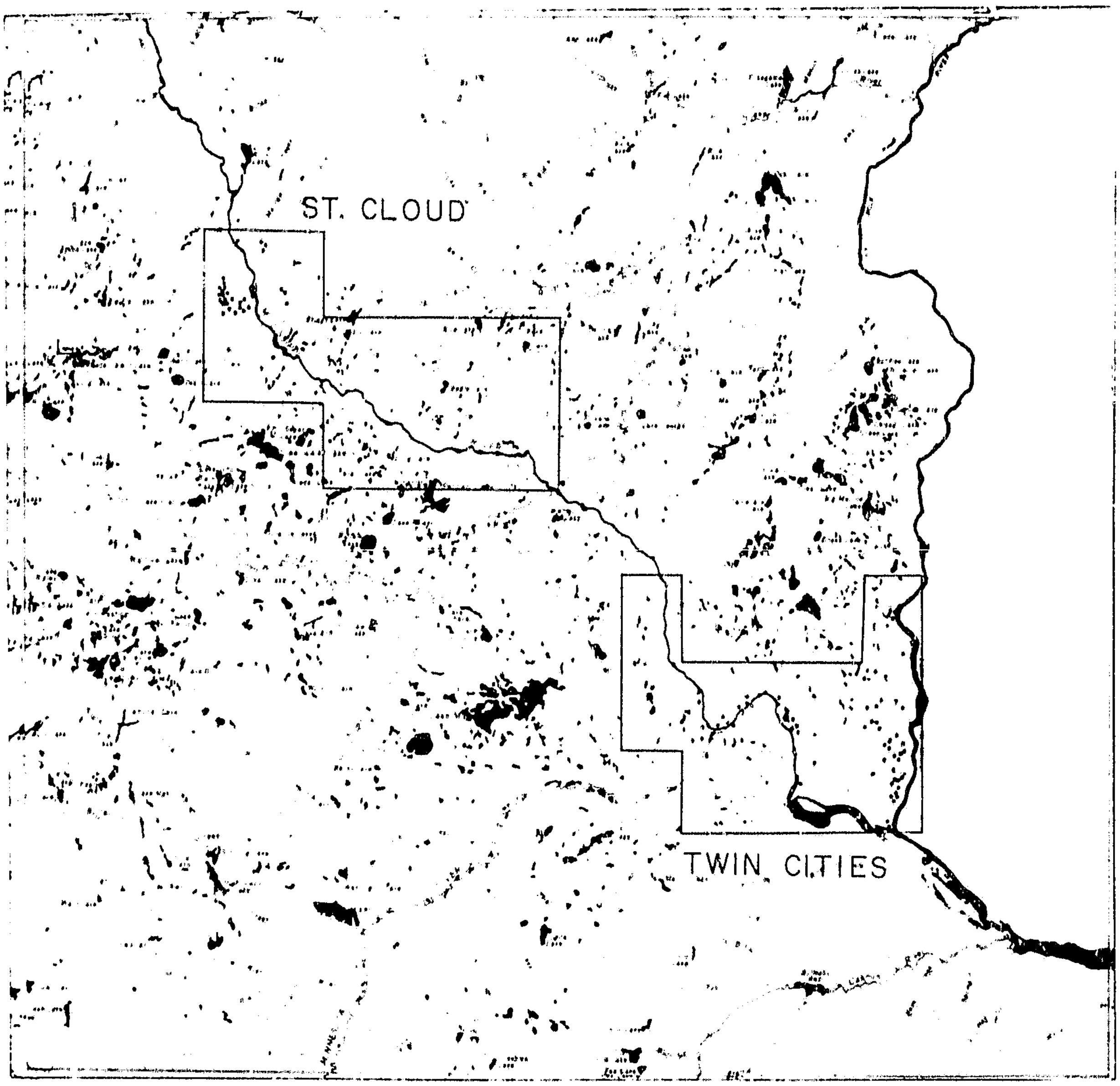

Figure 2. Bedrock outcrops located in the St. Cloud and Twin Cities training sites.

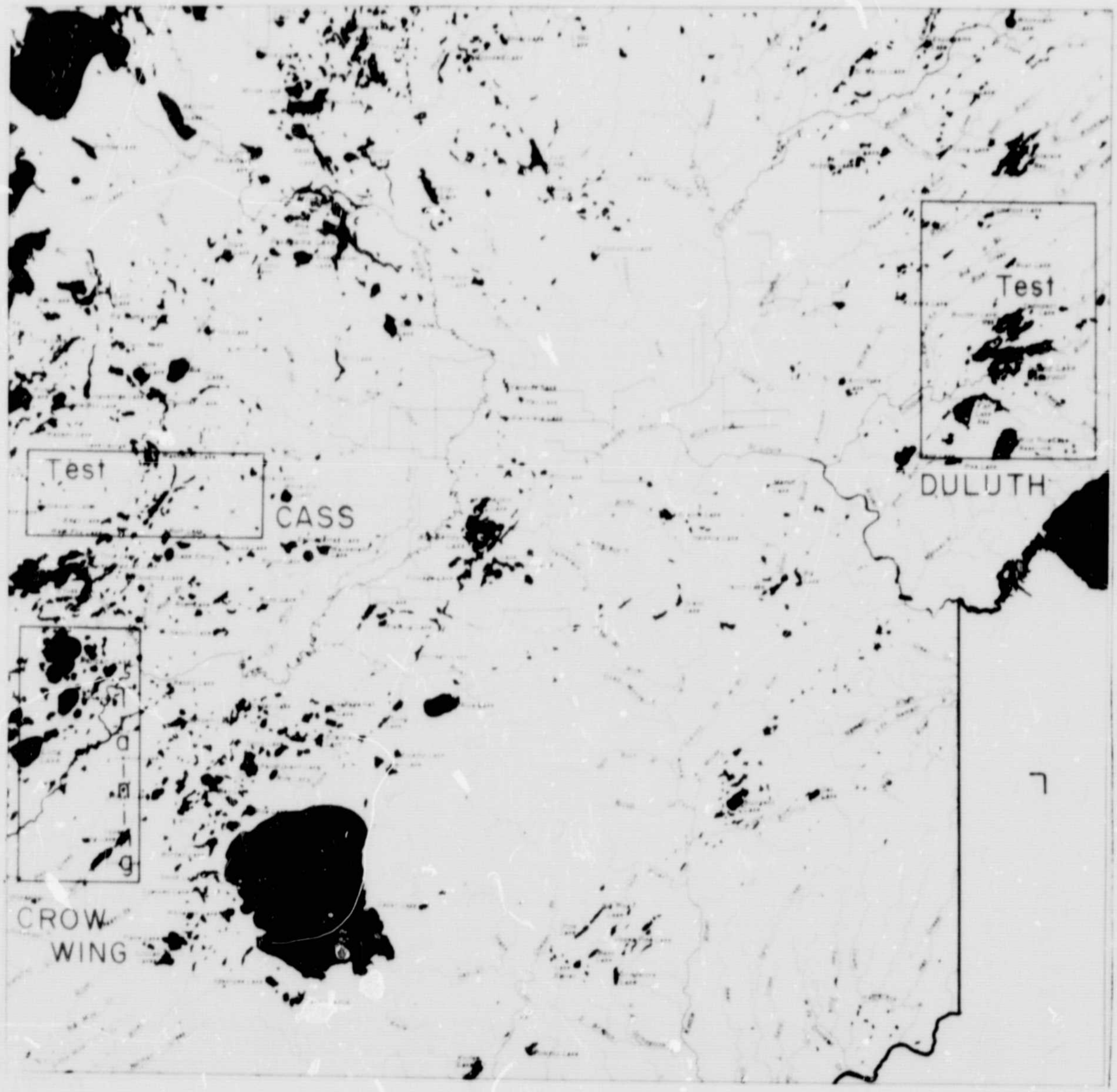

Figure 3. Bedrock outcrops located in the Crow Wing training site and the Cass and Duluth test sites.

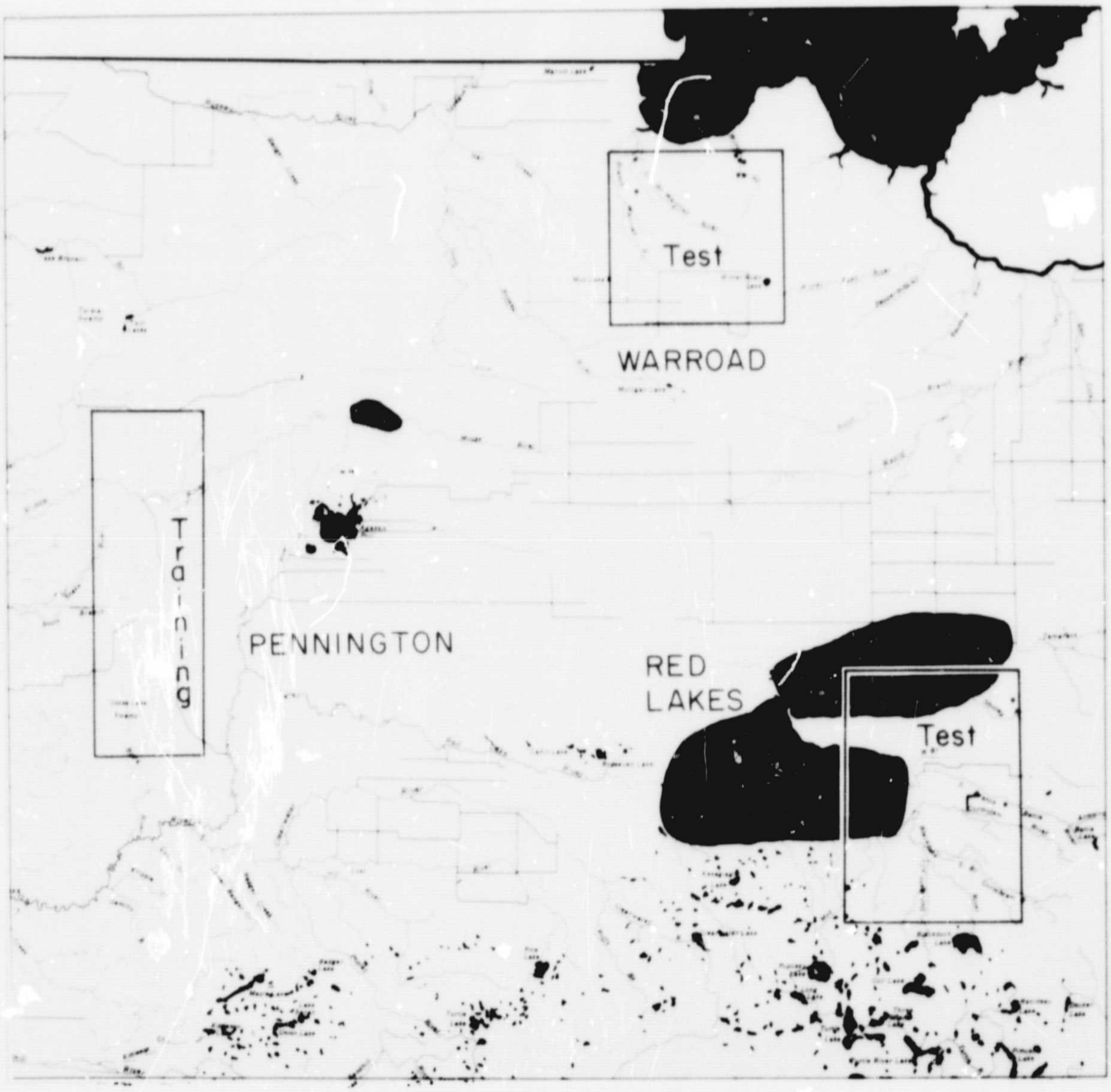

Figure 4. Bedrock outcrops located in the Red Lakes and Warroad test sites. No outcrops were located in the Pennington training site.

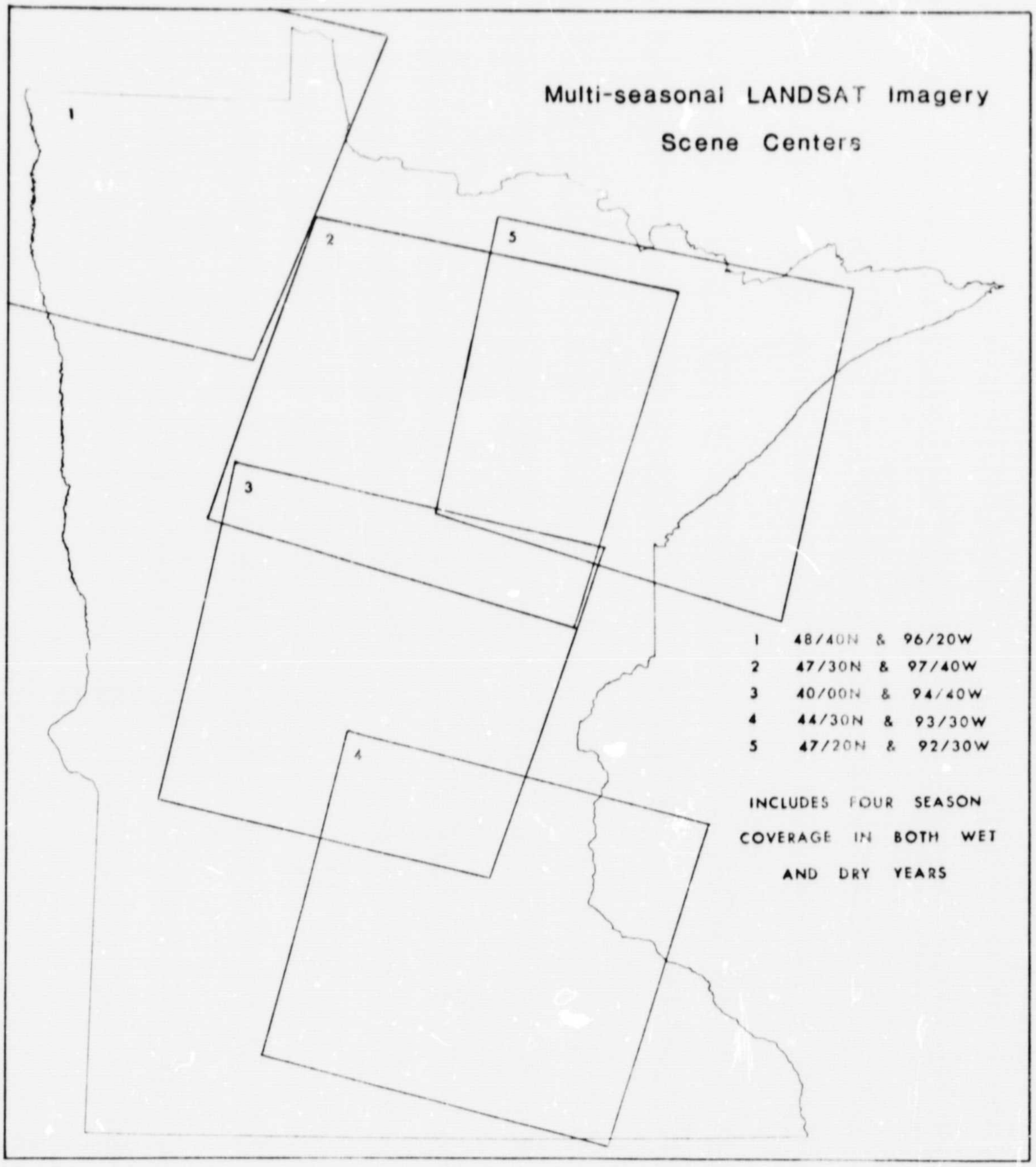

Figure 5. Index map for multiseasonal LANDSAT MSS imagery scene centers. Each scene center has imagery related to a wet and dry year for spring, summer and fall while winter has single coverage. For the list of all of the images used in this study, see Data Sources.

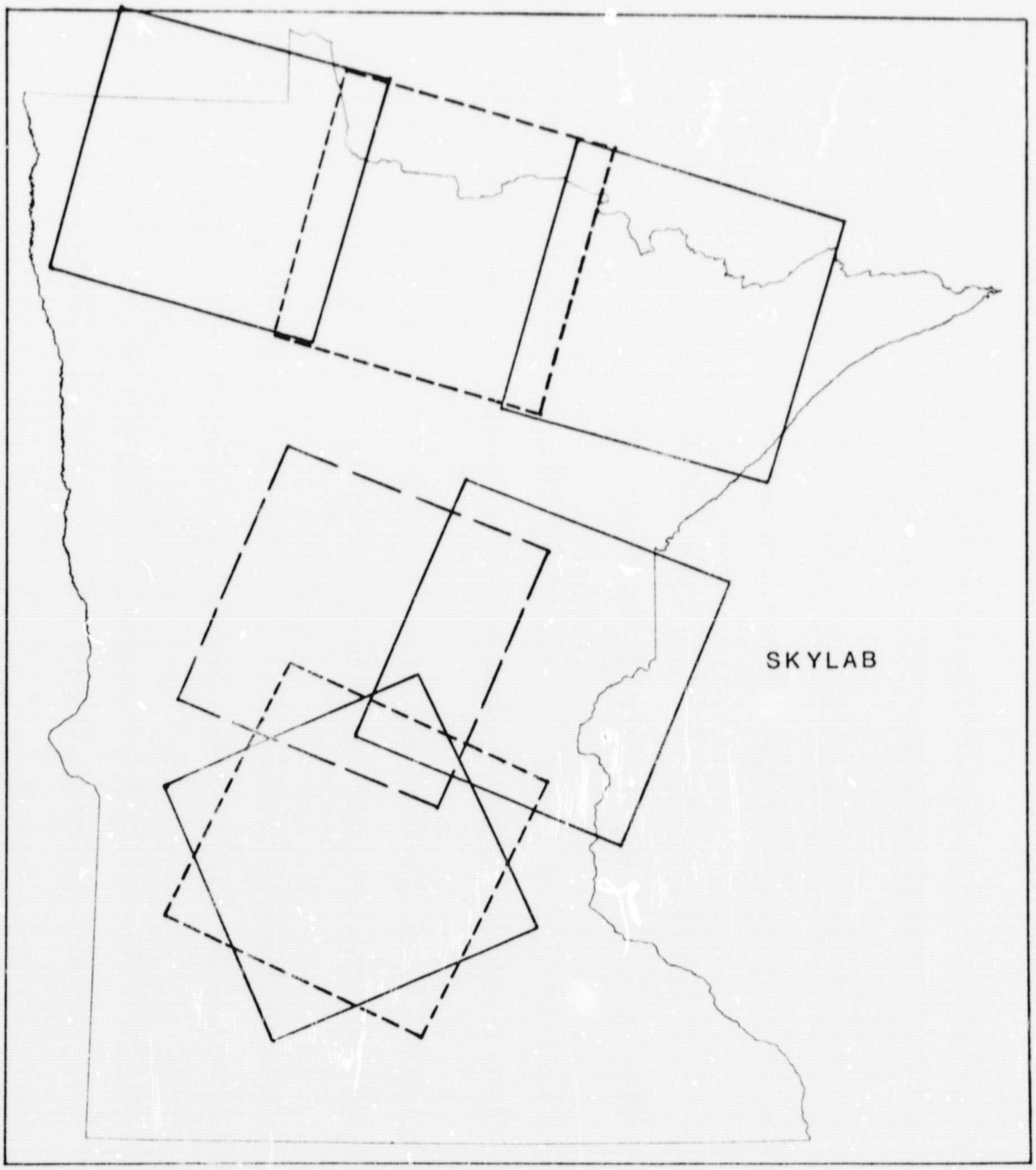

Figure 6. Index Map of Skylab photographs.

82

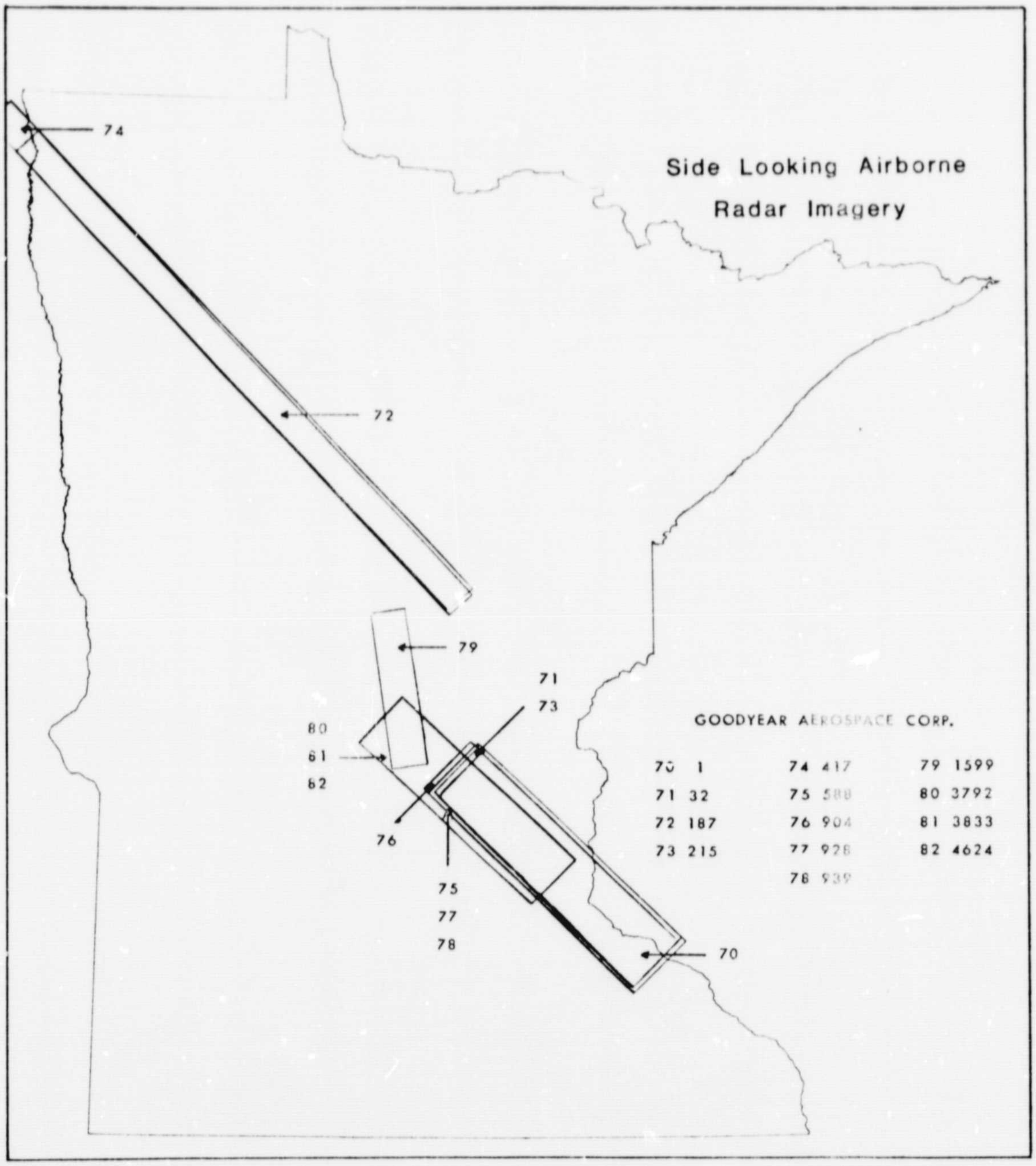

Figure 7. Index map of SLAR imagery.

**Magnetic contours**

*Showing total intensity magnetic field of the earth in gammas relative to arbitrary datum. Main magnetic field of the earth, from Cain and others, 1965, has been removed*

Figure 8. Reduced aeromagnetic map of Minnesota.

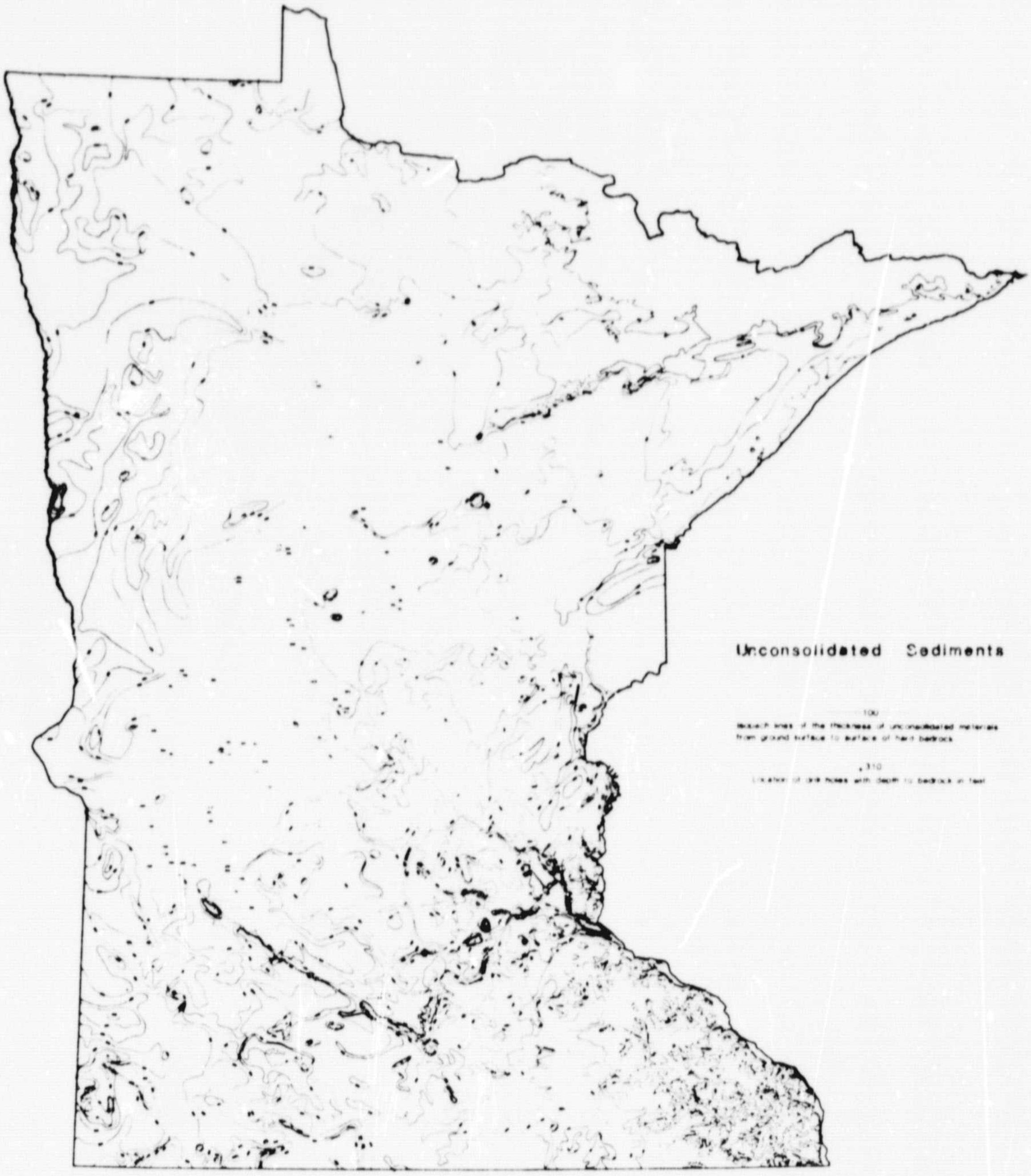

Figure 9. Reduced map of the thickness unconsolidated sediments in Minnesota.

Figure 10. Reduced map of areas where the bedrock is exposed or thinly covered with unconsolidated deposits.

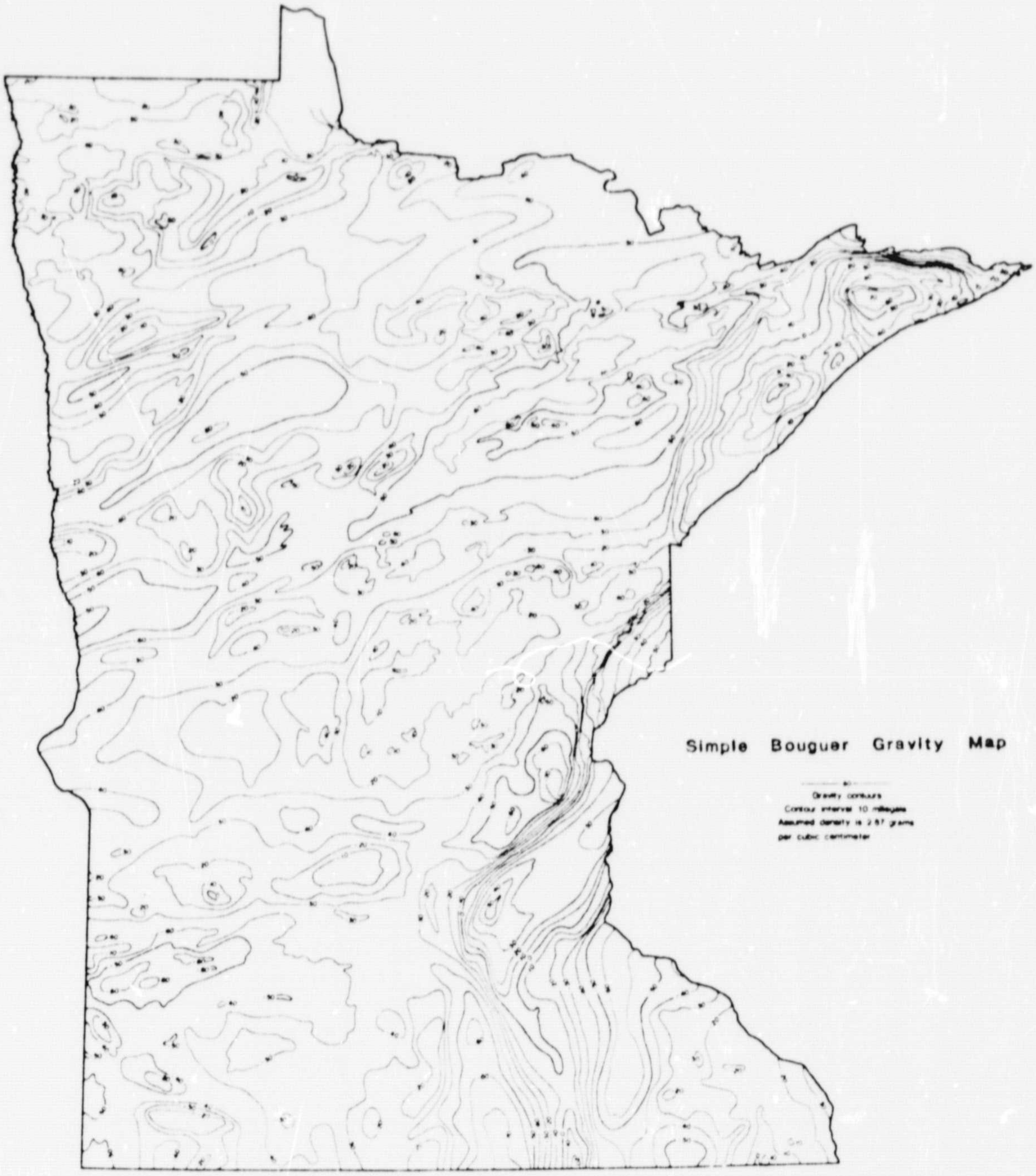

Figure 11. Reduced simple Bouguer gravity map of Minnesota.

24

N81-12509

## SECTION D

# A PROJECT TO EVALUATE MOISTURE STRESS IN CORN AND SOYBEAN AREAS OF WESTERN AND SOUTHWESTERN MINNESOTA

Dr. R. H. Rust
Pierre Robert
Department of Soil Science
St. Paul, Minnesota

---

## INDEX

---

# A PROJECT TO EVALUATE MOISTURE STRESS IN CORN AND SOYBEAN AREAS OF WESTERN AND SOUTHWESTERN MINNESOTA

Investigators: Dr. R. H. Rust
Pierre Robert
Department of Soil Science
St. Paul, Minnesota

## INTRODUCTION

This report summarizes a continuing effort to assess soil moisture stress through crop signatures in southwestern Minnesota using remote sensing techniques and particularly LANDSAT data (Rust and Robert, 1977, 78). Related objectives are: localization of droughty, well drained, and poorly drained soils; detection of stress from hail, wind, and disease damage; and the use of remote sensing data for agricultural management.

The 1979 ground data collection network was similar to that used in 1978, but site #10 in Chippewa County was dropped because the soil survey terminated. Generally similar procedures were used for ground data collection, greenhouse experiments, and remote sensing data types. The 1978 progress report gives the site locations (Figure 1: See Volume XII, 1978) and summarizes equipment characteristics and procedures.

Since the amount and distribution of precipitation were adequate during the 1977 and 1978 growing seasons, no significant stress occurred. Crop conditions were very favorable. As a result, crop signatures were too uniform to reflect soilscape variations and crop condition changes. In 1979 precipitation was again adequate to excess, particularly in June and August (Table 1). In some cases, poorly drained sites especially,

Table 1. 1979 growing season monthly precipitation and normals for some weather stations of SW Minnesota

| | | Precipitation (inches) | | | | | | | |
|---|---|---|---|---|---|---|---|---|---|
| Location | | April | May | June | July | August | Sept | Oct | Total |
| Montevideo | Normal | 2.29 | 3.31 | 4.72 | 3.48 | 3.69 | 2.92 | 1.62 | 22.03 |
| | 1979 | 3.26 | 3.98 | 8.32 | 2.17 | 6.87 | 0.40 | 3.60 | 28.60 |
| Marshall | Normal | 2.46 | 3.30 | 4.49 | 3.95 | 2.68 | 2.70 | 1.61 | 21.19 |
| | 1979 | 3.90 | 4.13 | 7.12 | 4.13 | 6.32 | 0.97 | 3.27 | 29.84 |
| Pipestone | Normal | 2.22 | 3.60 | 4.62 | 3.35 | 2.96 | 3.20 | 1.73 | 21.68 |
| | 1979 | 3.13 | 2.82 | 3.84 | 3.44 | 6.38 | 2.13 | 4.31 | 26.05 |
| Redwood Falls | Normal | 2.22 | 3.25 | 3.92 | 3.86 | 3.24 | 2.42 | 1.74 | 20.65 |
| | 1979 | 1.56 | 5.48 | 4.71 | 6.70 | 8.30 | 1.44 | 3.24 | 31.43 |
| Windom | Normal | 2.35 | 3.61 | 4.50 | 3.74 | 3.30 | 3.54 | 1.70 | 22.74 |
| | 1979 | 1.11 | 6.02 | 5.13 | 3.76 | 7.82 | 2.43 | 4.68 | 30.95 |
| Average | Normal | 2.38 | 3.49 | 4.42 | 3.69 | 2.99 | 3.07 | 1.70 | 21.66 |
| | 1979 | 2.59 | 4.78 | 4.98 | 4.04 | 7.14 | 1.47 | 3.82 | 28.82 |

stress conditions developed as a result of excess of water and could be identified on color infrared photographs.

## CORN LEAF REFLECTANCE IN GREENHOUSE EXPERIMENTS

Field reflectance[1] is the result of interactions between a variety of factors such as crop condition, soil type, and farming techniques. The relationship between water availability and plant reflectance can be most adequately isolated in a greenhouse experiment.

Five experiments measuring corn leaf reflectance were conducted from fall 78 to spring 79 using equipment and techniques previously described (1978 progress report). Figure 1 summarizes the main results of one experiment. We observe a general trend toward increased reflectance in response to increased plant water potential[2], a result also found in 1978 on soybean plants. However, the detailed relationship is much more variable, for example, as in the last measurement. Furthermore, correlations may be smaller in some other experiments, particularly in the near infrared waveband. Additional experiments will be conducted during the 1979-80 fall to spring period.

---

[1] Reflectance is use for "reflected energy intensity". The differential normalized reflected energy (DNRE) is defined as

$$\text{DNRE} = \frac{\text{E.I. of stressed leaf}}{\text{E.I. of standard}} - \frac{\text{E.I. of turgid leaf}}{\text{E.I. of standard}}$$

where
E.I. = Energy Intensity of the reflected light. The standard is magnesium oxide at 600 nm.

[2] Water potential is the energy status of the contained water in leaves (or other plant parts) expressed in units of pressure (bars).

C-2

D4

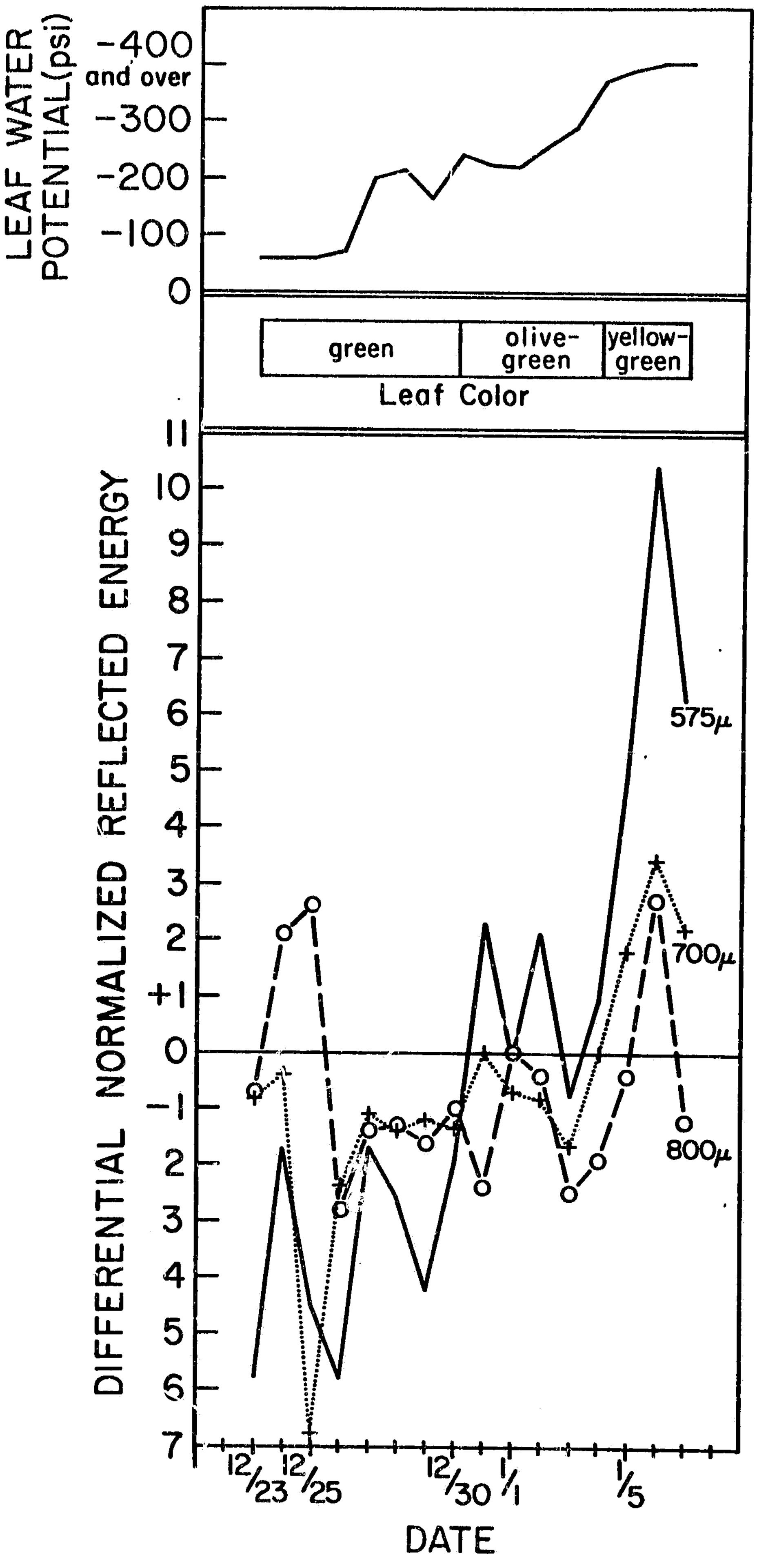

Figure 1. Differential Normalized Reflected Energy(3), Water Potential and Color of Progressively Stressed Corn Plants.

## ASSESSING CROP HAIL DAMAGE

Ground data on hail damage were collected and mapped by the field collaborators using local informaion.

The main hail damage in 1978 occurred on July 6 in Chippewa, Jackson, Pipestone, and Redwood counties. The July 15 LANDSAT imagery (near infrared B & W, 1:1,000,000 scale) gives the best signature of the damaged areas. Figure 2 shows the characteristic signature change of the damaged areas. A better identification could result from the ratio of the July 17 to June 23 data. The ratio might reduce background noise. This will be tested on the IMAGE 100 system during our next session at the Eros Data Center.

## LANDSAT DIGITAL DATA ANALYSIS

Data from the three related scenes of 1977 (June 23, July 29, and September 9) were analyzed at the EROS Data Center, Sioux Falls, during a three-day session. Most of the image processing was performed using the IMAGE 100 system (General Electric Co.). One information extraction was done using the more powerful IDIMS (interactive image processing) system (Electromagnetic System Laboratores, Inc.).

From the original computer compatible tape, overviews of the three scenes (3% sampling) were computed by sampling every sixth column and every fifth line. Windows (256 columns by 185 lines) corresponding to six sites were extracted from the three tapes and stored on a "working" tape.

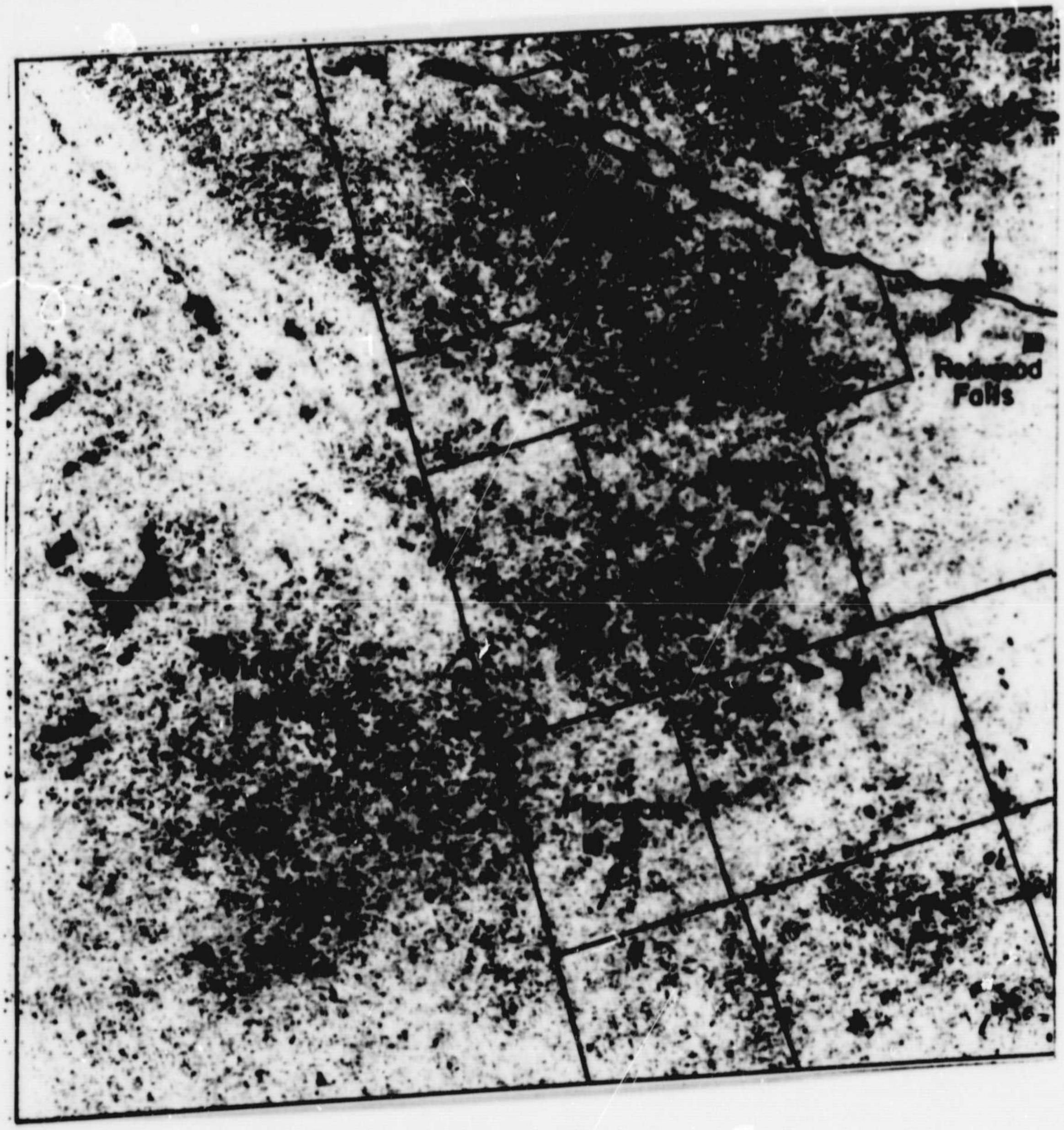

Figure 2. July 15, LANDSAT imagery over southwestern Minnesota (Band 7, 1:1,000,000 scale, path 31, row 24). Arrows indicate hail damage.

Site number 5 (Tracy) was selected for a detailed study on both image analysis systems.

On the IMAGE 100 system the following operations were performed: (1) dumping pixel values; (2) establishing video levels between 0 and 255 for each pixel within the cursored area, which are then printed so that a 1:1 map is obtained; (3) alphanumeric plotting of the training sections using 8 different themes corresponding to 8 equal groups of pixel values; (4) clustering the June (Figure 3) scene and displaying the result on the electrostatic plotter using a 1:1 and 9:1 ratio; (5) temporal overlaying of bands 5 and 7 for the June and July scenes with classification of the resulting image.

On the IDIMS system, alphanumeric maps with 64 classes for the June and July scenes were produced after clustering using the "Isoclass method" (nearest neighbor algorithm) on the 4 channels.

The most significant result came from the temporal signature of the June and July scenes. Corn, soybean, and small grain fields were readily identified. Because of the homogeneity of the signature within crops (the result of favorable weather conditions), it was not possible to make further differentiations, particularly in soil drainage classes.

## ANALYSIS OF SOIL WATER

Soil water content is one of the principal parameters correlated to the crop signatures. Its value is monitored throughout the growing season on each site.

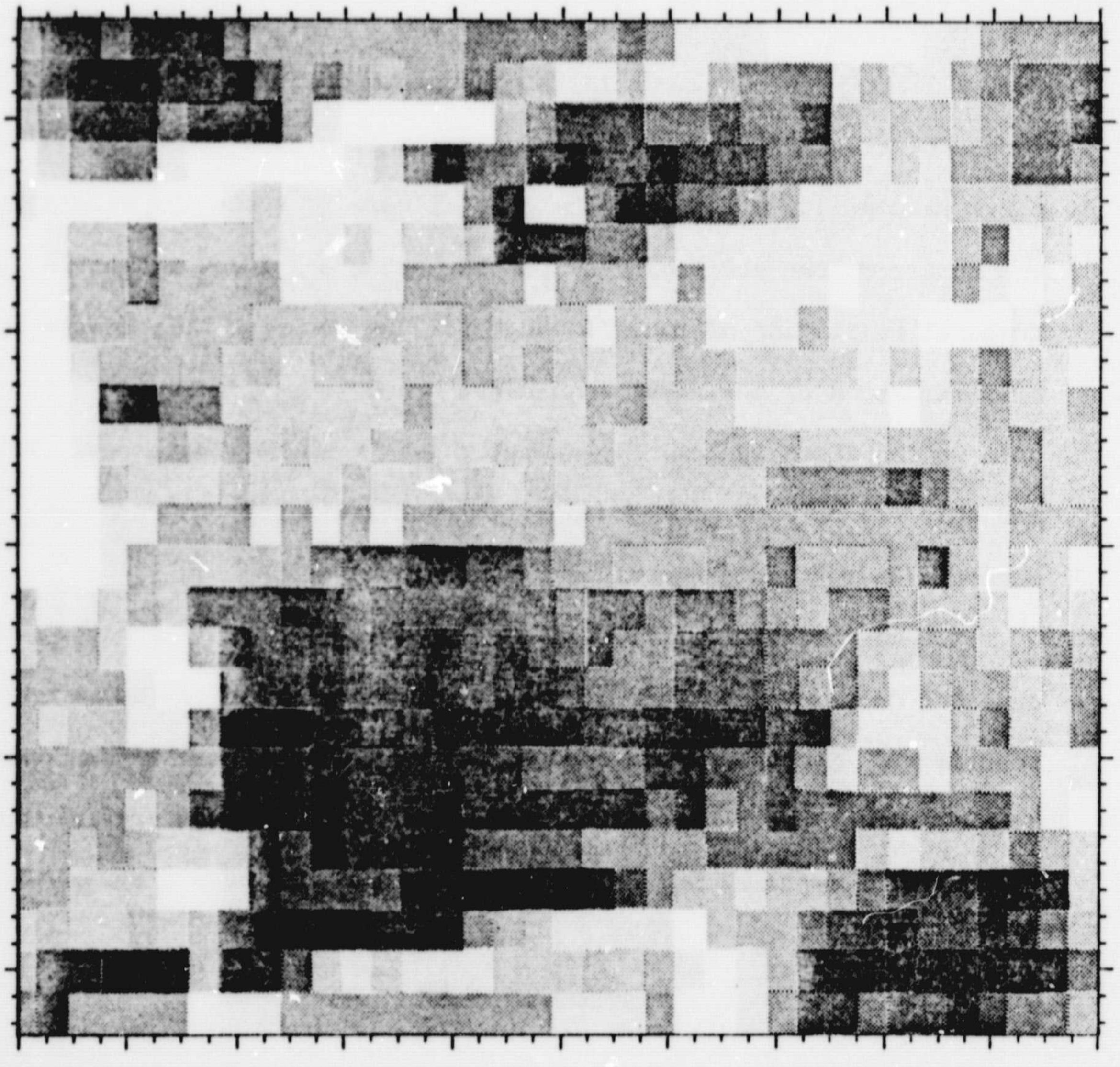

Figure 3. Clustering of the June, 1977 Scene (Band 5).

ORIGINAL PAGE IS
OF POOR QUALITY

Soil water content was previously expressed water per unit mass of soil because most of the soil bulk densities were not available. A preferred expression is water per unit volume of soil. This is a better evaluation of the soil water content since it takes account of soil texture and structure. However its computation requires a correct measure of the soil bulk density, which introduces some error due to soil variability and requires a lengthy laboratory analysis. Table 2 gives the oven dry and 0.3 bar soil bulk densities for most of the ground data soil sites. Values in parenthesis seem questionable.

Another expression of the soil moisture is the available water, which is the moisture retained in the soil between the field capacity (a pressure of 0.3 bar) and the permanent wilting coefficient (15 bars). Values are usually expressed on disturbed (crushed, artifically packed) samples because it is easier and faster to do so. However, such measurements eliminate the soil structure effect and have to be applied with caution to field situations, particularly for low matric potential (wet end of soil moisture range).

A method was developed to measure soil water retention on undisturbed soil cores. Soil cores are sampled using a hydraulic probe, saturated with water, frozen, installed in a special holder (Figure 4), mounted on a diamond saw, and cut to the thickness of the rubber ring used in the pressure chamber.

If the sawing produces a "polish" on the faces, the sample surface is roughened on a grinder covered with a medium sand paper to reopen all the pores.

Table 2. Oven dry and 1/3 bar soil bulk densities for ground data sites.

| | Oven dry density (g/cm$^3$) | | | | | 1/3 bar density (g/cm$^3$) | | | | |
|---|---|---|---|---|---|---|---|---|---|---|
| Soils (Sites) / Depth | - 0-6" | 6-12 | 12-24 | 24-36 | 36.48 | 0-6" | 6-12 | 12-24 | 24-36 | 36-48 |
| Ves (02) | 1.74 | 1.64 | 1.53 | 1.56 | 1.50 | 1.51 | 1.38 | 1.38 | 1.42 | 1.47 |
| Seaforth (03) | 1.39 | 1.32 | 1.32 | 1.38 | 1.48 | 1.18 | 1.15 | 1.15 | 1.26 | 1.35 |
| Letri (05) | 1.21 | 1.39 | 1.41 | 1.51 | 1.56 | 1.04 | 1.16 | 1.26 | 1.45 | 1.44 |
| Everly (05) | 1.46 | 1.39 | 1.40 | 1.42 | 1.47 | 1.32 | 1.32 | 1.30 | 1.30 | 1.34 |
| Okoboji (06) | (.95) | 1.19 | 1.27 | 1.23 | (1.19) | (.87) | 1.04 | 1.06 | 1.03 | (.99) |
| Everly (10) | 1.46 | 1.39 | 1.40 | 1.42 | 1.47 | 1.32 | 1.32 | 1.30 | 1.30 | 1.34 |
| Tara (10) | 1.30 | 1.42 | 1.44 | 1.45 | -- | 1.11 | 1.27 | 1.32 | 1.30 | -- |
| Kranzburg (11) | 1.48 | 1.40 | 1.47 | 1.61 | 1.58 | 1.40 | 1.24 | 1.25 | 1.46 | 1.48 |
| Ves (12) | 1.49 | 1.57 | 1.42 | 1.42 | 1.50 | 1.32 | 1.32 | 1.21 | (1.04) | 1.47 |

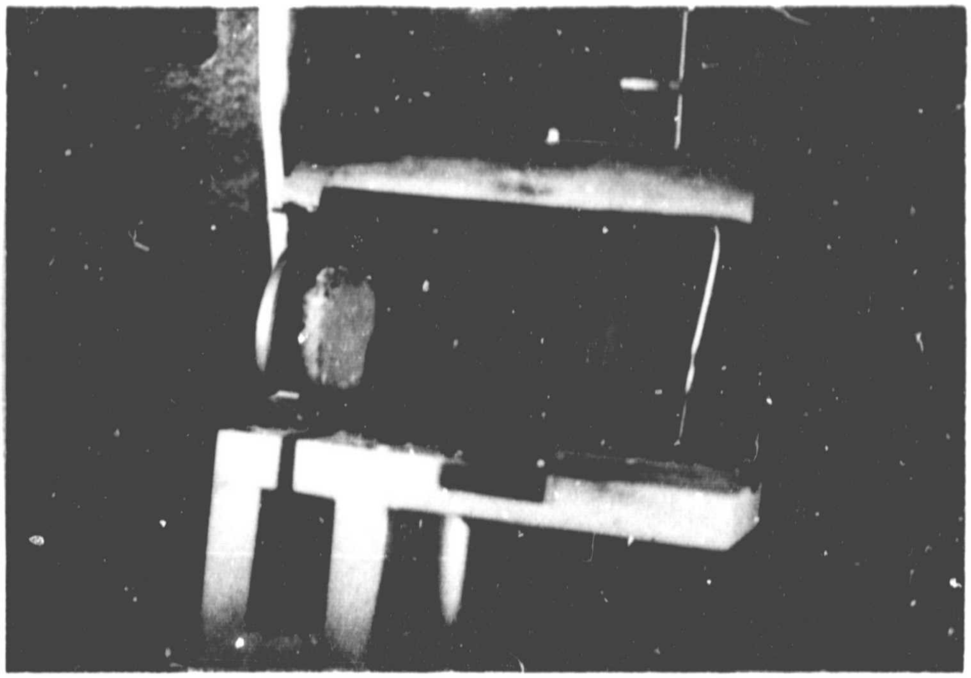

Figure 4. Cut soil core in the special petrographic saw holder.

Table 3 gives a summary of differential water content (disturbed less undisturbed samples) at 0.3 and 15 bars for on site soils. The differential values are statistically highly significant ($p < .001$) at 0.3 bar, but they are not significant at the .05 level for the 15 bars samples ($.05 < p$ value $< .10$). Therefore, water retention at 0.3 bar should always be measured on undisturbed samples.

## ATTEMPT TO DEVELOP REAL TIME AGRICULTURAL MANAGEMENT

The development of timely recommendations for crop and soil management was an initial objective of the project. It appears that this objective cannot presently be accomplished using Landsat data. The acquisition of imagery requires a long delay of at least two months. However,

Table 3. Difference in water content per unit volume between disturbed and undisturbed soil samples at 0.3 and 15 bars.

| Site | | Soil | Depth in inches for well-drained soils | | | | | Soil | Depth in inches for poorly-drained soils | | | | |
|---|---|---|---|---|---|---|---|---|---|---|---|---|---|
| | | | 0-6 | 6-12 | 12-18 | 18-24 | 24-36 | | 0-6 | 6-12 | 12-18 | 18-24 | 24-36 |
| 02 | 1/3 bar | Ves | 1.6 | 5.9 | 5.1 | - | 3.4 | Canisteo | 3.2 | 0.8 | 0 | 4.2 | 0.7 |
| | 15 bars | | -0.9 | -2.0 | - | -5.0 | - | | | | | | |
| 03 | 1/3 | Seaforth | 1.9 | 0.9 | 2.8 | 3.2 | 3.9 | | | | | | |
| | 15 | | -0.5 | -0.4 | 0.5 | 0.6 | - | | | | | | |
| 04 | 1/3 | Clarion | 0.5 | 3.4 | 2.9 | 1.9 | 2.5 | | | | | | |
| | 15 | | -0.5 | 0.5 | -1.3 | -0.1 | - | | | | | | |
| 05 | 1/3 | Everly | 3.8 | 1.9 | 0.7 | 5.2 | - | Letri | 3.0 | 1.4 | 0.4 | 4.5 | 3.6 |
| | 15 | | 0.4 | -1.1 | -0.2 | 1.1 | - | | 1.0 | -0.7 | -1.7 | -0.2 | 0.8 |
| 06 | 1/3 | Ves | | | | | | Okoboji | 8.2 | 9.5 | 3.3 | 2.7 | 8.6 |
| | 15 | | | | | | | | - | - | 0.4 | - | 0.3 |
| 10 | 1/3 | Tara | 5.2 | 4.7 | - | 3.7 | - | Sletten | 5.0 | 3.2 | 6.9 | 1.8 | 3.8 |
| | 15 | | -0.4 | -0.8 | -3.9 | -1.8 | - | | 0 | -1.7 | -0.8 | -1.0 | 0.3 |
| 11 | 1/3 | Kranzburg | | | | | | Hidewood | 6.9 | 4.6 | 5.1 | 4.9 | 4.9 |
| | 15 | | | | | | | | -3.3 | -3.4 | -2.8 | -0.2 | -1.0 |
| 12 | 1/3 | Ves | 3.0 | 2.3 | 3.4 | 6.9 | 5.0 | Webster | -1.0 | 1.5 | -0.7 | - | -0.3 |
| | 15 | | | | | | | | | | | | |

since improvements in processing time and in data resolution are expected in the near future, a cooperative project between the Waseca and Lamberton experimental stations, and twelve farmers located in southcentral and southwestern Minnesota (see Figure 5) was started in Spring 1979 to test the practical use of remote sensing techniques for "on time" corn and soybean field management.

The objective was to give the cooperators, throughout the growing season, a color infrared print within ten days of flight date at approximately 1:10,000 scale and contain interpretation of soils - and crop-conditions on an overlay (Figure 6). Information which can be extracted from aerial photographs includes germination success (equipment failure, disease, herbicide effectiveness), a check on stand growth and development (plant damage, misapplication of chemicals), drainage effectiveness, soil moisture stress, harvesting problems (lodging, weed infestation, variable ripening), regrowth pattern, and hail, wind and flood damages.

Unfortunately, the cloudy conditions encountered during most of the 1979 growing season allowed only two flights, July 15 and September 16. Table 4 gives the features we were able to distinguish on the September photographs. An important practical result was to show a precise spatial distribution of drainage effectivness.

Interest in continuing the project was expressed at the evaluation meeting held in St. James on November 14 by the farmers, county agents and extension agents.

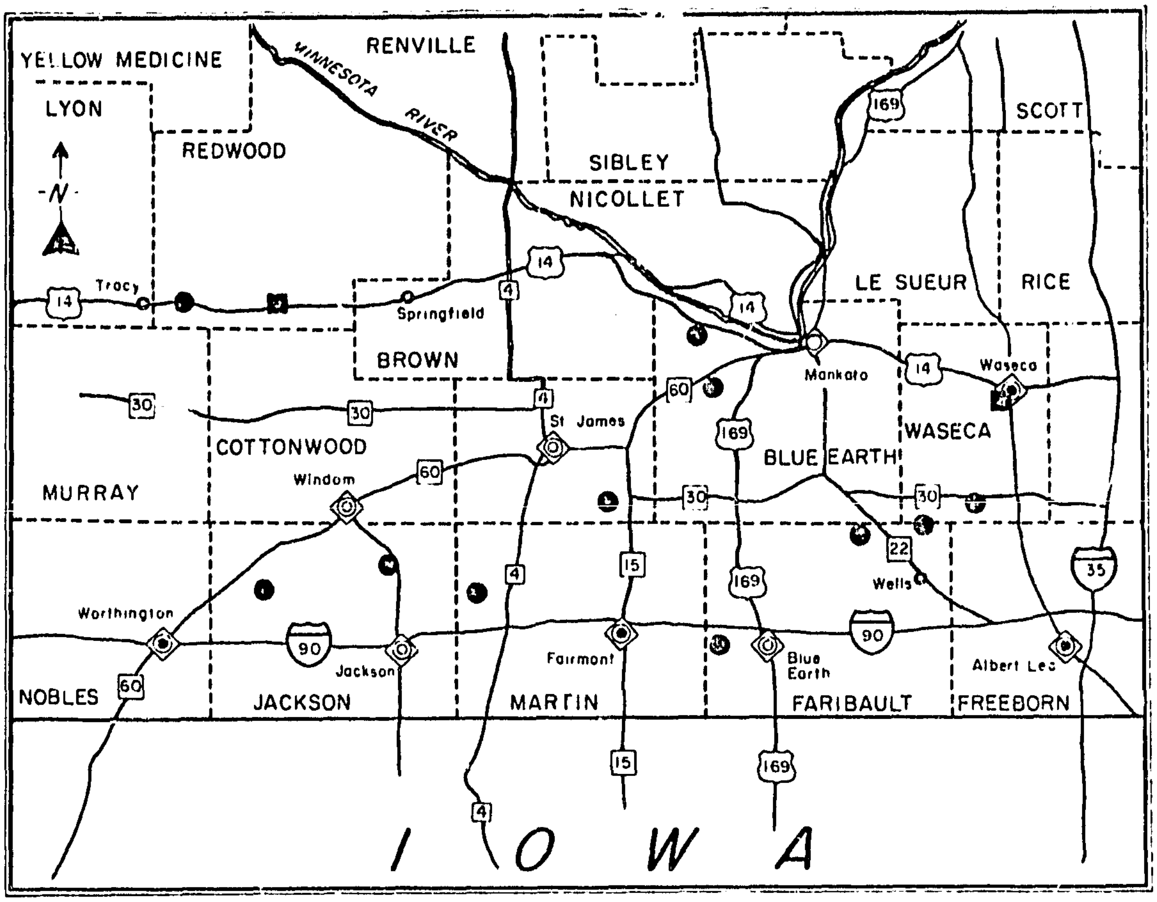

Figure 5. Locations of Cooperators in the Agricultural Management Project

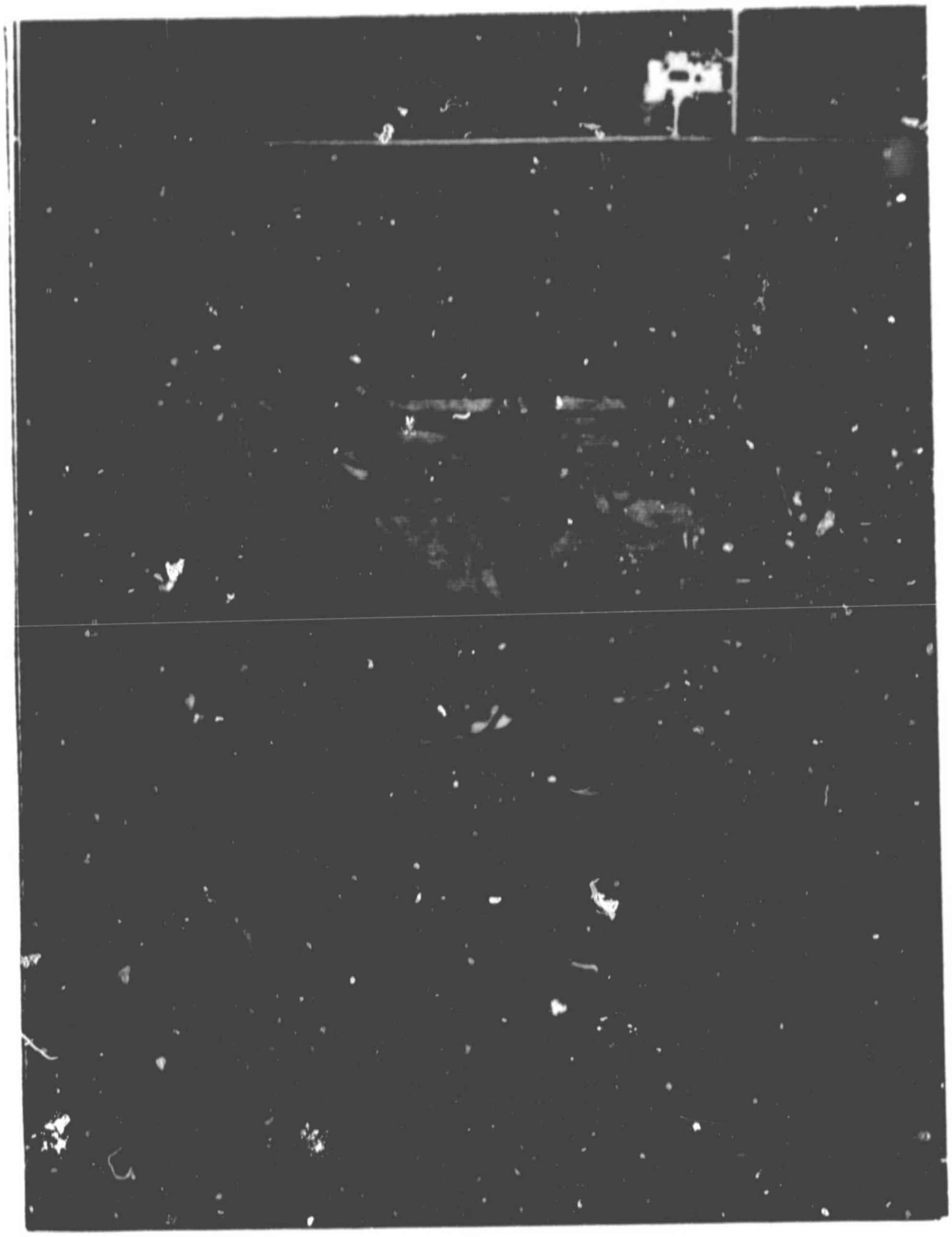

ORIGINAL PAGE IS
OF POOR QUALITY

Figure 6. Color infrared print with interpretation of soils and crop conditions (at 1:10,000 scale).

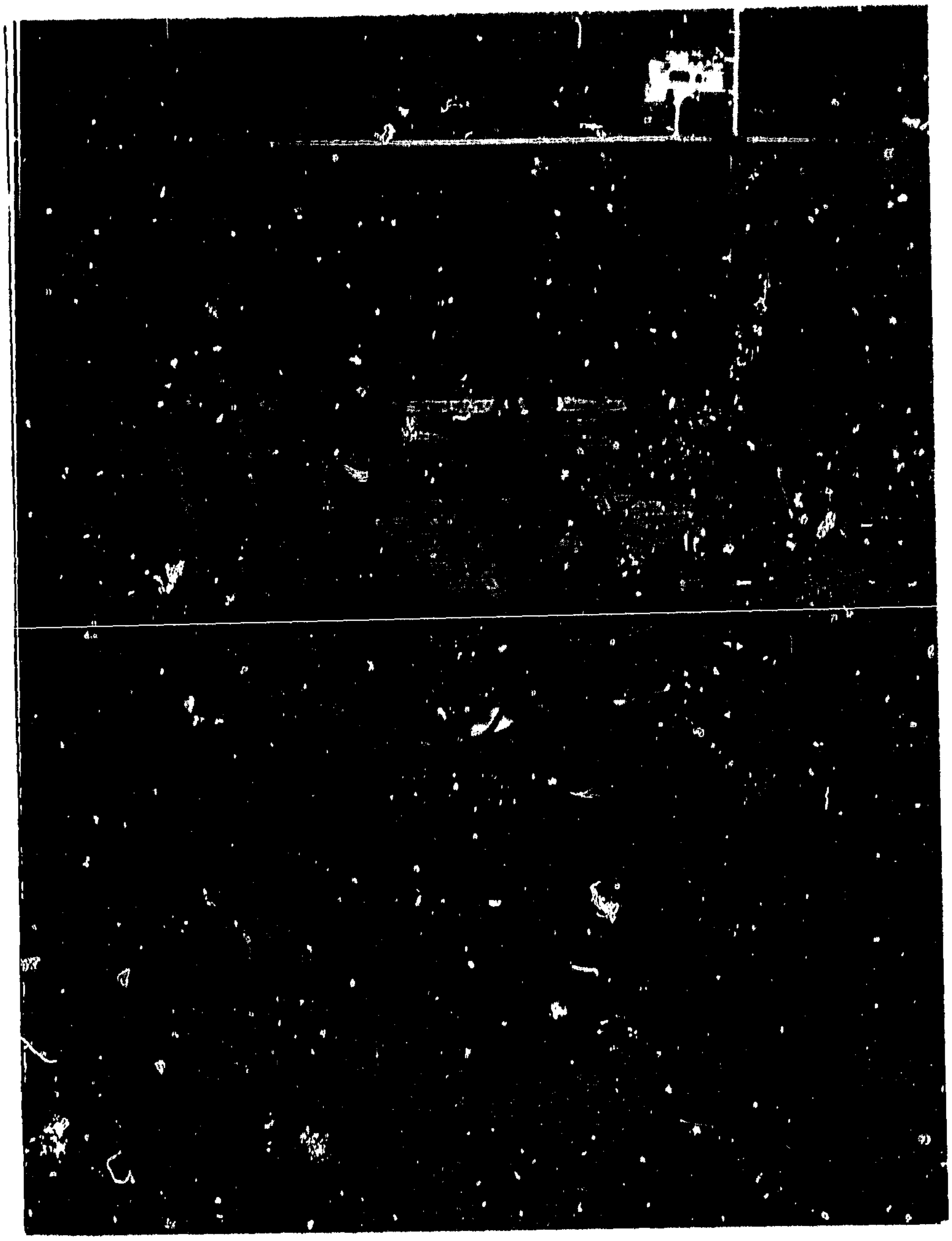

ORIGINAL PAGE IS
OF POOR QUALITY

Figure 6. Color infrared print with interpretation of soils and crop conditions (at 1:10,000 scale).

Table 4. Interpretative legend for the September 16 photographs.

1 : slight reduction in growth or crop stand by excess of moisture;

2 : significant reduction in growth or crop stand by excess of moisture;

3 : plant loss or damage by high excess of moisture;

5 : reduced growth by soil erosion.

S1: (greenish color) soybeans, reduced stand, delayed maturity.

S2: (brownish color) soybeans, good stand;

C1: (darker brown) corn, reduced stand, delayed maturity;

C2: (lighter brown) corn, good stand;

B1: (darker green) bare field, poorly drained soil type;

B2: (lighter green) bare field, well drained soil type;

T1: (light tone) thin surface horizon, sandy;

T2: (light tone) thin surface horizon, high lime;

Df: differential maturity related to planting date or seed variety;

W : (reddish color) significant weed problem;

? : unknown problem.

## SUMMARY AND CONCLUSIONS

The 1979 growing season received significantly above average precipitation in the study area. As a result, the poorly drained soils had some moisture excess which probably will be reflected in the LANDSAT data.

As a result of the wet season, the percentage of cloud cover was also higher than usual. This greatly reduced the availability of LANDSAT scenes. There are only 3 scenes available with less than 10% cloud cover for the study area. There is no usable scene available from June 6 to September 20, 1979.

Corn leaf reflectance does not show a strong relationship with plant stress or plant water potential as measured with the technique used for soybeans in the 1978 greenhouse experiment. Additional measurements will be made in 1980.

Hail-damaged areas show a characteristic signature on the LANDSAT black and white infrared product. Further identificaion will be tested using the digital data.

Information extraction from the 1977 digital tapes was performed at the Eros Data Center using the IMAGE 100 and the IDIMS systems. The study of one site showed that crop identification is feasible using temporal signatures. But because of uniformly excellent crop conditions, reflected in nearly homogeneous signatures, it was not possible to make further differentiations, e.g., soil drainage classes.

To evaluate more accurately the soil water content of the ground data sites, their soil bulk densities and soil water retentions at 0.3

and 15 bars were measured. A method to prepare undisturbed soil samples was developed. A highly significant difference in water retention was found between disturbed and undisturbed samples at 0.3 bar. Undisturbed samples should be used.

A cooperative project between the Waseca and Lamberton Experiment Stations and 12 farmers tested the feasibility of using remote sensing techniques for real time agricultural management. The objective was to produce, within 10 days of the flight date, color infrared prints and interpretation of soils and crop conditions related to plant growth, equipment failure, chemical efficiency, drainage effectiveness, and stress as a result of moisture extremes, hail, and diseases. Cloud cover and the processing time of color infrared films were the two main problems. Positive results were obtained such as indication of a need of drainage, weed control, and the management of eroded fields. Interest in continuing the project was expressed by the cooperators.

## REFERENCES

Rust, R. H. and P. Robert. 1977. Evaluation of soil moisture stress in W. and SW. Minnesota. Section F in NASA Progress Report (NGL 24-005-263, Vol. XI).

Rust, R. H. and P. Robert. 1978. A project to evaluate moisture stress and weather modification procedures in Corn and Soybean areas of W. and SW. Minnesota. Section B in NASA Progress Report (NGL 24-005-263, Vol. XII).

D5

N81-12510

## SECTION E

# MEASUREMENT OF SUSPENDED SOLIDS IN LAKES AND OCEANS USING SATELLITE REMOTE SENSING DATA

Dr. Michael Sydor
Department of Physics
University of Minnesota, Duluth
Duluth, Minnesota

---

## INDEX

---

# MEASUREMENT OF SUSPENDED SOLIDS IN LAKES AND OCEANS USING SATELLITE REMOTE SENSING DATA

Investigator: Dr. Michael Sydor
Department of Physics
University of Minnesota, Duluth
Duluth, Minnesota

## ABSTRACT

Using satellite remote sensing data to measure low concentrations of suspended solids in lakes and oceans requires careful evaluation of background signals from the atmosphere and the water surface. We present here typical background corrections for Lake Superior and determine the spectral distribution of the residual radiance from three major categories of turbidity in the lake. The results indicate that for large bodies of water, some general information on atmospheric scattering, water clarity, and the optical properties of suspended solids allows estimates of concentrations of suspended solids to within ± 0.5 mg/ℓ without using real time ground truth data. Under calibrated conditions the threshold detection level is 0.3 mg/ℓ for the fine particulates dispersed throughout the lake and 1 mg/ℓ for the highly light absorbing effluent from rivers. Comparisons of the minimum reflectance over the open lake areas with reflection from the highly absorbing tannin water from rivers, provides a check on the clarity of the atmosphere and the excessive background scatter from the water surface.

## METHOD AND RESULTS

The spectral and the angular distributions of radiance from Lake Superior were measured with an optical probe which has a flat response from 400 to 900 nm. The detector had an acceptance cone of 5.65 x $10^{-2}$ steradians and an area of 1 $cm^2$. The spectral distributions of radiance were measured using a set of filters spanning the 380 to 1050 nm range. The filters had nominal band pass values of 10 nm. Measurements of the direct solar intensity were made with the probe and with an auxiliary narrow-angle NASA radiometer designed to measure the optical thickness of atmosphere.

The direct solar radiation per unit area normal to the incident solar ray is shown in Figure 1. The time of the measurements coincided with the LANDSAT 2 overpass. The sun elevation was 57°. The measurements represent average radiation for June 24, 26, 27, and 29, 1979. Curve 1 in Figure 1 is based on solar radiation values at the top of the atmosphere. The values are based on measurements by Thekaekara (1971) and are accepted as standard by NASA (Coulson 1975). Curve 2 shows the radiation at lake level.

The angular dependence of the radiation from Lake Superior was measured at several angles in the incidence plane (the plane containing the solar incidence ray and the normal to the water surface). The measurements were made looking towards the sun (forward angles), away from the sun (backscattered), and at right angles to the plane of incidence (side-scattered). Forward scatter is susceptible to glare and is not generally used in remote sensing of suspended solids. For light emerging at angles near the Zenith, the backscattered and sidescattered radiances were similar when the sea conditions were calm. The radiances at the Zenith were devoid of the excessive specular reflection. However, at angles approaching 45° from the Zenith, the specular reflection of sky light overwhelmed the backscattered signal due to volume reflectance, as shown in Figure 2. The intensity and the spectral distribution of the overhead sky light, measured at 90° to the solar incidence along a line in the plane of incidence, are shown in Figure 3. The overhead sky intensity provides a measure of the specular reflection by the water surface. The specular reflection must be subtracted from radiance measurements to determine the residual radiance from the particulates. Figure 4 shows the spectral distribution of radiance for calm water containing less than 0.2 mg/ℓ of suspended solids. The radiances are measured near the nadir unless otherwise specified. The radiance in Figure 4 is broken down into the specular component, taken as 6% of the overhead sky intensity, and the remainder of the signal which is attributed to the volume scattering from the 0.2 mg/ℓ concentration of suspended solids. This remaining signal is assumed to be the volume reflectance by the carrying medium.

In analysis of remote sensing data for turbid water where concentrations exceed 1 mg/ℓ, the scatter from the carrying medium was diminished exponentially according to the ratio of secchi transparencies. The correction term is small, so the use of secchi transparencies is justified. Although the secchi transparencies are not precisely measureable, the parameter is a convenient and commonly available measure of the transparency of lakes and oceans. The decrease in the scatter from the carrying medium is important because it implies that for highly turbid or highly absorbing water, the background is due mainly to atmospheric scattering and specular reflection by the water surface. This provides an important check on the clarity of the atmosphere and the clarity of water in the reference area when real time ground truth data are not available. For instance, when the minimum signal in the image is high because the reference area, assumed to be clear water, actually has turbidity on the order of 1 mg/ℓ, the corresponding residual radiance from the known areas of highly absorbing tannin water will be unusually low or negative in band 4 of the Landsat data. In a known system this will serve as a test of the assumption that the minimum reflectance area contains clear water. On the other hand, if the subtraction of the minimum radiance in the image yields residual radiances which are high in band 4 over the normally clear open lake areas and the areas with highly absorbing water, then the excessive background for the day is due to a turbid atmosphere.

The dependence of volume reflectance on angle is shown in Figure 5. The scatter is quite flat over the angles encompassing the range of LANDSAT observation angles and the acceptance angles for the probe, when measurements were made at or near nadir.

To obtain residual radiance due to turbidity, the measurements were corrected for surface and volume scattering according to Figure 4. As previously stated, the volume reflectance from the carrying medium was reduced exponentially according to the average secchi transparencies. Figures 6, 7 and 8 show the spectral distribution of the residual radiance for red clay, taconite tailings, and tannin. These are the dominant

111

types of suspended solids in Lake Superior. The fine red clay particulates shown in Figure 6 originate from extensive erosion along the Wisconsin shore of Lake Superior. Banks of clay are also present near Ontonagon, Michigan. Erosion of clay is the dominant natural source of inorganic particulates in the lake. The reflected sunlight peaks at 630 nm for the red clay. Red clay concentrations from 1 -15 mg/ℓ cover large sections of the lake, especially in extreme western Lake Superior.

Taconite tailings give a residual reflectance peak at 560 nm. The tailings are discharged from a point source at Silver Bay, Minnesota. The discharge, in excess of 6 x $10^4$ tons/day, causes extensive plumes ranging in concentration from 1 to 4 mg/ℓ. Some of the fine tailings and the red clay particulates spread throughout the lake and form the main background of suspended solids in western Lake Superior.

Tannin is a term applied to the brown colored river water common around Lake Superior. Tannin is highly organic (∿ 35%). It has low transparency, with secchi lengths ranging from .5 - 2 m in comparison with 3 - 5 m for western Lake Superior containing ∿ 1 mg/ℓ of red clay or tailings. The background clear water exceeds 10 m secchi transparency.

Figure 9 shows the spectral distribution of radiance from rough seas. It was obtained from the difference between radiance measured by looking into the wind (corresponding in this case to the sidescatter angles) and the backscattered radiance at right angles to the wind.

The spectral distribution of the residual radiances allow us to identify particulates in the lake (Sydor, Stortz, and Swain 1978). Using the data in Figures 5 and 6 we can estimate the reflectance for each particulate type and concentration. We can also treat mixtures of particulates, since the reflectances are reasonably linear with the concentrations as shown for red clay in Figure 6. However, to be able to use the data in conjunction with the remote sensing information from the satellites, one needs to be able to predict the radiances at the satellite altitude. Furthermore, one needs to account for the seasonal changes in solar radiation at lake level and the attenuation of the residual radiance by the atmosphere. The attenuation by atmosphere can be obtained from Figure 1 by taking the ratio of the solar radiation at the lake and at the top of the atmosphere. The seasonal variation of the minimum background radiance from clear water and the atmosphere is shown by curve 1 in Figure 10. This variation arises mainly from the effects of solar elevation and changes of atmospheric attenuation at various solar angles (Coulson 1975). The broken line in Figure 10 approximates the effect of solar elevation and is given by

$$R = R_o(\cos\beta + \alpha\sec\beta)e^{-\mu\sec\beta}$$

where R is the radiance for clear water and clear atmosphere, β is the Zenith angle of the sun, α is the scattering coefficient for one atmosphere, and μ is the absorption coefficient for one atmosphere, which can be evaluated from Figure 1. The limits of fluctuation for background radiance are shown by curve 2 in Figure 10. The shape of curve 2 departs from the seasonal behavior during the winter. This departure can be attributed to rescattering. During the summer and fall the albedo over the lake is low. Thus correction for atmospheric rescattering of the light reflected from waters adjacent to the observation area can be ignored. In the winter a high albedo from snow and ice packs surrounding the observed water area accounts for a substantial increase in the sky light intensity. In the summer and fall curve 2 also corresponds to the reflectance for .5 mg/ℓ of suspended solids and minimum atmospheric and surface background. In a sense curve 2, for May - November constitutes the average background radiance for the western Lake Superior. The .5 mg/ℓ concentration is an equilibrium concentration of particulates in extreme western Lake Superior. The open lake waters in western Lake Superior stay within the .2 - .8 mg/ℓ limits 97% of the time. Curve 2 is the upper limit on the acceptable background signal level for routine analysis of remote sensing data in the absence of the real time ground truth data. The atmospheric effects are most pronounced in band 4. For bands 5 and 6 only the best fit to minimum background values is given in Figure 10. Figure 11 shows the direct and diffuse components of solar radiation. The curves were obtained by fitting equation (1) to the minimum values of background radiation for clear atmosphere in bands 4, 5, and 6. This determined $\alpha$, $\mu$, and $R_o$. By scaling $R_o$ to the value of solar radiation at the top of the atmosphere, we obtain solar radiation at lake level. The first term gives the direct component, while the second one approximates the diffuse component. The diffuse component is not the same as the total sky light.

## PROCEDURE FOR REMOTE SENSING DATA ANALYSIS

When real time sampling data are available, the background signal can be calculated and subtracted from the image to produce residual radiances for the suspended solids. However in analysing satellite data without ground truth, we first examine the image to locate the open lake area with the minimum signal. If the lowest intensity on the image for the open lake areas lies within the 0.2 mg/ℓ - .5 mg/ℓ limits shown in Figure 10, an assumption of .2 mg/ℓ suspended solids and clear atmospheric conditions is made. The residual radiance at satellite altitude is then obtained by subtracting from the image intensities the minimum background intensity given by curve 1 in Figure 10. The resulting data can subsequently be used to identify suspended solids to determine their concentrations according to Figures 6, 7, and 8. However, if the minimum signal in the image is substantially above the .2 - .5 mg/ℓ limits shown in Figure 10, a determination must be made of whether the background is high because of high overall turbidity of the water or because of excessive atmospheric scattering. Visual examination for extensive plumes, thin clouds or haze can be made. Normally, only tapes with clear images of the lake are purchased. However, a test of excessive background signal levels can be made by first subtracting from the image the minimum background according to curve 1, Figure 10, and then examining whether the excess in the background has the spectral character attributable to the atmosphere (according to Figure 11), rough seas (Figure 9), or suspended solids, (according to Figures 6, 7, and 8). If the spectral dependence of the excess in background indicates that the atmosphere is turbid, the satellite data may still be usable provided the atmospheric turbidity is uniform. However, the resulting error for the estimates of concentration of suspended solids can be as high as 1 mg/ℓ and the identification of the suspended solids at low concentrations will be hampered because of the unpredictable spectral behavior of the turbid atmosphere.

The unambiguous identification of the suspended solids relies on identifying the spectral shape of the residual radiance, and it requires a signal at least two or three digital steps above background. This in turn requires that the horizontal concentration gradients in suspended solids be large enough to provide a change of 1 mg/ℓ for red clay and tailings and of 3 mg/ℓ for tannin, over the entire area of the lake covered by the image. Such gradients are readily available for most images containing near shore areas and are usually satisfied in the images of Great Lakes. However, this condition does impose some bothersome restrictions. In Lake Superior, for example, tannin concentrations in the lake must be usually compared with those in the Duluth harbor, or a comparable tannin area large enough to be well resolved in the image.

Although unambiguous identification of particulates from LANDSAT data cannot be made for concentrations lower than 1 mg/ℓ in absence of ground truth data, estimates of suspended solids concentration can be made to within .5 mg/ℓ above background. Furthermore, some decisions on the identity of particulates can also be made at those concentration levels. When no ground truth is available, but the lowest reflectance over the lake is within the clearly acceptable background limits, the assumption of .2 mg/ℓ concentration for the lowest intensity area introduces a probable error of ± .3 mg/ℓ in the estimates of concentration of red clay and the tailings. The identity of the low concentration of suspended solids can also be deduced from spectral dependence based on magnitude of signals in two bands. For western Lake Superior, for instance, the background is usually red clay or tailings, so the decision on the identity of the low concentration of particulates in the lake can be made by examining the relative magnitude of the signal in bands 4 and

5. For the tannin water, which usually has higher intensity in band 6 than band 4, the identity can be based on the relative signal in bands 6 and 4. Unfortunately, concentrations of tannin lower than 1 mg/ℓ cannot be detected in LANDSAT data. At high concentrations, various algorithms can be devised to automatically extract from the residual radiances the identity and concentrations of the suspended solids. Figures 12, 13, and 14 show application of previously published algorithms (Sydor, Stortz, and Swain 1978) to the data for June 29, 1979. The identity of suspended solids in the image agrees closely with the sampling data all along the transects of our 1979 cruise of the western Lake Superior.

## COMPARISON OF CALCULATED AND MEASURED RADIANCE AT SATELLITE ALTITUDE

To examine how well the results in the previous sections can be used to analyse remote sensing data, we calculate the radiances at the satellite altitude and compare them with the satellite data for specific sampling sites on Lake Superior. The sampling points are shown in Figure 15. These points correspond to some of the stations for our 1979 experimental cruise of Lake Superior using research vessel Crockett.

The predicted radiance values shown in Table 1 are close to the observed satellite values. The corrections for atmospheric attenuation were taken into consideration according to Figure 1. The satellite data were obtained from the Canada Centre for Remote Sensing. The Canadian data for LANDSAT 2 provides a signal resolution level of 1/255.

Some results discussed in previous sections are evident from Figure 15 and Table 1. Notice, for instance, that the signal level in band 4 for the Duluth harbor tannin water is lower than the signal in the open

| Station | | Minimum Background at Satellite | | | Residual Radiance | | | | | | Expected Radiance at Satellite | | | Landsat 2 Radiances | | |
|---|---|---|---|---|---|---|---|---|---|---|---|---|---|---|---|---|
| | | | | | at Ground | | | at Satellite | | | | | | | | |
| Western Lake Superior | Landsat Bands | 4 | 5 | 6 | 4 | 5 | 6 | 4 | 5 | 6 | 4 | 5 | 6 | 4 | 5 | 6 |
| | Clean Water | .26 | .11 | .07 | | | | .06 | .04 | .01 | | | | .32 | .15 | .08 |
| A | Tailings 1.8 mg/ℓ | .26 | .11 | .07 | .124 | .089 | .026 | .11 | .08 | .021 | .37 | .19 | .09 | .37 | .18 | .09 |
| B | Red Clay 8 mg/ℓ | .26 | .11 | .07 | .196 | .21 | .07 | .175 | .19 | .06 | .44 | .30 | .13 | .45 | .29 | .13 |
| C | Tannin 3 mg/ℓ | .26 | .11 | .07 | .093 | .096 | .045 | .083 | .086 | .036 | .34 | .20 | .11 | .35 | .21 | .11 |

Radiances in mw/(cm$^2$SR)

Overall background turbidity in western Lake Superior shows spectral character most like tailings having concentration 1 mg/ℓ - actual value .8 mg/ℓ. Tailings at station A 1 mg/ℓ above background - just on the verge of positive identification from Landsat data.

Table 1.

lake areas. This indicates excessive background. Thus in absence of real time ground truth data, a check on the lowest background signal could have been made to ascertain the clarity of the atmosphere or the clarity of the open lake water. In this case it would have shown that the overall turbidity of the lake was high. The spectral character of the residual signal for low intensity open lake areas indicates, according to Table 1, approximately a 1 mg/ℓ background of tailings. Actually the open lake was more turbid than normal, having a background suspended solids of level of .7 mg/ℓ of tailings. Thus it is realistic to assume that for background conditions falling within the accepted values shown in Figure 10, an estimate of the suspended solids could be made to within ± .5 mg/ℓ in absence of the ground truth data. Nimbus G data promise to provide an even better sensitivity for Lake Superior work. However, the angular dependence for the volume and surface scattering may be more difficult to handle in the Nimbus G data. In anticipation of Nimbus G data, it is interesting to compare the spectral shape for the difference in volume reflectances observed at a 40° Zenith angle, for 8 mg/ℓ and 14 mg/ℓ red clay concentrations. This difference is shown in Figure 16. We notice that measurements at Zenith for the 5.6 mg/ℓ concentration yield a similar spectral response. We might thus expect that for Zenith angles smaller than 40° (Figure 2), we might still be able to use remote sensing data from the Nimbus Coastal Zone Scanner to identify the particulates in plumes, without resorting to elaborate models for angular scattering by small particulates.

## FIGURE CAPTIONS

Figure 1. Direct solar radiation at lake level. The experimental values represent 4 day averages. Measurements were made in .01 μm bands spaced at 05 - .08 μm intervals. Curve 1 shows the reference radiation at the top of the atmosphere, which is based on standard N.A.S.A. values derived from measurements by Thekaekara (1971).

Figure 2. Angular distribution of 0.4 - 0.9 μm light backscattered and specularly reflected from clear lake water (.2 - .5 mg/ℓ suspended solids). Measurements were made in the plane of incidence with the instrument pointing away from the sun. Specular reflection of sky light becomes dominant at Zenith angles exceeding 40°.

Figure 3. Diffuse overhead solar radiation measured in the plane of incidence, along a line perpendicular to the incident sun ray. The sun was at 23° Zenith angle.

Figure 4. Curve 1 shows the spectral distribution at nadir of the radiance from clearest lake water (less than .2 mg/ℓ suspended solids). Curve 2 shows the fraction of this radiance attributable to specular reflection of the overhead sky light by the calm water surface.

Figure 5. Laboratory determination of the angular distribution of .646 μm light scattered by fine red clay particulates and fine mining waste particulates. These particulates are the prevalent constituent of suspended solids in western Lake Superior.

Figure 6. Spectral distribution at nadir of light reflected from red clay turbidity in Lake Superior. The residual radiance from particulates is linear for concentrations of suspended solids lower than 10 mg/ℓ.

Figure 7. Spectral distribution at nadir of light reflected from mining tailings. Tailings often upwell from a broad deposit of discharge slurry at the bottom of the lake.

Figure 8. Spectral distribution at nadir of light reflected from highly organic, opaque river water commonly referred to as tannin. The above turbidity contained .5 mg/ℓ of red clay particulates.

Figure 9. Spectral distribution at nadir of light scattered from rough seas (white caps). The reflectivity has a flat spectral dependence. Rough seas can be easily identified in remote sensing data because of their high reflectance at long wavelengths (.8 - 1.1 μm) and unstructured geometric patterns.

Figure 10. Seasonal behavior of the background radiance due to light scattered by the atmosphere, the water surface, and the low concentration of particulates in clear water (.2 mg/ℓ suspended solids). The volume scatter by the clear water is taken as the intrinsic scatter by the carrying medium. Curve 1 represents LANDSAT derived measurements of radiance in band 4 (.5 - .6 μm) for the clearest atmospheric conditions. Curve 2 corresponds to the maximum value of acceptable radiance from clear water and uniform atmosphere - defining the clear viewing conditions when straightforward analysis for suspended solids may be made in absence of real time ground truth data. The broken line in band 4 corresponds to the seasonal dependence of radiance as a function of sun elevation. The curves for band 5 (.6 - .7 μm) and band 6 (.7 - .8 μm) show average radiance for clear viewing conditions. The minimum cutoff radiance in bands 5 and 6 for LANDSAT 2 and 3 is indicated by the dotted lines.

Figure 11. Curves 1, 2, and 3 show the calculated values of direct solar radiation at lake level for bands 4, 5, and 6 respectively. Curves A, B, and C give the respective total solar radiations in bands 4, 5, and 6, including the diffuse component from the overhead sky. The experimental points represent measurements of the direct solar radiation plus the fraction of forward scattered sunlight included within the acceptance angle of the instrument.

Figure 12. Distribution of red clay particulate (in excess of .5 mg/ℓ) in western Lake Superior. The identifications for suspended solids are based on the relative magnitudes of the residual LANDSAT intensity readings in bands 4, 5, and 6 and the ratios of the residual intensities.

Figure 13. Distribution of mining waste tailings in the 1 - 1.5 mg/ℓ range.

Figure 14. Distribution of output from the St. Louis River (lower left corner) into western Lake Superior. The output from smaller rivers in Wisconsin can also be seen along lower shoreline.

Figure 15. Band 4, LANDSAT 2 digital output averaged over 90 pixels. Note the low readings in the lower left corner of the image showing the St. Louis River estuary and the Duluth harbor. The overall turbidity in the lake is higher than average, thus opaque river water shows lower apparent background than the open lake areas.

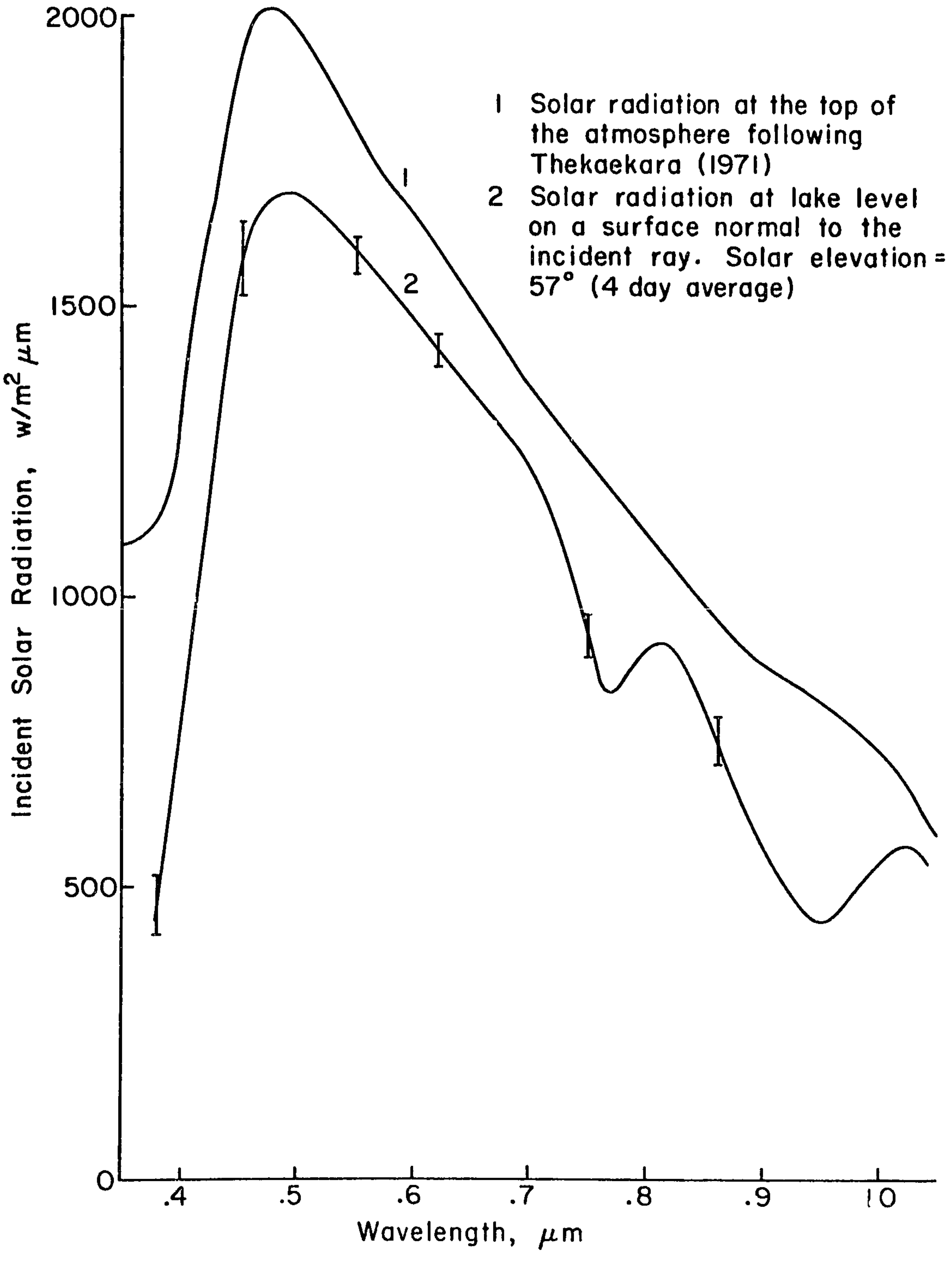
2000
1500
1000
500
0
Incident Solar Radiation, w/m² μm
.4
.5
.6
.7
.8
.9
1.0
Wavelength, μm
1
2
1 Solar radiation at the top of the atmosphere following Thekaekara (1971)
2 Solar radiation at lake level on a surface normal to the incident ray. Solar elevation = 57° (4 day average)

Figure 1

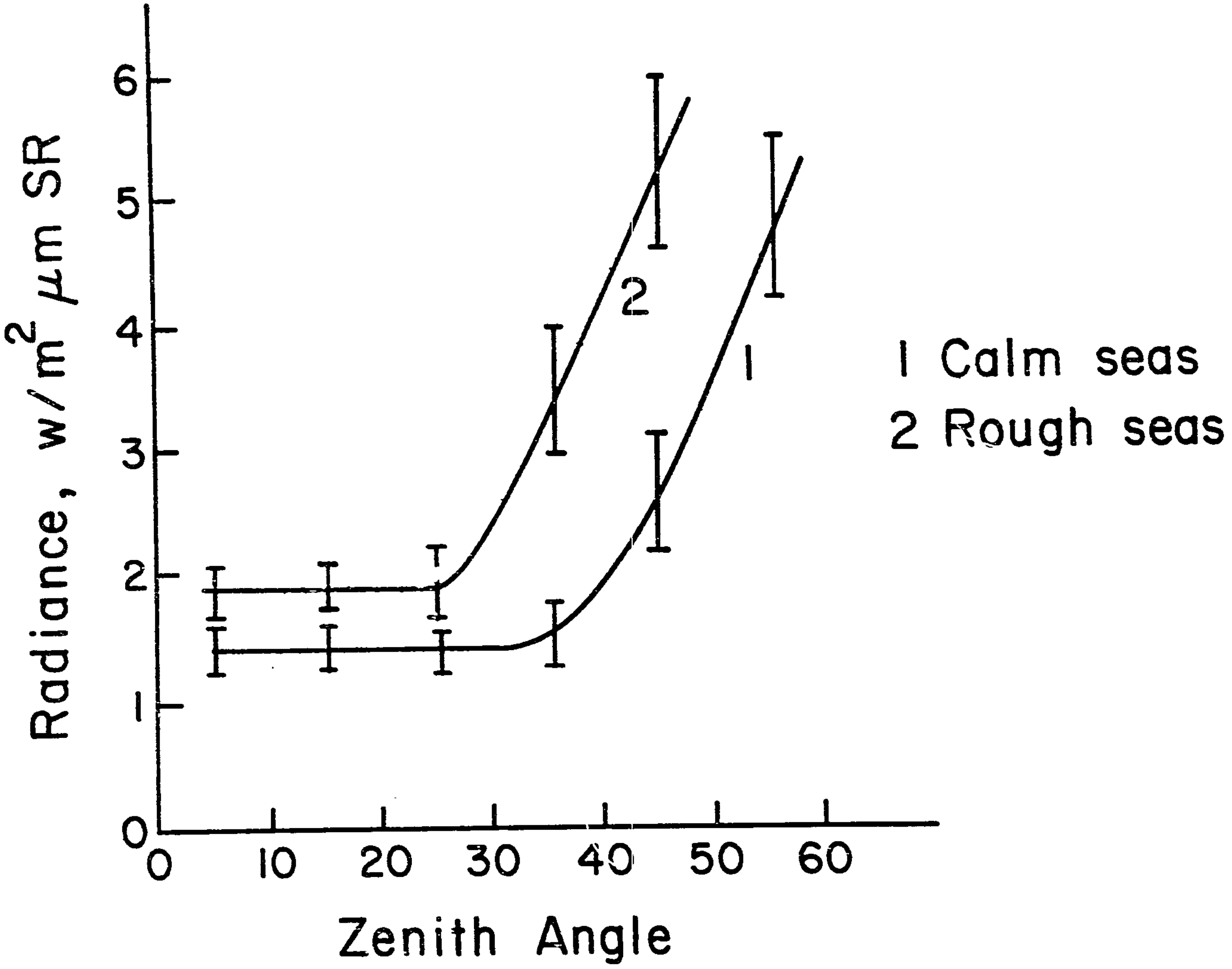
Radiance, $w/m^2 \mu m$ SR
0
1
2
3
4
5
6
Zenith Angle
0
10
20
30
40
50
60
1
2
1 Calm seas
2 Rough seas

Figure 2

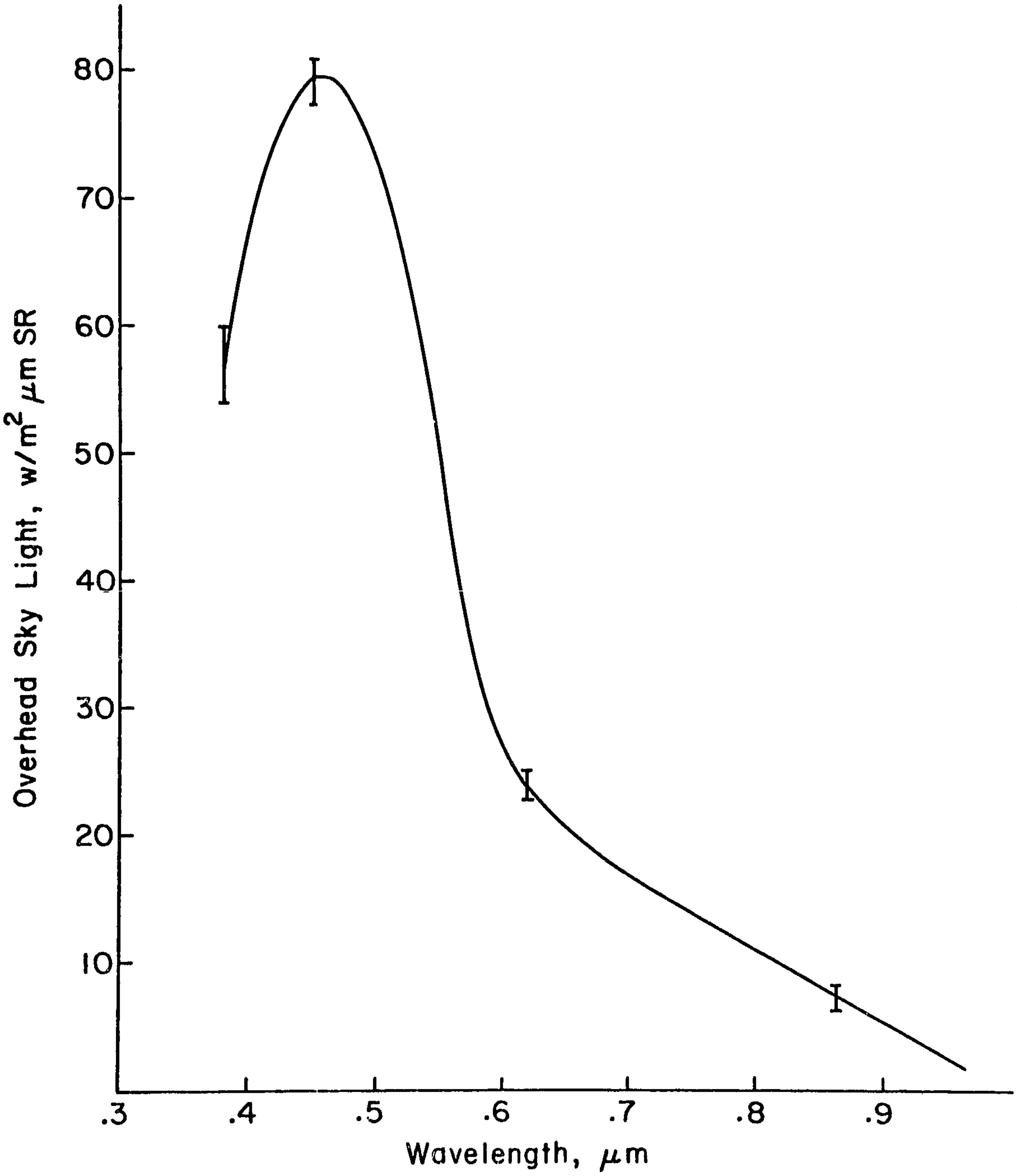
Overhead Sky Light, w/m$^2$ $\mu$m SR
80
70
60
50
40
30
20
10
.3
.4
.5
.6
.7
.8
.9
Wavelength, $\mu$m

Figure 3

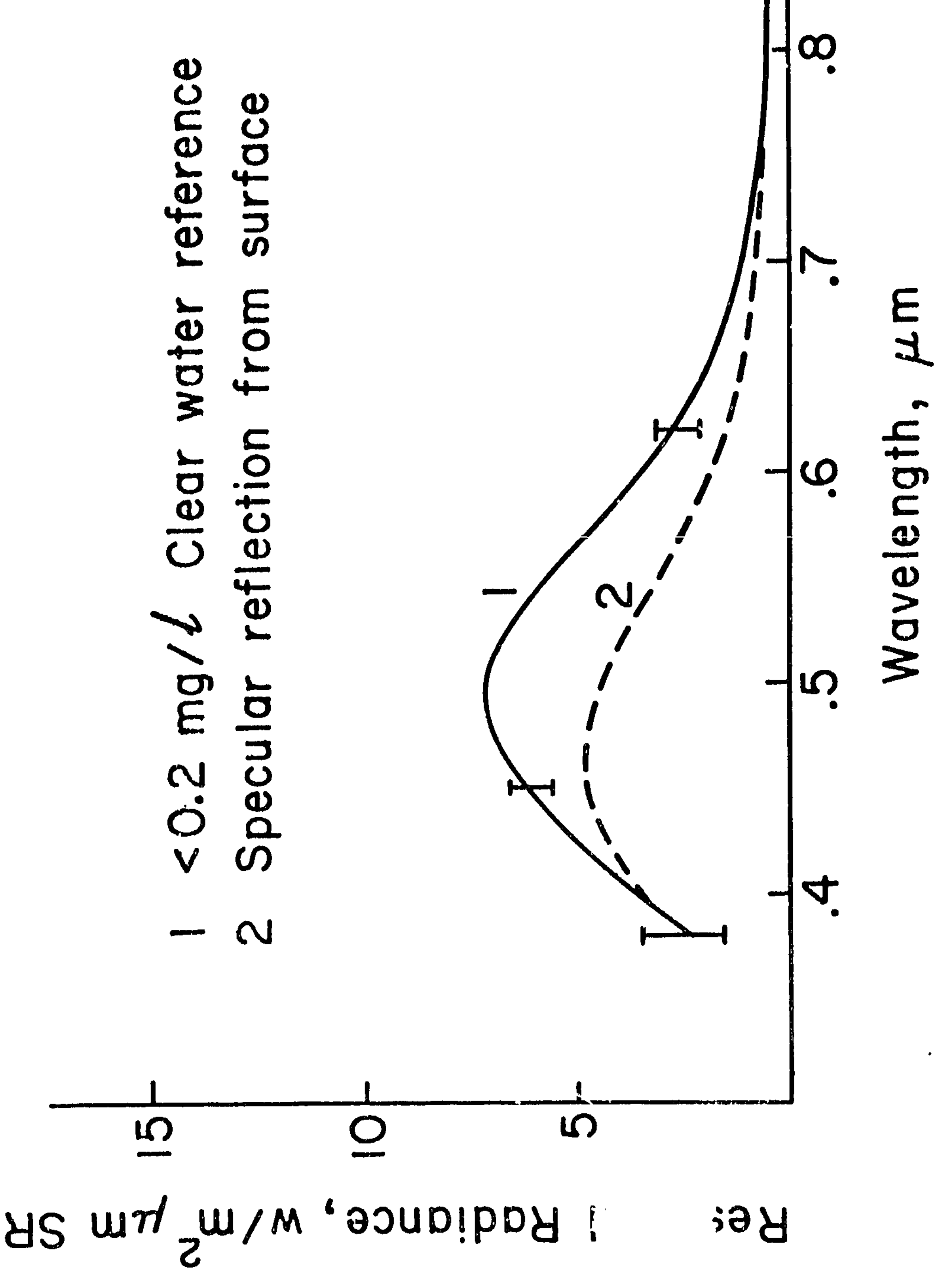
1 <0.2 mg/ℓ Clear water reference
2 Specular reflection from surface
1
2
Re Radiance, w/m$^2\mu$m SR
15
10
5
.4
.5
.6
.7
.8
.9
Wavelength, $\mu$m

Figure 4

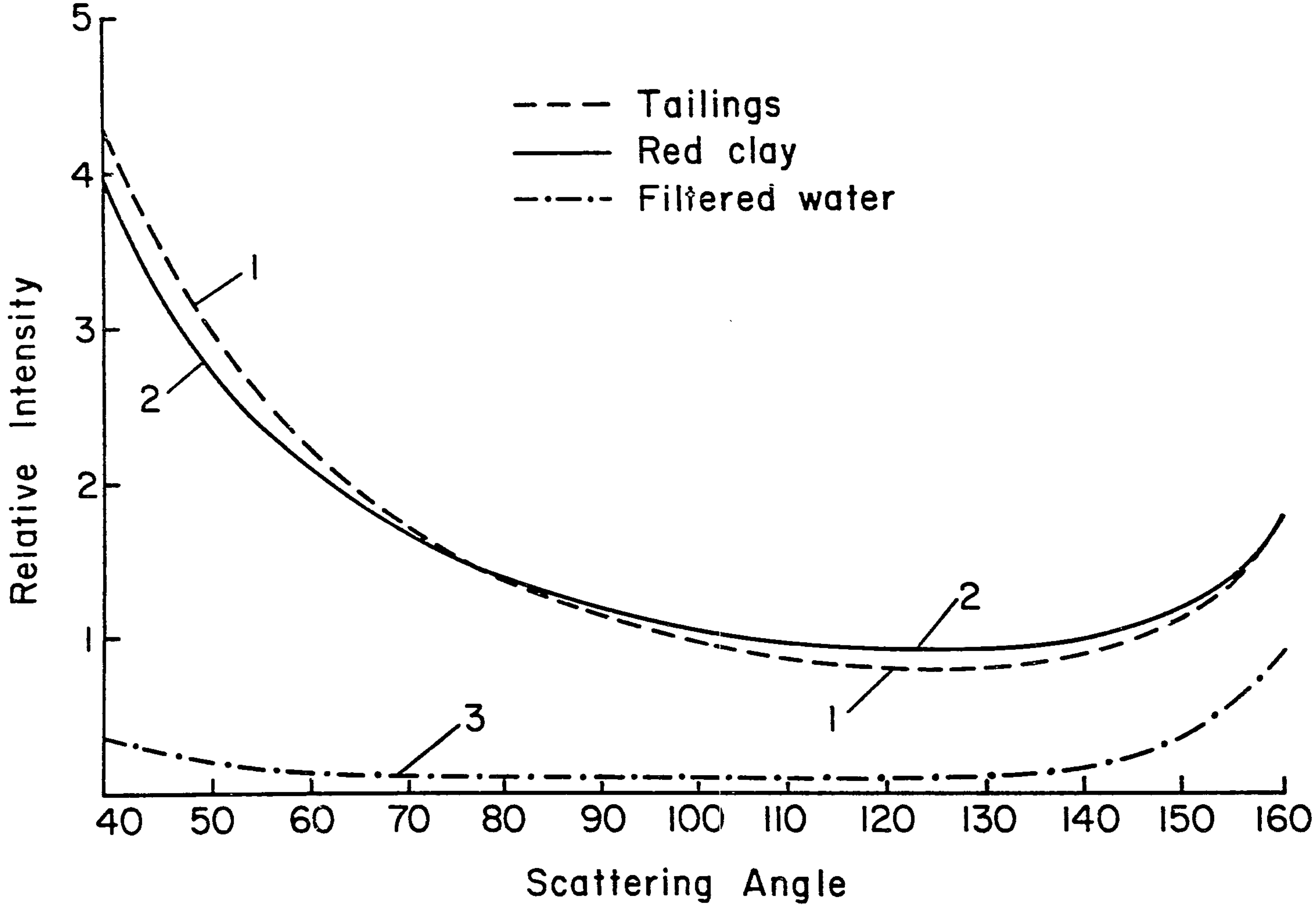
Tailings
Red clay
Filtered water
Relative Intensity
5
4
3
2
1
1
2
2
1
3
40
50
60
70
80
90
100
110
120
130
140
150
160
Scattering Angle

Figure 5

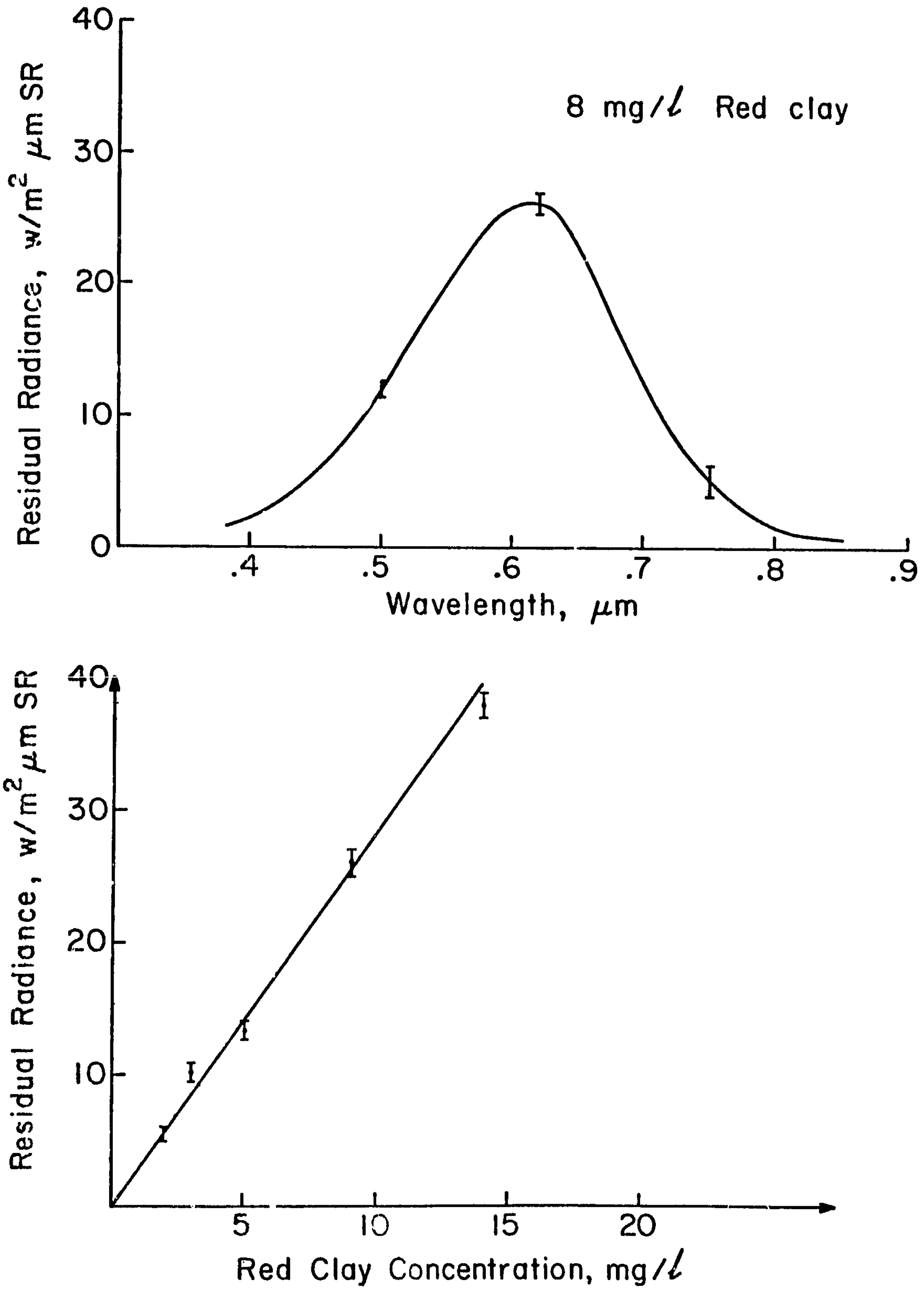
8 mg/l Red clay
Residual Radiance, w/m² μm SR
0
10
20
30
40
.4
.5
.6
.7
.8
.9
Wavelength, μm
Residual Radiance, w/m² μm SR
10
20
30
40
5
10
15
20
Red Clay Concentration, mg/l

Figure 6

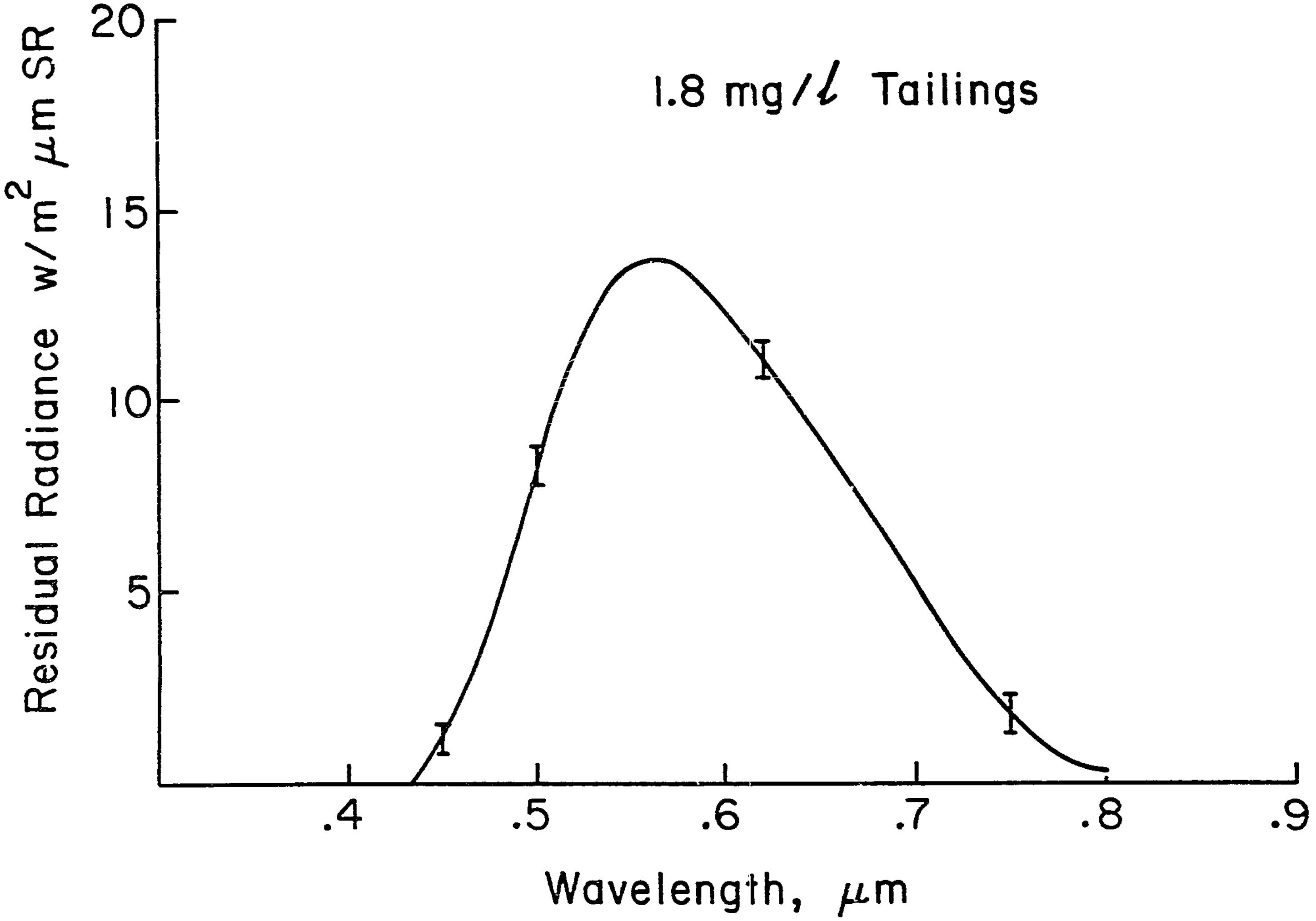
1.8 mg/ℓ Tailings
Residual Radiance w/m² μm SR
20
15
10
5
.4
.5
.6
.7
.8
.9
Wavelength, μm

Figure 7

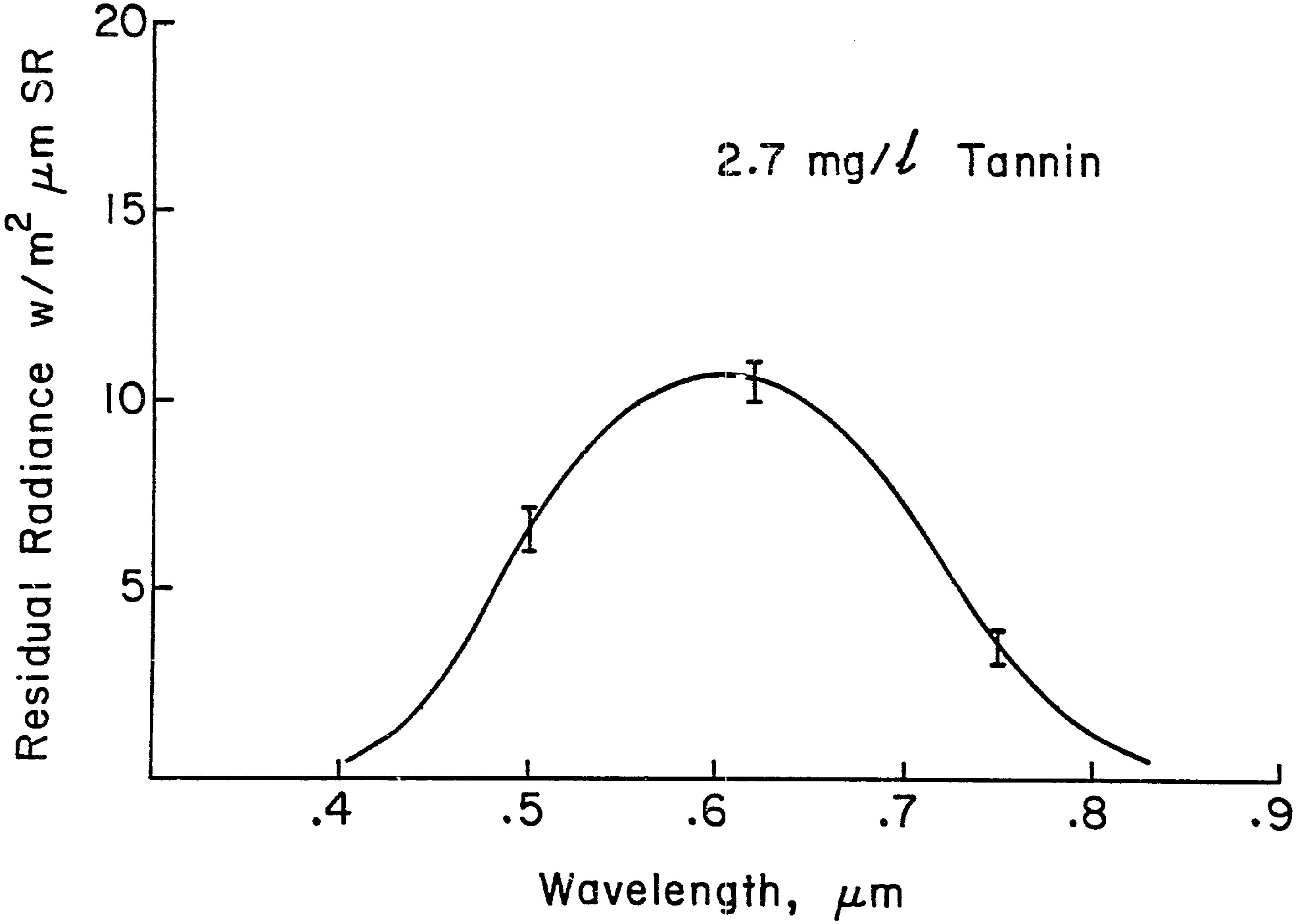
2.7 mg/l Tannin
Residual Radiance w/m² μm SR
20
15
10
5
.4
.5
.6
.7
.8
.9
Wavelength, μm

Figure 8

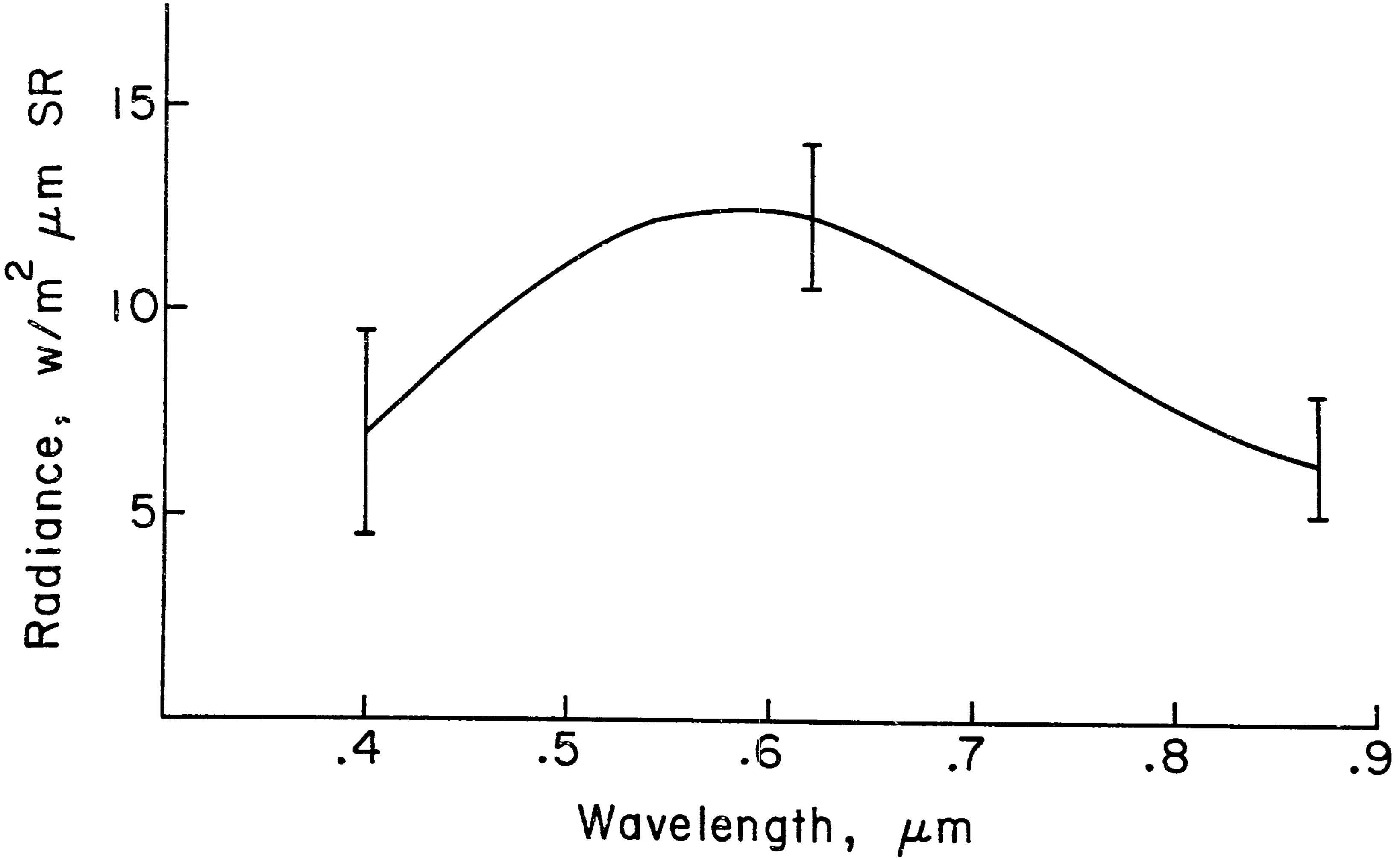

Figure 9

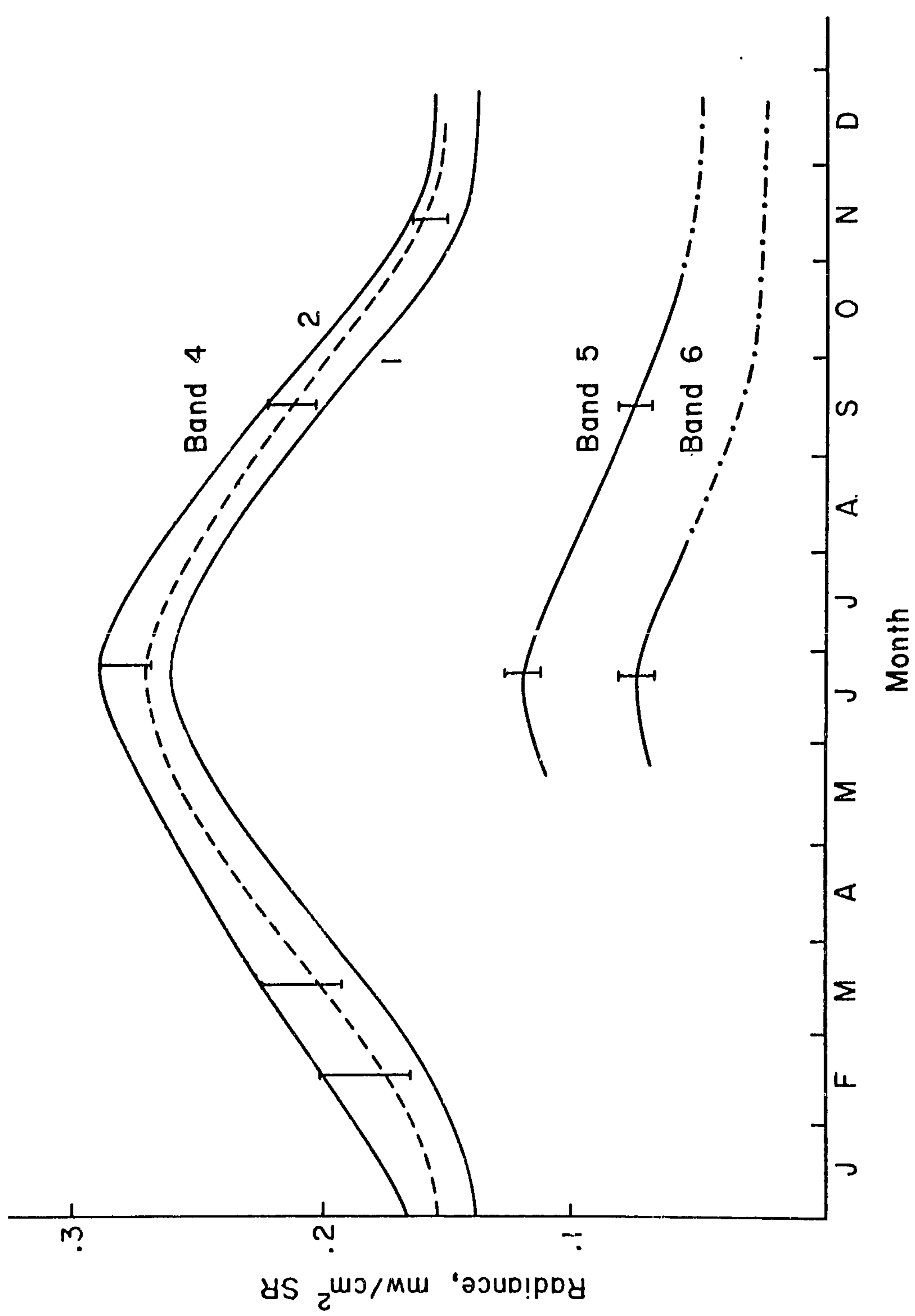
Radiance, mw/cm² SR
.3
.2
.1
J
F
M
A
M
J
J
A
S
O
N
D
Month
Band 4
2
1
Band 5
Band 6

Figure 10

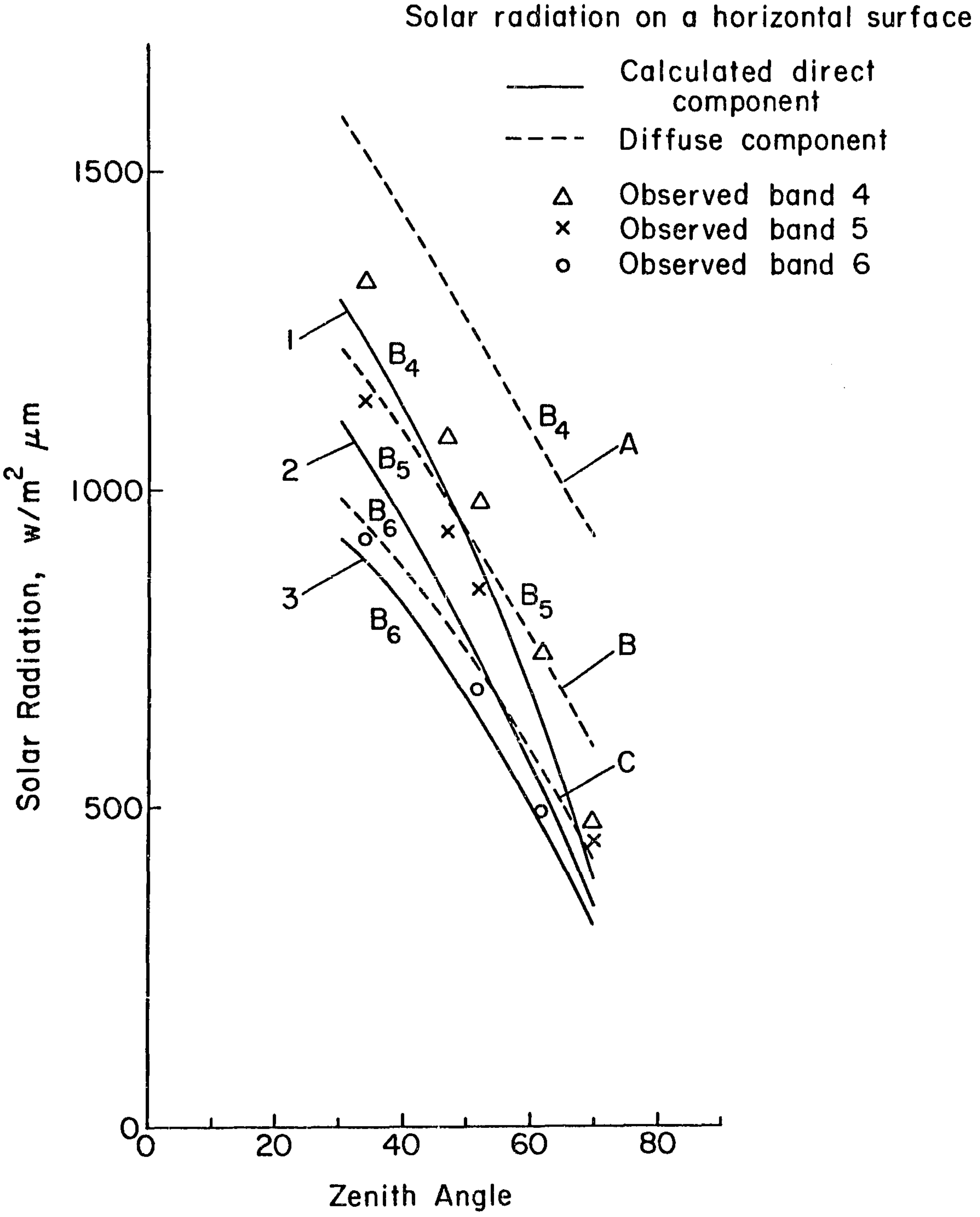
Solar radiation on a horizontal surface
Calculated direct component
Diffuse component
△ Observed band 4
× Observed band 5
o Observed band 6
1500
1000
500
0
0
20
40
60
80
Solar Radiation, $w/m^2\ \mu m$
Zenith Angle
1
2
3
$B_4$
$B_5$
$B_6$
$B_4$
$B_5$
$B_6$
A
B
C

Figure 11

Figure 12

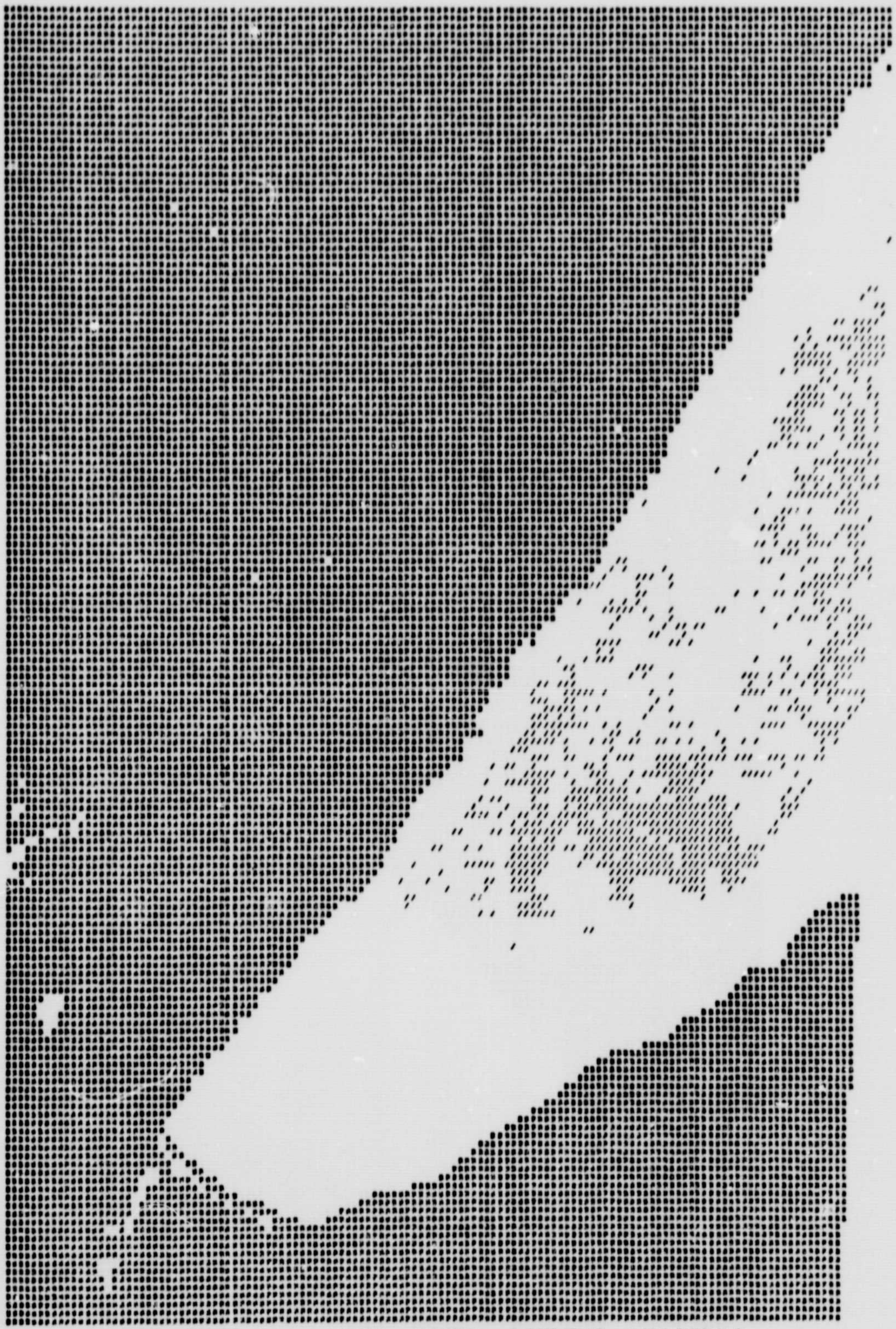
24JUN75 TAILINGS. (840)>3. (840-850)*1. 2.*(850-870)≤3. 1.5≤(840/850)≤1.7
(/) = TAILINGS.

Figure 13

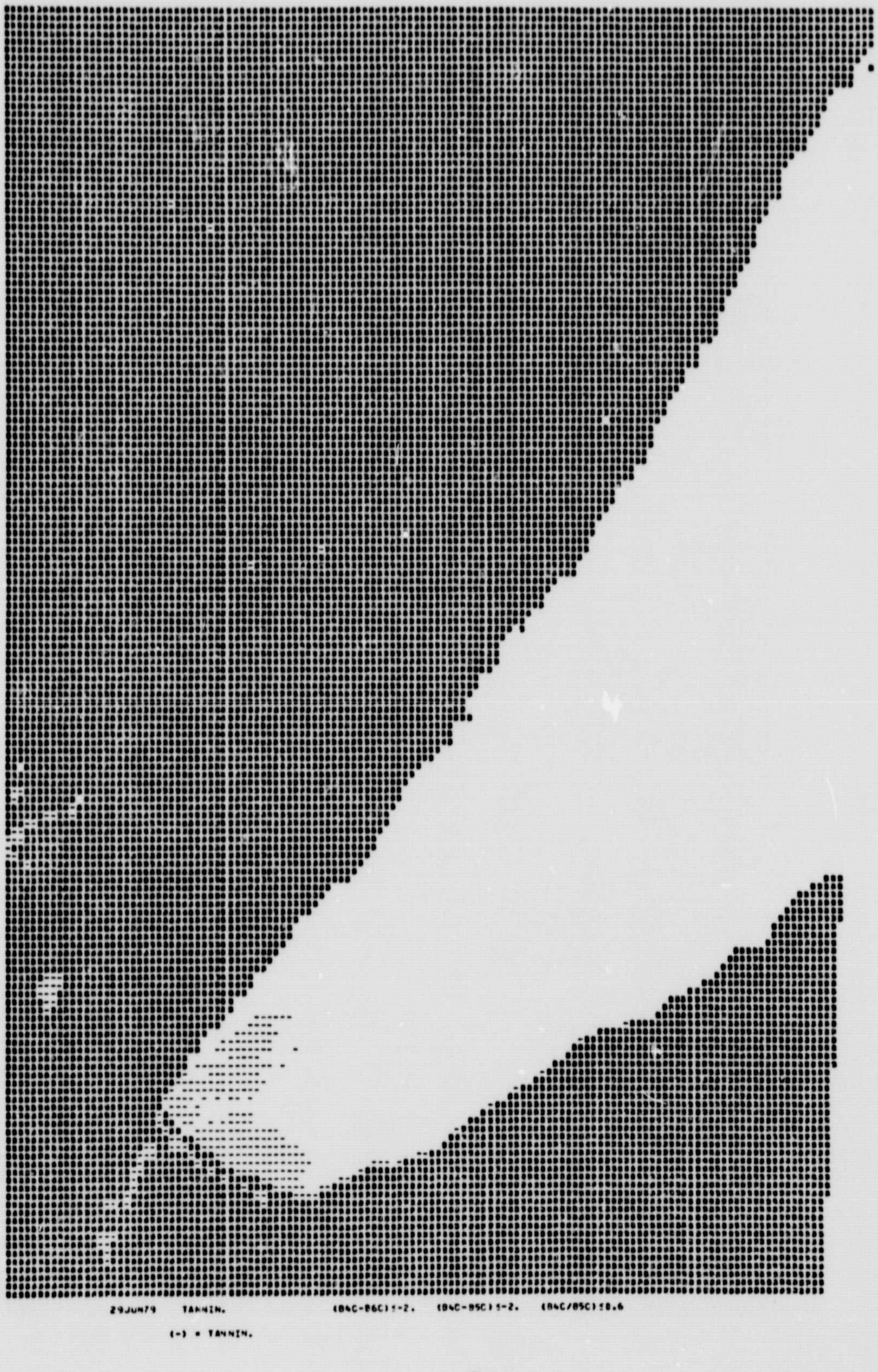

29JUN79 TANNIN. (B4C-B6C)≤-2. (B4C-B5C)≤-2. (B4C/B5C)≤0.6

(-) = TANNIN.

Figure 14

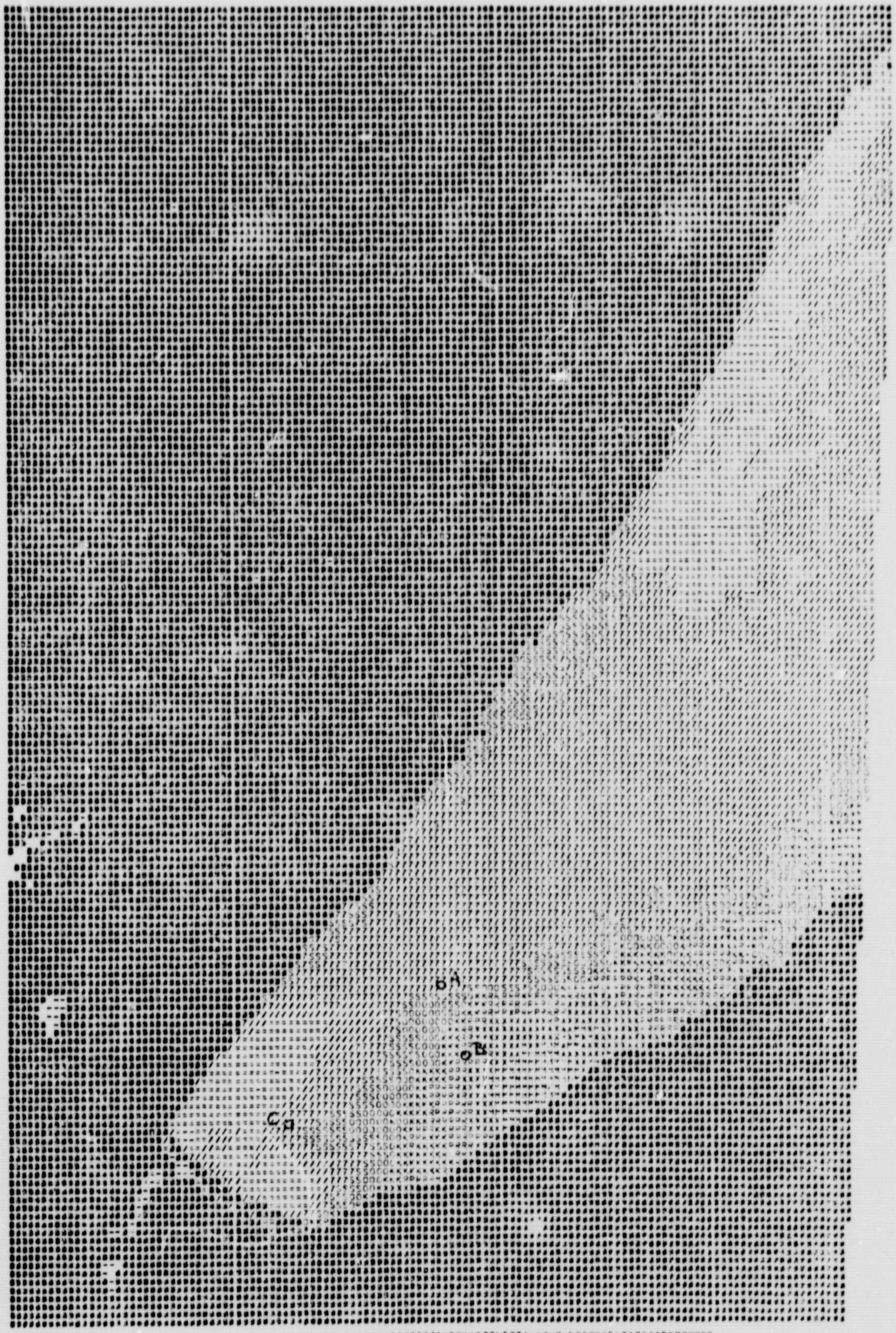

Figure 15